



CENTER FOR INFRASTRUCTURE ENGINEERING STUDIES

EXPERIMENTAL BEHAVIOR OF PRESTRESSED CONCRETE BEAMS STRENGTHENED WITH FRP

By

Marco Di Ludovico

University of Missouri-Rolla

**CIES
03-42**

Disclaimer

The contents of this report reflect the views of the author(s), who are responsible for the facts and the accuracy of information presented herein. This document is disseminated under the sponsorship of the Center for Infrastructure Engineering Studies (CIES), University of Missouri -Rolla, in the interest of information exchange. CIES assumes no liability for the contents or use thereof.

The mission of CIES is to provide leadership in research and education for solving society's problems affecting the nation's infrastructure systems. CIES is the primary conduit for communication among those on the UMR campus interested in infrastructure studies and provides coordination for collaborative efforts. CIES activities include interdisciplinary research and development with projects tailored to address needs of federal agencies, state agencies, and private industry as well as technology transfer and continuing/distance education to the engineering community and industry.

Center for Infrastructure Engineering Studies (CIES)
University of Missouri-Rolla
223 Engineering Research Lab
1870 Miner Circle
Rolla, MO 65409-0710
Tel: (573) 341-6223; fax -6215
E-mail: cies@umr.edu
www.cies.umr.edu

**UNIVERSITA' DEGLI STUDI DI NAPOLI
FEDERICOII**

FACOLTA' DI INGEGNERIA

**DIPARTIMENTO DI ANALISI E PROGETTAZIONE
STRUTTURALE**

TESI DI LAUREA

**EXPERIMENTAL BEHAVIOR OF PRESTRESSED
CONCRETE BEAMS STRENGTHENED WITH FRP**

Relatore
Ch.mo Prof. Ing. Edoardo Cosenza

Candidato:
Di Ludovico Marco

Correlatore
Ch.mo Prof. Ing. Antonio Nanni

Matr. 37/2290

ANNO ACCADEMICO 2001 - 2002

UNIVERSITA DEGLI STUDI DI NAPOLI
FEDERICO II

FACOLTA' DI INGEGNERIA

Dipartimento di Analisi e Progettazione Strutturale

TESI DI LAUREA

EXPERIMENTAL BEHAVIOUR OF PRESTRESSED
CONCRETE BEAMS STRENGTHENED WITH FRP

Relatore
Ch.mo Prof. Ing. Edoardo Cosenza

Candidato:
Di Ludovico Marco

Correlatore
Ch.mo Prof. Ing. Antonio Nanni

Matr. 37/2290

ANNO ACCADEMICO 2001 – 2002

EXPERIMENTAL BEHAVIOUR OF PRESTRESSED BEAMS STRENGTHENED WITH FRP

TABLE OF CONTENTS

CHAPTER I	1
FIBER REINFORCED COMPOSITES	1
1. INTRODUCTION	1
2. GENERAL PROPERTIES OF COMPOSITES	2
3. FIBER REINFORCED POLYMERS	7
-Reinforcing phase: fibers	9
-Matrix	11
-Fillers	14
-Additivies	15
4. FRP MANUFACTURING PROCESS	16
-Pultrusion	17
-Resin Transfer Molding (RTM)	18
-Vacuum Assisted Resin Transfer Molding (VARTM)	19
-Hand Lay-up, Open Molding Process	21
-Compression Molding	22
-Filament winding	23
-Braiding	
5. DURABILITY OF FRP COMPOSITES	26
-Moisture (water) absorption	27
-Alkaline solution	27
-Aggressive chemical solution	28
-Sub zero and freeze-thaw exposure	29
-Temperature and thermal cycling (above zero)	29
-Creep and relaxtion	29
-Fatigue	30
-Ultraviolet (UV) radiation	31
-Fire and high thermal exposure	31

6. FRP SOLUTION IN CONSTRUCTION	33
7. EXTERNALLY BONDED REINFORCEMENT	35
-Laminates	35
-Mechanical properties	36
-Tensile and compressive behaviour	39
-Time-dependent behaviour	41
-Installation technique : Manual Lay-up	42
-Pre-cured systems	46
-Hand Lay-up systems	46
-Near surface mounted bars	
8. INTERNAL REINFORCEMENT	49
-Rebars	49
-Mechanical properties	50
-Tensile and compressive behaviour	51
-Bond behaviour	53
-Time-dependent behaviour	54
-Durability	55
-Grids	58
-Cages	60
-Prestressing Tendons	60
9. CONCLUSIVE REMARKS	62

CHAPTER II	65
STRENGTHENING OF IMPACT-DAMAGED	
BRIDGE GIRDER USING FRP LAMINATES	65
1. INTRODUCTION	65
2. A CASE OF STUDY	68
3. MATERIAL PROPERTIES	71
-PC Girder deck	71
-FRP Laminate	73
4. CFRP DESIGN CALCULATIONS	75
-Strengthening Design	75
-Design criteria	76
-Development length	78
5. INSTALLATION	82
-Inspection and maintenance	83

CHAPTER III	85
RESEARCH PROGRAM	85
1. INTRODUCTION	85
2. THEORETICAL BACKGROUND	86
-Nominal moment strength of undamaged beam	86
-Nominal moment strength of CFRP upgraded beam	96
-Length of FRP reinforcement	104
-Cracking-Load Moment	106
3. SPECIMEN DESCRIPTION	108
-Specimen 1 (undamaged)	108
-Specimen 2 (intentionally damaged and upgraded)	112
4. MATERIALS CHARACTERIZATION	117
-Girder concrete	117
-Deck concrete	118
-Prestressed concrete strand	120
-Mild steel	121
5. THEORETICAL PREDICTIONS	122
-Undamaged beam	122
-Virgin damaged beam	124
-Intentionally damaged and CFRP upgraded beam	126
6. TEST SET UP AND INSTRUMENTATION	131
-Instrumentation Specimen 1 (Undamaged)	133
-Instrumentation Specimen 2 (Intentionally damaged and upgraded)	136
7. TEST RESULTS	140
-Specimen 1 (undamaged)	140 -
Specimen 2 (intentionally damaged and upgraded)1	147
8. DISCUSSION OF TEST RESULTS	167
-Experimental comparison	167
-Theoretical and experimental comparison)	171

CHAPTER IV	174
REPAIR AND STRENGTHENING OF A PC BRIDGE GIRDER WITH NSM CFRP RECTANGULAR BARS	174
1. BACKGROUND	174
2. TEST PHASE II	178
-Flexural Strengthening	179
-Shear Strengthening	181
-Test Setup	183
- Experimental Results	185
3. DISCUSSION	188
-Flexural Evaluation	188
-Shear Evaluation	189
4. MODELING CONSIDERATION	192
5. CONCLUSIVE REMARKS	195

LIST OF FIGURES

Figure I-2-1- <i>Reinforcement of matrix material</i>	3
Figure I-2-2 – <i>SPI Composites Institute, May 1999-Includes shipments Figure I-2-3of reinforced thermoset and thermoplastic resin composites, reinforcements and fillers</i>	5
Figure I-2-3– <i>Growth of FRP composites from 1970 to 2000</i>	6
Figure I-3-1- <i>Comparison among fiber’s, resin’s and composite’s tensile properties</i>	7
Figure I-3-2- <i>FRP rods (left) and laminates (right)</i>	9
Figure I-3-3- <i>Comparison among AFRP, CFRP, GFRP and Steel</i>	11
Figure I-4-1- <i>Pultrusion process</i>	17
Figure I-4-2- <i>Resin Transfer Molding</i>	19
Figure I-4-3- <i>VARTM process</i>	20
Figure I-4-4- <i>Compression molding</i>	23
Figure I-4-5- <i>Filament winding process</i>	24
Figure I-4-6- <i>Two-dimensional braiding process</i>	25
Figure I-7-1- <i>FRP Laminates</i>	36
Figure I-7-2- <i>Installation step by step</i>	46

Figure I-7-3- <i>Near Surface Mounted Bars</i>	48
Figure I-8-1- <i>Rebars with different surfaces</i>	50
Figure I-8-2- <i>FRP grids</i>	59
Figure I-8-3- <i>Applications of FRP grids</i>	59
Figure II-1-1- <i>Accidental Damage Repair Using FRP Technology</i>	67
Figure II-2-1- <i>Bridge A5657 side view</i>	68
Figure II-2-2- <i>Bridge A5657</i>	69
Figure II-2-3- <i>Damaged Area in the girder</i>	69
Figure II-3-1- <i>Girder Dimensions(1 in.=2.54 cm)</i>	71
Figure II-3-2- <i>Prestressing Details (1 in.=2.54 cm)</i>	72
Figure II-4-1- <i>Stress Distribution in a PC section at ultimate</i>	75
Figure II-4-2- <i>Three-Ply CFRP laminate(1 in.=2.54 cm)</i>	77
Figure II-4-3- <i>CFRP Strips U-Wrapped around the giredr bulb(1 in.=2.54 cm)</i>	78
Figure II-4-4- <i>Strand and FRP development length</i>	79
Figure III-2-1- <i>Stress distribution throughout loading history for a PC beam. (a) Beam section. (b) Initial prestressing stage. (c) Self-weight and effective prestress. (d) Full dead load plus effective prestress. (e) Full service load plus effective prestress. (f) Limit state of stress at ultimate load for underreinforced beam. (Edward G. Navy, Prestressed concrete)</i>	87
Figure III-2-2- <i>Load-deformation curve of typical prestressed beam. (Edward G. Navy, Prestressed concrete)</i>	88
Figure III-2-3- <i>(a)strain distribution due to self weight and effective prestress-(b)strain distribution due to full service load- (c)strain distribution due to (a) plus (b).</i>	90
Figure III-2-4- <i>Stress and strain distribution across beam depth at ultimate load . (a) strain distribution due to self weight and effective prestress; (b) strain distribution due to external load; (c) strain distribution at failure[(a) plus (b)];(d) actual stress block;(e) assumed equivalent stress block</i>	91
Figure III-2-5- <i>Typical stress-strain curve, 7 wire low-relaxation prestressing strand.</i>	95

Figure III-2-6- <i>Internal strain and stress distribution under flexure at ultimate stage</i>	101
Figure III-3-1- <i>Girder cross section (1 in.=2.54 cm)</i>	109
Figure III-3-2- <i>Specimen 1 cross section (1 in.=2.54 cm)</i>	110
Figure III-3-3- <i>Tendons cut and intentionally damaged area on specimen 2</i>	112
Figure III-3-4- <i>Two plies of CFRP laminate (1 in.=2.54 cm)</i>	113
Figure III-3-5- <i>CFRP Strips U-Wrapped around the Girder Bulb on specimen 2 (1 in.=2.54 cm)</i>	114
Figure III-3-6- <i>Second Specimen mid-span cross section (1 in.=2.54 cm)</i>	116
Figure III-4-1- <i>Girder concrete cylinders</i>	117
Figure III-4-2- <i>Compression test under a Tinius Olsen Machine</i>	118
Figure III-4-3- <i>Deck concrete cylinders</i>	119
Figure III-6-1- <i>Test set up</i>	132
Figure III-6-2- <i>Strain gages on the specimen 1 (1 in.=2.54cm)</i>	134
Figure III-6-3- <i>Detail strain gages on the tendon and on the concrete</i>	135
Figure III-6-4- <i>Stringer LVDTs and LVDTs positions</i>	136
Figure III-6-5- <i>Strain gage on CFRP detail</i>	138
Figure III-6-6- <i>Strain gages on specimen 2 (1 in.=2.54 cm)</i>	138
Figure III-7-1- <i>Flexural cracks</i>	141
Figure III-7-2- <i>Load-displacement stringer LVDTs #1 and LVDTs #2</i>	142
Figure III-7-3- <i>Load-displacement stringer LVDTs #3 (1.37 m(4.5 ft) from mid-span</i>	142
Figure III-7-4- <i>Strain on tendons placed at mid-span</i>	144
Figure III-7-5- <i>Strain on concrete at mid-span</i>	144
Figure III-7-6- <i>Moment curvature (curvature 1c/1-3t)</i>	146
Figure III-7-7- <i>Moment curvature (curvature 2c/1-9t)</i>	146
Figure III-7-8- <i>Cracks pattern</i>	148
Figure III-7-9- <i>CFRP failure</i>	149
Figure III-7-10- <i>Load-displacement stringer LVDTs #1 (mid-span)</i>	150
Figure III-7-11- <i>Load-displacement stringer LVDTs #2 (mid-span)</i>	150
Figure III-7-12- <i>Load-displacement LVDTs # 3(1.37 m(4.5 ft) from mid-span</i>	151

Figure III-7-13- <i>Load-strain on tendon 9(mid-span cross-section)</i>	153
Figure III-7-14- <i>Load-strain on tendon 3(mid-span cross-section)</i>	153
Figure III-7-15- <i>Load-strain on tendon 1(20.3 cm(8 in.) from mid-span cross-section)</i>	154
Figure III-7-16- <i>Load-strain on tendon 1(66 c m(26 in.) from mid-span cross-section)</i>	154
Figure III-7-17- <i>Load-strain on concrete deck(mid-span cross-section strain gage 1c)</i>	156
Figure III-7-18- <i>Load-strain on concrete deck(mid-span cross-section strain gage 2c)</i>	156
Figure III-7-19- <i>Load-strain on concrete deck (20.3 cm (8 in.) from mid-span cross-section strain gage 3c)</i>	157
Figure III-7-20- <i>Load-strain on concrete deck(66.0 cm (26 in.) from mid-span cross-section strain gage 4c)</i>	157
Figure III-7-21- <i>Load-strain on CFRP bottom surface (mid-span cross-section strain gage 1 frp)</i>	158
Figure III-7-22- <i>Load-strain on CFRP bottom surface (mid-span cross-section strain gage 2 frp)</i>	159
Figure III-7-23- <i>Load-strain on CFRP bottom surface (10.2 cm (4 in.) from mid-span cross-section strain gage 3 frp)</i>	159
Figure III-7-24- <i>Load-strain on CFRP bottom surface (55.9 cm (22 in.) from mid-span cross-section strain gage 4 frp)</i>	159
Figure III-7-25- <i>Moment- curvature 1c-1frp</i>	162
Figure III-7-26- <i>Moment- curvature 2c-2frp</i>	162
Figure III-8-1- <i>Load displacement string LVDT's comparison between virgin and CFRP upgraded specimen</i>	165
Figure III-8-2- <i>Load-displacement LVDT's 3 comparison between virgin and CFRP upgraded specimens</i>	166
Figure III-8-3- <i>Comparison between strain in the tendons between virgin and CFRP upgraded specimens</i>	167
Figure III-8-4- <i>Comparison between strain in concrete between virgin and CFRP upgraded specimens</i>	167
Figure III-8-5 <i>Moment-curvature comparison between virgin and CFRP upgraded specimens1</i>	168
Figure III-8-6 <i>Moment-curvature theoretical and experimental comparison virgin specimen</i>	169
Figure III-8-7 <i>Moment-curvature theoretical and experimental comparison upgraded specimen</i>	169
Figure III-8-8 <i>Load –displacement virgin specimen,cracking and yielding load</i>	170

Figure III-8-9	<i>Load –displacement upgraded specimen, cracking and yielding load</i>	171
Figure IV-1-1-	<i>Dimensions of test specimen before cutting (25.4 mm=1 in.)</i>	176
Figure IV-1-2-	<i>Geometry of test setup for Phase 1</i>	176
Figure IV-1-3-	<i>FRP layout of specimen S2 (25.4 mm = 1 in, 1 m = 3.28 ft)</i>	177
Figure IV-1-4-	<i>FRP layout of specimen S3 (25.4 mm = 1 in)</i>	178
Figure IV-2-1-	<i>Flexural strengthening installation</i>	179
Figure IV-2-2-	<i>Removal of excess resin</i>	180
Figure IV-2-3-	<i>Installation of rectangular CFRP bar for shear strengthening</i>	182
Figure IV-2-4-	<i>Instrumented bars for shear strengthening</i>	183
Figure IV-2-5-	<i>Test setup for specimen S4 (25.4 mm = 1 in, 1 m = 3.28 ft)</i>	184
Figure IV-2-6-	<i>Strain gage positions for specimen S4 (25.4 mm = 1 in, 1 m = 3.28 ft)</i>	185
Figure IV-2-7-	<i>Load-displacement as measured at the location of the jack (stringer LVDTs)</i>	186
Figure IV-2-8-	<i>Strain measured in the flexural pre-cured FRP Laminate</i>	187
Figure IV-2-9-	<i>Strain measured in the FRP rectangular bar for shear</i>	187

LIST OF TABLES

Table I-3-1-	<i>Typical epoxy resin properties</i>	14
Table I-7-1-	<i>Mechanical properties for primer, putty and saturant</i>	37
Table II-3-1-	<i>Material properties</i>	71
Table II-3-2-	<i>Mechanical properties for carbon fibers</i>	72
Table II-3-2-	<i>Properties of Carbon FRP (MBT, 1998)</i>	74
Table II-4-1-	<i>Moment capacity of the cross-section</i>	76
Table III-3-1-	<i>Material quantity and properties</i>	111
Table III-3-2-	<i>CFRP 130 properties</i>	115
Table III-4-1-	<i>Test results for girder concrete cylinders</i>	118
Table III-4-2-	<i>Test results for deck concrete cylinders</i>	116
Table III-4-3-	<i>Prestressed concrete strands properties</i>	117
Table III-4-4-	<i>Mild steel properties</i>	121

Table III-5-1- <i>Theoretical results</i>	129
Table III-6-1- <i>Load cycles</i>	132
Table III-6-2- <i>Strain on tendons due to prestress</i>	132
Table III-6-3- <i>Strain on tendons due to prestress</i>	136
Table III-7-1- <i>Displacement cm (in.) at cracking and maximum load</i>	142
Table III-7-2- <i>Strain on concrete and tendons</i>	144
Table III-7-3- <i>Curvature value at cracking and maximum load</i>	146
Table III-7-4- <i>Displacement cm (in.) at cracking and maximum load</i>	151
Table III-7-5- <i>Strain on concrete and tendons</i>	161
Table III-7-6- <i>Curvature value at cracking and ultimate load respectively</i>	163
Table III-8-1- <i>Final results comparison, cracking, yielding, ultimate load</i>	172
Table III-8-2- <i>Final results comparison cracking, yielding, ultimate curvature</i>	172
Table IV-1-1- <i>Test results of Phase 1</i>	178
Table IV-2-1- <i>FRP system properties for specimen S4</i>	183
Table IV-2-2- <i>Load-unload cycles for specimen S4</i>	185
Table IV-3-1- <i>Comparison of test results for Phases 1 and 2 – flexure (cross-section at 914 mm (3 ft) from mid-span)</i>	189
Table IV-3-2- <i>Comparison of test results for Phases 1 and 2 - shear (cross-section at 914 mm (3 ft) from mid-span)</i>	191
Table IV-4-1- <i>Shear theoretical predictions</i>	194

CHAPTER I

FIBER REINFORCED COMPOSITES

1. INTRODUCTION

The idea of combining two different materials to make a single, superior composite material is not new. Some of the earliest building materials were composite. The ancient Egyptians reinforced their mud bricks with straw to make them stronger. Although the concept of fiber reinforced materials can be traced back to the use of straw as reinforcement in bricks manufactured by the Israelites in 800 B.C., and in the early 1930's to the use of short glass fibers in cement in United States, fiber reinforced resin matrix materials (or fiber reinforced composites as we know them today) were not developed until the early 1940's.

After World War II, US manufacturers began producing *fiberglass* and *polyester resin* composite boat hulls and radomes (i.e., radar cover). The automotive industry first introduced composites into vehicle bodies in the early 1950's. Because of the highly desirable light weight, corrosion resistance, and high strength characteristics in composites, research emphasis went into improving the material science and manufacturing process. That effort led to the development of two new manufacturing techniques known as *filament winding* and *pultrusion*, which helped advance the composite technology into new markets. There was a great

demand by the recreation industry for composite fishing rods, tennis rackets, ski equipment and golf clubs. The aerospace industry began to use composites in pressure vessels, containers, and non-structural aircraft components. The US Navy applied composites in mine sweeping vessels, crew boats and submarine parts. The domestic consumers began installing composite bath tubs, covers, railings, ladders and electrical equipment. The first civil application in composites was a dome structure built in Benghazi in 1968, and other structures followed slowly.

2. GENERAL PROPERTIES OF COMPOSITES

A composite is a combination of two or more materials into a single system that exhibits combined properties of its individual components. The system constituents retain their distinct identities (they do not dissolve or merge completely into each other) and act in concert as a hybrid to provide new, desirable properties. Reinforced concrete (RC), for example, is a composite consisting of steel reinforcement, sand and gravel fillers, and a cement matrix. .

Composite materials are composed of a *matrix* material reinforced with any of a variety of fibers (reinforcing phase) made from ceramics, metals, or polymers. The reinforcing fibers are the primary load carriers of the material, with the matrix component transferring the load from fiber to fiber. Reinforcement of the matrix material may be achieved in a variety of ways: fibers may be either continuous or discontinuous, and the reinforcement may also be in the form of particles (see Figure I-2-1).

The matrix material is usually one of the many available engineering plastics/polymers. Selection of the optimal reinforcement form and material is dependent on the property requirements of the finished part.

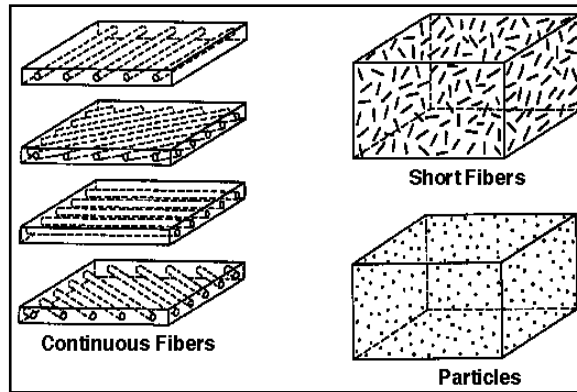


Figure I-2-1 - Reinforcement of matrix material

The advantages of composite materials over metals are:

- Light weight
- Possibility to tailor the fiber/resin mix to meet
- Possibility to meet stiffness/strength/manufacturing requirements
- Reduced machining
- Resistance to corrosion
- Resistance to fatigue damage
- Low coefficient of thermal expansion

Some of the most significant properties are described as follow:

Weight: A weight saving of 27% is attainable in most structures. This is due to the lower density of composites, which range (depending on material form) from 1246 daN/m³(0.045 lb/in³) to 1800 daN/m³(0.065

lb/in³) as compared to 2768 daN/m³(0.10 lb/in³) for aluminum. Some applications may require thicker composite sections to meet strength/stiffness requirements, however, a weight savings will still result.

Cost: Low cost, high volume manufacturing methods are used to make composites cost competitive with metals: tooling costs for high volume production of metals and composites parts are similar and also the production labor time is similar, so the higher cost of composite parts is mostly due to high raw material costs; a judicious selection of the optimal material for the part and of the suppliers will control these costs and can minimize the cost penalty.

Composite performance: Composites have inherent properties that provide performance benefits over metals. A wide range of fibers and resins are available to select the optimal material combination to meet the structural requirements. The strength-to-weight and stiffness-to-weight ratios are the primary reasons for using composites. The fracture toughness of composites is better than aluminum castings; by their nature, castings basically have built-in notches that can catastrophically fracture under impact. The fiber reinforcement of composites alter this failure sequence resulting in an increased resistance to impact. The impact toughness of composites can be maximized by fiber selection, length of fiber and use of tougher resin such as thermoplastics.

Composite materials will provide a structure that saves weight and has better performance over the competing metallic structure. The structure will be more durable and tougher.

The composite industry associations and materials producers track the FRP's composites material shipments in eight primary markets like shown in Figure I-2-2:

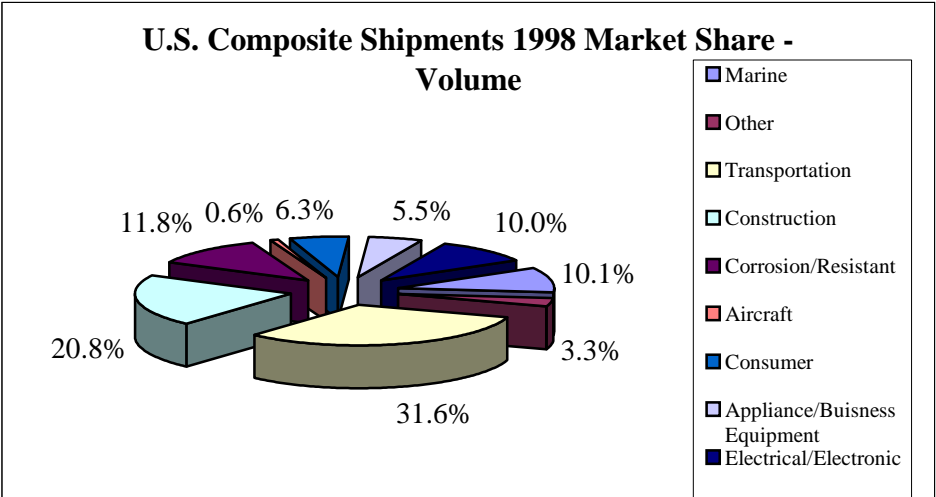
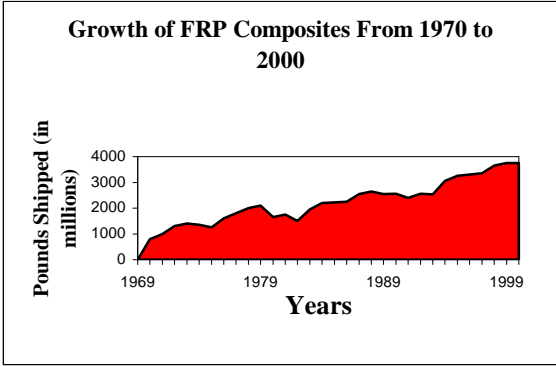


Figure I-2-2- *SPI Composites Institute, May 1999 – Includes shipments of reinforced thermoset and thermoplastic resin composites, reinforcements and fillers*

The composites industry has shown growth over the past ten years and is projected to increase as FRP composites are accepted in new markets. The FRP increase is presented in FigureI-2-3:



FigureI-2-3 - Growth of FRP composites from 1970 to 2000

3. FIBER REINFORCED POLYMERS

Fiber reinforced polymers (FRP) are a particular typology of composite materials, made of high resistance fibers impregnated with polymeric resins. The mixing result is a material with properties between fiber and resin.(see Figure I-3-1)

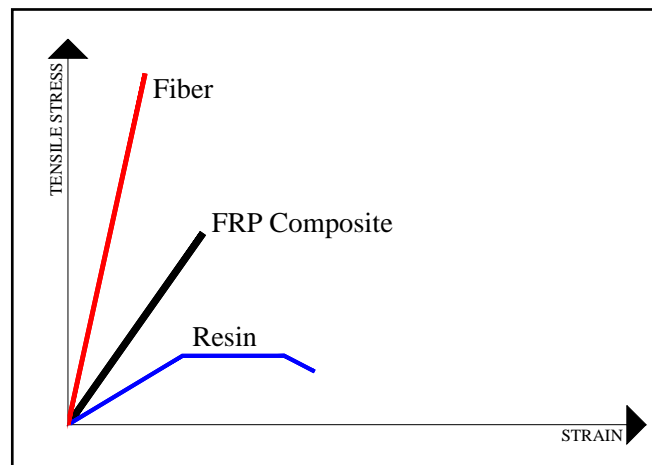


Figure I-3-1-*Comparison among fiber's, resin's and composite's tensile properties*

FRP materials are characterized by excellent tensile strength in the direction of the fibers and by negligible strength in the direction transverse to the fibers; this illustrates the anisotropic nature of these materials. FRP composites do not exhibit yielding, but instead are elastic up to failure and they are also characterized by relatively low modulus of elasticity in tension and low compressive properties.

Their function usually consists in adsorbing tensile stress due to shear and flexural actions. Often, among the reachable advantages, are also the increase of the overall stiffness and ductility.

FRP properties make these materials particularly suitable for structural applications, especially in support or substitution of steel.

The general advantages of FRP reinforcement compared to steel are:

- Durability in aggressive environments
- High strength-to-density ratio
- Magnetic and electric neutrality
- Low specific weight
- Low axial coefficient of thermal expansion

Without underlining the importance of a lower installation cost, the use of FRP composites possesses some advantages compared to traditional retrofitting methods; as an example, the disturbance of both occupants and facilities are minimal and there is no loss of valuable space. In addition, from the structural point of view, the dynamic properties of the structure remain unchanged because there is no addition of weight that would lead to increase the seismic forces.

FRP products are commercialized in different shapes: rods, tendons, laminates and three-dimensional components.

FRP reinforcement comes in the shape of rods of circular cross-sections, strips of rectangular cross-sections, strands, and laminates, which enable different types of applications.(see Figure I-3-2)

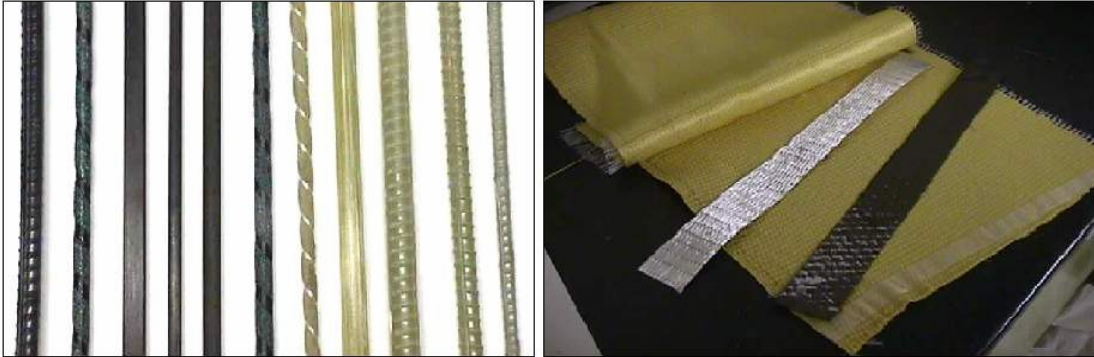


Figure I-3-2 - *FRP rods (left) and laminates (right)*

The main characteristics of FRP components are briefly described in the following paragraph

-Reinforcing phase: fibers

The three most common types of FRP used in construction are made of *carbon, aramid* or *glass fibers*.

- ***Carbon Fibers:*** Fiber produced by heating organic precursor materials containing a substantial amount of carbon (93÷95%), such as rayon, polyacrylonitrile (PAN), or pitch (a black residue from the distillation of petroleum) in an inert environment. This kind of fibers is the strongest, stiffest, and most durable; they are more expensive than glass fibers but offer an excellent combination of strength, low weight, high modulus and fatigue properties.

- **Aramid Fibers (ex. Kevlar):** Highly oriented organic fiber derived from polyamide incorporating into aromatic ring structure. This kind of fibers offers excellent impact resistance, a good electric and temperature insulating properties and they are also resistant to organic solvents, fuels and lubricants.

They have a medium modulus and a very low density as compared to glass and carbon.

It is available in tows, yarns and various woven cloth products.

- **Glass Fibers:** Fiber drawn from an inorganic product of fusion that has cooled without crystallizing. **E-Glass** fibers are considered the predominant reinforcement for polymer matrix composites, due to their high electrical insulating properties and low susceptibility to moisture. Other commercial composition includes **S-Glass**, with higher strength, heat resistance and modulus, as well as some specialized glass reinforcements with improved chemical resistance, such as AR Glass (alkali resistant). On the other hand, these products are very expensive. Glass produces a common, low-cost reinforcing fiber, but they weight more than carbon or aramid and the lower modulus requires special design treatment where stiffness is critical. Glass has been the predominant fiber for many civil engineering applications because of an economical balance of cost and specific strength properties.

A comparison based on fiber area among sheets made of carbon (CFRP), aramid (AFRP), glass (GFRP) and reinforcing steel in terms of stress-strain relationship is depicted in

Figure I-3-3 :

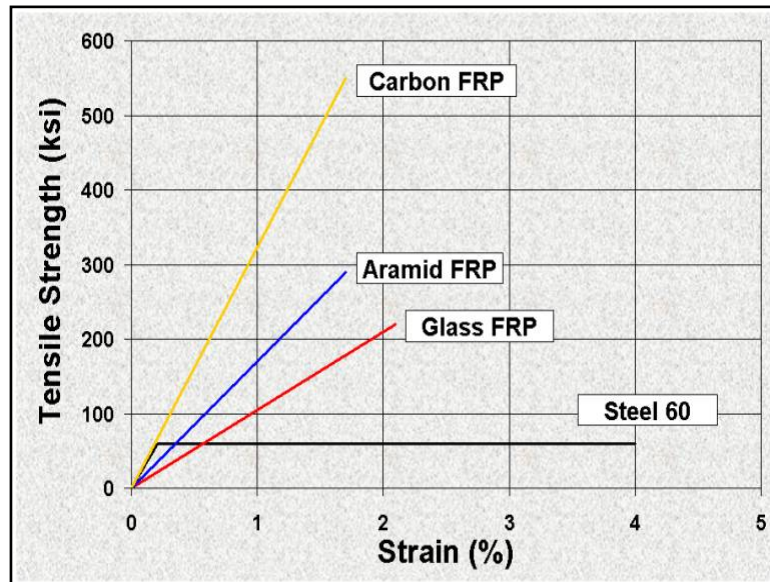


Figure I-3-3- Comparison among AFRP, CFRP, GFRP and Steel

- Matrix

The *FRP matrix* consists of a polymer, or resin, used as a binder for the reinforcing fibers, and it has the functions of enabling the load to be transferred among fibers and protecting them from environmental effects. The resin is fundamental for interlaminar and in-plane shear strength: the interlaminar strength is important for the structure inflection and the in-plane strength is important for the torsion. Furthermore, FRP workability and defects depend on some physical-thermal resin's properties such as viscosity, vulcanization temperature and melting point. Polymeric resins are subdivided in two big categories, thermoset and thermoplastic:

- The *thermoset polymers* after the vulcanization (with energy under appearances of heat energy or with catalysts) are insoluble and not melt also with high temperature.
- The *thermoplastic polymers* are instead soluble, because they have a low molecular bond; so, these resins can be weak, melted and mold all times want.
- The *glass transition temperature* (T_g) is used to measure the softening of cured resins. Generally the resins are isotropic and they have an elastic-brittle behaviour.
- Also if the *thermoplastic resins* had a large development as for thermosetting polymers, there are still many problems to soak the fibers, so, in the building's field, there are three types of commonly available thermo-setting resins: epoxy, vinyl ester and phenolic. The main properties of such resins are below outlined:
- *Epoxy* resins are the most common and have excellent structural properties as well as excellent adhesion characteristics; a major benefit of epoxy resins is their lower shrinkage. Epoxy can also be formulated with different materials or blended with other epoxy resins to achieve specific performance features. Epoxies are used primarily for fabricating high performance composites with superior mechanical properties and good performance at elevated temperatures; this kind of resin has particularly good UV resistance and their maximum use temperature is on the order of 200° F (93.3° C). Epoxy resins are available in a range of

viscosity, and will work with a number of curing agents or hardeners.

- **Vinyl ester** resins are a lower cost matrix material with good durability characteristics, excellent corrosion resistance and very good mechanical toughness, but have lower structural performance and low resistance to heat. Vinyl esters were developed to combine the advantages of epoxy resin with the better handling/faster cure, which are typical for unsaturated polyester resins.
- **Phenolic** are a class of resins commonly based on phenol and formaldehyde. Phenolic composites have many desirable performance qualities include high temperature resistance, creep resistance, excellent thermal insulation and sound damping properties, corrosion resistance and excellent fire/smoke toxicity properties.

Phenolic appears to be the most important resin, but epoxy and vinylester are the most commonly used because of durability and adhesion properties.

The main mechanical properties of a typical epoxy resin are shown in Table I-3-1:

Density	1200 Kg/m ³ (0.043 lb/in ³)
---------	--

Elastic modulus	3.4 GPa (493128 psi)
Shear modulus	1.308 Gpa (189710 psi)
Tensile strength	72 Mpa (10443 psi)

Table I-3-1 - Typical epoxy resin properties

Thermoset resins are generally heat activated, or cured, from an initial liquid state. Resins are often combined with additives and fillers for environmental resistance, flame resistance, appearance, and cost reduction.

- Fillers

The use of inorganic fillers in composites is increasing; not only they reduce the cost of composites, but also frequently impart performance that might not otherwise be achieved by the reinforcement and resin ingredients alone. These materials improve the following performance:

- They reduce the shrinkage of the composites part
- They influence the fire resistance of laminates
- Fillers can influence the mechanical strengths of composites
- Crack resistance and crack prevention properties are improved with filled resin systems
- Uniformity of the laminate can be enhanced by use of fillers

There are a lot of inorganic filler materials that can be used with composites including *Calcium Carbonate, Kaolin, Alumina trihydrate, Calcium sulfata* etc...

- Additives

A wide range of additives are used in composites to modify material properties and tailor the FRP performance. Additives used in thermosetting composites include the following:

- Fire resistance (in place of fillers)
- Viscosity control
- Toughness
- Heat stabilizers
- Ultraviolet stabilizers

4. FRP MANUFACTURING PROCESS

In this section, the manufacturing processes typical of products used in civil infrastructure are covered. Unique to the composites industry is the ability to create a product by many different manufacturing processes. There is a wide variety of processes available to the composites manufacturer to produce cost efficient products. Each of the fabrication processes has characteristics that define the type of products. This is advantageous because a high level of expertise allows the manufacturer to provide the best solution for the customer. In order to select the most efficient manufacturing process, the manufacturing team should consider several factors such as:

- user needs
- performance requirements
- size of the product
- surface complexity
- appearance
- production rate
- total production volume
- economic targets/limitations
- labor
- materials
- tooling/assembly
- equipment

The manufacturing processes typically used to make products found in construction/civil infrastructure market are below described:

- Pultrusion

Pultrusion is a continuous molding process that combines fiber reinforcements and thermosetting resin. The pultrusion process is used in the fabrication of composite parts that have a constant cross-section profile. Typical examples include various rods and bar section, ladder side rails, tool handles, and electrical cable tray components and now bridge beams and decks. Most pultruded laminates are formed using rovings aligned down the major axis of the part. Various continuous strand mats, fabrics (braided, woven and knitted), and texturized or bulked rovings are used to obtain strength in the cross axis or transverse direction (see Figure I-4-1)

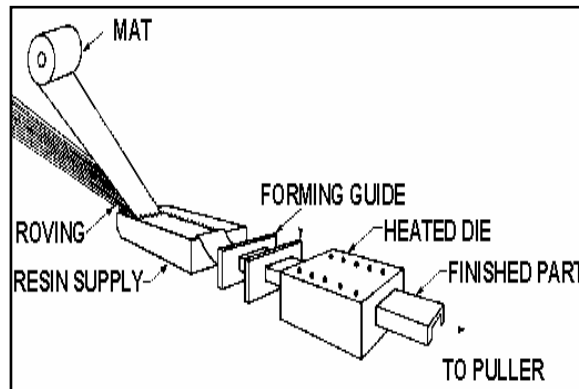


Figure I-4-1 - Pultrusion process

The process is normally continuous and highly automated. Reinforcement materials, such as roving, mat or fabrics, positioned in a specific location using preforming shapers or guides to form the profile. The reinforcements are drawn through a resin bath or wet-out where the material is thoroughly coated or impregnated with a liquid thermosetting

resin. The resin-saturated reinforcements enter a heated metal pultrusion die. The dimensions and shape of the die will define the finished part being fabricated. Inside the metal die, heat is transferred initiated by precise temperature control to the reinforcements and liquid resin. The heat energy activates the curing or polymerization of the thermoset resin changing it from a liquid to a solid. The solid laminate emerges from the pultrusion die to the exact shape of the die cavity. The laminate solidifies when cooled and it is continuously pulled through the pultrusion machine and cut to the desired length. The process is driven by a system of caterpillar or tandem pullers located between the die exit and the cut-off mechanism.

-Resin Transfer Molding (RTM)

Resin Transfer Molding, commonly known as (RTM) is a “Closed Mold Process” in which reinforcement material is placed between two matching mold surfaces – one being male and one being female. The matching mold set is then closed and clamped and a low-viscosity thermoset resin is injected under moderate pressures (345 – 689 kPa (50 – 100 psi) typical) into the mold cavity through a port or series of ports within the mold. The resin is injected to fill all voids within the mold set and thus penetrates and wets out all surfaces of the reinforcing materials. The reinforcements may include a variety of fiber types, in various forms such as continuous fibers, mat or woven type construction as well as a hybrid of more than one fiber type. Vacuum is sometimes used to enhance the resin flow and reduce void formation. The part is typically cured with

heat. In some applications, the exothermic reaction of the resin may be sufficient for proper cure (see Figure I-4-2)

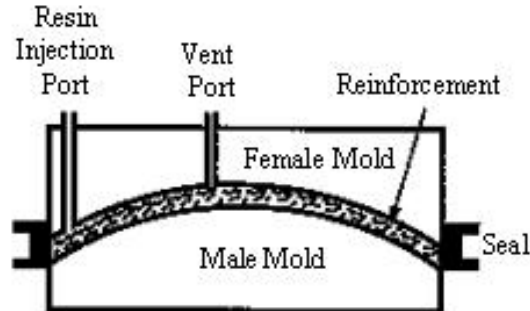


Figure I-4-2 - Resin Transfer Molding

-Vacuum Assisted Resin Transfer Molding (VARTM)

In the traditional RTM process, a matched set of molds or “closed mold” is used. The fiber reinforcements are usually preformed off line to enhance the production cycle time of the molds to perform at a respectable production rate. Resin is injected at high pressures and the process is sometimes assisted with vacuum.

However, Vacuum Assisted Resin Transfer Molding (VARTM) is different for many reasons. First, the fabrication of parts can be accomplished on a single open mold. Second, the process uses the injection of resin in combination with a vacuum and captured under a bag to thoroughly impregnate the fiber reinforcement. In the late 1980’s, Bill Seemann invented and patented a variation to the VARTM process called SCRIMPTM, which is Seemann Composite Resin Infusion Molding Process. This process has been used in many new and large applications ranging from turbine blades and boats to rail cars and bridge decks.

Unique to this process is the manufacturing method that allows the efficient processing of VARTM to produce large structural shapes that are virtually void-free. This process has been used to make both thin and very thick laminates. In addition, complex shapes with unique fiber architectures allow the fabrication of large parts that have a high structural performance (see Figure I-4-3)

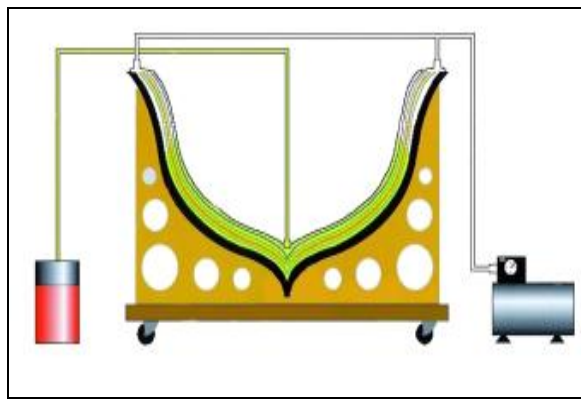


Figure I-4-3 -VARTM process

Parts using VARTM are made by placing dry fiber reinforcing fabrics into a mold, applying a vacuum bag to the open surface and pulling a vacuum while at the same time infusing a resin to saturate the fibers until the part is fully cured. This process allows for easy visual monitoring of the resin to ensure complete coverage to produce good parts without defects.

-Hand Lay-up, Open Molding Process

Hand lay up is the oldest and simplest method used for producing reinforced plastic laminates. Capital investment for hand lay up processes

is relatively low. The most expensive piece of equipment typically is a spray gun for resin and gel coat application. Some fabricators pour or brush the resin into the molds so that a spray gun is not required for this step. There is virtually no limit to the size of the part that can be made. The molds can be made of wood, sheet metal, plaster, and FRP composites.

In a particular hand lay up process (otherwise known as *wet lay up*), high solubility resin is sprayed, poured, or brushed into a mold. The reinforcement is then wet out with resin. The reinforcement is placed in the mold. Depending upon the thickness or density of the reinforcement, it may receive additional resin to improve wet out and allow better drapeability into the mold surface. The reinforcement is then rolled, brushed, or applied using a squeegee to remove entrapped air and to compact it against the mold surface.

Chopped strand mat is the lowest cost form of reinforcement used in wet lay up. It also provides equal reinforcing strength in all directions due to the random orientation of the fibers that form the mat. Woven roving is especially suitable for thick laminates requiring greater strength. Woven fabric and braid can also provide a low cost reinforcement. Once the reinforcement is thoroughly wet out with resin, it can be easily formed into complex shapes.

A key step toward a successful lamination is the *bonding process* of the layers. There are three basic components, which make up the bonding process. First is the surface preparation of the laminate, which improves the substrate's ability to accept and adhere to an adhesive. Surface preparation varies depending on material type. Composites use sanding

and grinding, surface texturing, or solvent cleaning. The second component is the adhesive itself, including epoxies, urethanes, phenolics, polyesters, solvents, acrylics and others. Each adhesive has its attributes depending on substrate type, in use requirements and process constraints. As a general rule, a maximum bond is achieved for a given substrate type when the material itself fails during an ultimate strength test. The maximum lap shear strength of an adhesive is achieved when the adhesive exhibits a cohesive failure in the bond line. The third component of lamination is the process by which the materials are bonded together. This involves a host of parameters primarily time, heat pressure, mixture, moisture and catalysts. It is important that the three basic components of bonding are properly employed to achieve a successful lamination.

-Compression molding

Compression molding is the most common method of molding thermoset materials such as SMC (sheet molding compound) and BMC (bulk molding compound). This molding technique involves compressing materials containing a temperature-activated catalyst in a heated matched metal die using a vertical press. The molding process begins with the delivery of high viscosity uncured composite material to the mold. Mold temperatures typically are in the range of 350° - 400° F. As the mold closes, composite viscosity is reduced under the heat and pressure approximating 6.9 MPa (1000 psi). The resin and the isotropically distributed reinforcements flow to fill the mold cavity. While the mold remains closed, the thermoset material undergoes a chemical change

(cure) that permanently hardens it into the shape of the mold cavity. Mold closure times vary from 30 seconds up to several minutes depending on part design and material formulation.

When the mold opens, parts are ready for finishing operations such as deflashing, painting, bonding, and installation of inserts for fasteners. By varying the formulation of the thermoset material and the reinforcements, parts can be molded to meet applications ranging from automotive class 'A' exterior body panels to structural members such as automobile bumper beams (see Figure I-4-4)

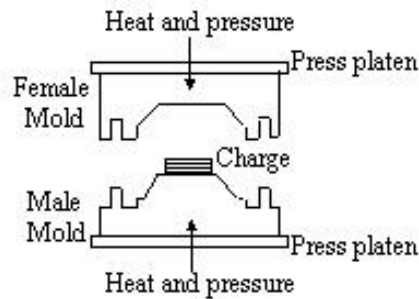


Figure I-4-4 - Compression molding

-Filament winding

The filament winding process is used in the fabrication of tubular composite parts. Typical examples are composite pipe, electrical conduit, and composite tanks. Fiberglass roving strands are impregnated with a liquid thermosetting resin and wrapped onto a rotating mandrel in a specific pattern. When the winding operation is completed, the resin is cured or polymerized and the composite part is removed from the mandrel. Capital investment is relatively higher compared to open mold

processes. The primary expense for an existing filament winder would be the cost of the winding mandrel for a specific application.

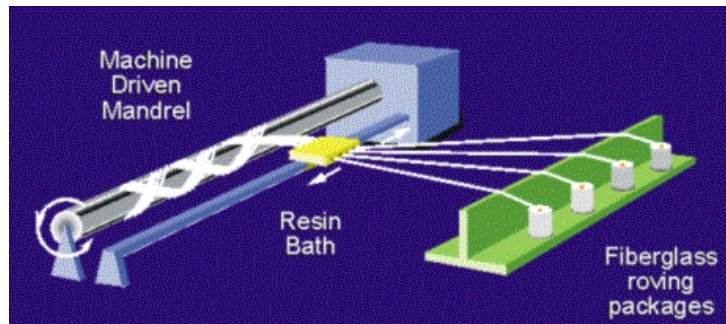


Figure I-4-5 - Filament winding process

-Braiding

Braiding is a manufacturing process by which different shapes can be formed. The basic concept of braiding method is to entail the interlocking of two or more yarns in order to form an integrated structure. Examples of two-dimensional braiding process are depicted in Figure I-4-6. A Japanese production forms also FRP rods by the braiding of fiber tows followed by epoxy resin impregnation and curing

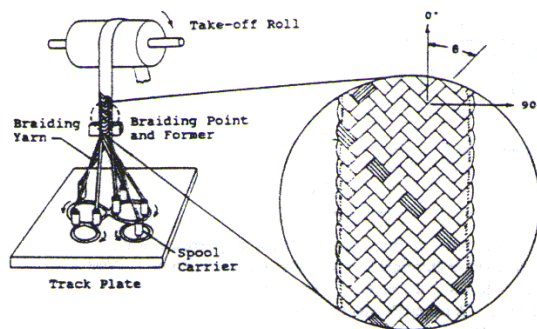


Figure I-4-6 - *Two-dimensional braiding process*

5. DURABILITY OF FRP COMPOSITES

The most significant technical obstacle preventing the extended use of FRP is a lack of data on long-term and durability performance comparable to those available for more traditional construction materials. Although there have been numerous studies on creep, stress corrosion,

fatigue, environmental fatigue, chemical and physical ageing and natural weathering of composites, most of these are not related to civil engineering application. Therefore the lack of durability data generate, at the moment, a big obstacle: the majority of civil engineers is not familiar with composites and is skeptical about using FRP to replace conventional materials in the structures.

It was already mentioned that corrosion problems of steel reinforcement and the good mechanical properties of FRP materials open a large field for the use of composites in construction, but the assessment of the durability is one of the most important issues.

The durability of a material can be defined as its ability to resist cracking, oxidation, chemical degradation, delamination, wear and the effects of foreign object damage over a specified period of time under specified environmental conditions.

Damage tolerance is defined as the ability of a material or structure to resist failure and continue performing at prescribed levels of performance in the presence of damage for a specified period of time under specified environmental conditions.

In most applications, the visible signs of deterioration appear gradually and can include one or more of the following: cracks of various kinds, surface pitting, blisters, swelling, delamination and occasionally softening.

The most significant durability issues are below described:

-Moisture (water) absorption

All resins adsorb moisture with the percentage of moisture absorption depending on the resin structure, degree of cure and water temperature. In general moisture effects over the short-term cause degradation in strength rather than stiffness levels in a composite.

Moisture absorption in FRP composite depends on type of resins, laminate composition, thickness, laminate quality, curing condition, fiber/resin interface and manufacturing process. In some applications, performance is improved with the use of corrosion barrier.

- Alkaline solutions

Alkaline solutions, such as the pore water of concrete, have a high PH and high concentration of alkali ions; this combination has no relevant effect on carbon reinforcement but may lead to degradation at the resin matrix and/or interface levels (strength and stiffness have been reported to each decrease between 0-20%).

Tensile strength reductions in GFRP bars ranging from zero to 75% of initial values have been reported in literature, while tensile stiffness reductions in GFRP bars range between zero and 20%.

Tensile strength and stiffness of AFRP rods in elevated temperature alkaline solutions either with and without tensile stress applied have been reported to decrease between 10-50% and 0-20% of initial values, respectively.

Resin damage via alkali is generally more severe than that due to moisture.

- Aggressive chemical solutions

FRP composites generally exhibit a variable performance when exposed to solution such as acids or corrosives; the resin type primarily influences this performance.

In the case of CFRP immersed in hydrochloric acid at the temperature of 80°C, the tensile strength reduced about 20% after 120 days.

The tensile of glass fiber reduced rapidly with time when immersed in any of the solution (NaOH, HCl, H₂O) at the temperature of 80°C; when immersed in sodium hydroxide, the strength reduction is tremendous: 96% within 9 hours at the same temperature.

For the AFRP (Technora fiber), after immersing for 90 days, strength reduced about 80% in hydrochloric acid and about 45% in sodium hydroxide solution.

However no particular sign of degradation were observed when the FRP were immersed in distilled water at temperatures of 20, 40 and 80°C (T.Uomoto and T.Nishimura,1999).

-Sub-zero and freeze-thaw exposure

Composites display excellent freeze-thaw resistance and are expected to withstand years of sub-zero conditions and hundreds of freeze-thaw cycles, with minimal loss of properties.

In general, freeze-thaw exposure does not affect fibers although it can affect the resin and the fiber/resin interface.

- Temperature and thermal cycling (above zero)

The primary effects of temperature are on viscoelastic response of the resin and hence of the composites; if the temperature exceeds the glass transition temperature (T_g), FRP composite performance can be expected to drop.

Thermal cycling in general does not cause deleterious effects, although extended cycles of brittle resin systems can result in microcrack formation.

- Creep and relaxation

FRP subjected to a constant load over time can suddenly fail after a time period called the endurance time; this phenomenon is known as creep rupture (or static fatigue).

Creep rupture is not an issue with steel bars in reinforced concrete except in extremely high temperatures such as those encountered in a fire.

The creep rupture endurance time can also irreversibly decrease under sufficiently adverse environmental conditions, such as high temperature, ultraviolet radiation exposure, high alkalinity, wet and dry cycles, or freezing-thawing cycles. In general, carbon fibers are the least susceptible to creep rupture, aramid fibers are moderately susceptible, and glass fibers are most susceptible to creep rupture.

Results indicated that a linear relationship exists between creep rupture strength and the logarithm of time for times up to nearly 100 hr. The ratios of stress level at creep rupture to the initial strength of the GFRP, AFRP, and CFRP bars after 500,000 hours (more than 50 years) were linearly extrapolated to be 0.29, 0.47, and 0.93, respectively.

Creep will not be a significant factor if the load to the structure are kept within manufacturer recommended stress levels.

For a typical civil infrastructure composite application, the creep-stress relaxation properties are dominated by the resin-dependent properties, rather than on the fiber or interfacial properties.

Traditionally glass-fiber reinforced composites have been designed to ensure that stress levels under sustained do not exceed 25-30% of ultimate to avoid premature failure due to stress rupture.

- Fatigue

FRP composites show significantly enhanced fatigue resistance over metallic materials. However, FRP composites structures are still susceptible to failure at joints and connections under fatigue loading and must be designed to reduce stress concentrations and geometrical discontinuities, which decrease overall fatigue resistance.

Fatigue failure in FRP composites is usually initiated through fiber/matrix debonding and matrix microcracking.

Although the data on fatigue in large structural application is limited, the data that is available indicates that fatigue failure is unlikely to occur at the lower stress levels used in design except at the joints and connection details.

Of all types of current FRP composites for infrastructure application, CFRP is generally thought to be the least prone to fatigue failure like E-glass and S-glass, but, for the last two types, environmental factors play an important role in the fatigue behavior due to their susceptibility to moisture, alkaline and acidic solutions.

Aramid fibers, for which substantial durability data are available, appear to behave similarly to carbon and glass fibers in fatigue.

- Ultraviolet (UV) radiation

In general, effects are rarely severe in terms of mechanical performance, although some resins can show significant embrittlement (are you sure about this term?) and surface erosion.

The most deleterious effect of UV exposure is probably not the UV-related damage, but the potential for increased penetration of moisture and other agents via the damaged region.

FRP composites can be protected from UV-related degradation through the use of appropriate additives in the resin and/or use of appropriate coatings.

- Fire and high thermal exposure

All polymeric systems degrade in the presence of extreme heat over extended periods. The primary effect in most fires is that of resin degradation and softening followed by charring of surface layers, which often causes the FRP composites to self-extinguish.

In critical applications, the FRP may be fireproofed with the use of special fire-resistant additives, intumescent coatings and the addition of inorganic fillers. The usual method to achieve the necessary structural fire rating is to use the FRP reinforcement as supplemental reinforcement: with this concept, the existing structure will not be able of total collapse without FRP reinforcement In FRP reinforced concrete the concrete itself acts as a thermal barrier reducing effects of thermal load.

6. FRP SOLUTIONS IN CONSTRUCTION

Currently, many FRP products are available to build or repair civil engineering structures. These include:

- New structural shapes applied to beams for bridge decks
- Bridge deck panels and pedestrian bridge systems
- FRP rebars and tendons for concrete reinforcement
- FRP composite systems for repair, strengthening, seismic retrofit for beams, columns and walls

As partially mentioned, reasons for the use of FRP in concrete structures are its:

- Corrosion resistance
- Low weight
- High tensile strength
- Low mechanical relaxation
- Good toughness
- High fatigue resistance
- Dimensional stability
- Stiffness
- Magnetic permeability
- Electrical conductivity
- Easy installation

A slight disadvantage of FRP today is its initial costs. The optimization of the manufacturing process and the development of new application methods could determine a wider use and then decrease such costs in the future. There are two main types of reinforcements:

- EXTERNAL
- INTERNAL

7. EXTERNALLY BONDED REINFORCEMENT

It is used for the strengthening of structures and for the seismic upgrade. The principles behind externally bonding of FRP plates or wraps to concrete and masonry structures are very similar to those used in the application of bonded steel plates (i.e., beton plaque). In general, the flexural, shear or axial strength, or blast resistance, is increased or better mobilized by the external application of high tensile strength material. Reasons for applying FRP systems as an external reinforcement for structures include:

- Capacity upgrade due to a change in use of a structure
- Passive confinement to improve seismic resistance
- Crack control
- Strengthening around new openings in slabs
- Correction of a design deficiency (flexural, shear or confinement)

The following are some of the most important products available in commerce:

- Laminates
 - Pre-cured elements
 - Hand lay-up systems
- Near Surface Mounted bars
- FRP Spray-up

-Laminates

Laminates are made by stacking a number of thin layers (laminate) of fibers and matrix and consolidating them into the desired thickness.

Fiber orientation in each layer, as well as the stacking sequence of the various layers, can be controlled to generate a range of physical and mechanical properties. Different systems of laminates exist, related to the constituent materials, the form and the technique of the FRP application. In general, these can be subdivided into “wet lay-up” (or “cured in-situ”) systems and “prefab” (or “pre-cured”) systems. The most common form of fiber-reinforced composites used in structural applications is called a “laminate”. Two types of FRP laminates (GFRP and CFRP) are shown in Figure I-7-1



Figure I-7-1- FRP Laminates

The main aspects of laminates are below described:

-Mechanical properties

Three basic component materials are commonly used for the installation process of the FRP sheets, namely: primer, putty and impregnating resin or saturant. The combination of the latter and the fibers form the FRP laminate.

The impregnating resin forms the matrix, which acts as a binder for the reinforcing fibers. The matrix has two functions: to enable the load to be

transferred among fibers and and to protect the fibers from environmental effects. Properties for primer, putty and saturant are shown in Table I-7-1.

Material	Tensile Strength, kPa , (psi)	Tensile Elastic Modulus, MPa (ksi)	Tensile Strain (%)	Compressive Strength kPa , (psi)	Compressive Modulus MPa , (ksi)
<i>Primer</i>	12400 (1800)	723.5 (105)	3	24100 (3500)	654.5 (95)
<i>Putty</i>	12400 (1800)	1791.4 (260)	1.5	24100 (3500)	1068.0 (155)
<i>Saturant</i>	54400 (7900)	3031.6 (440)	2.5	86100 (12500)	2618.2 (380)

Table I-7-1- Mechanical properties for primer, putty and saturant

The most common FRP sheets available and their properties are reported in Table I-7-2

Designation	Fabric Architecture	Nominal Thickness mm per ply (in. per ply)	Ultimate tensile Strength Mpa (ksi)	Tensile Modulus of elasticity GPa (Ksi)	Rupture strain
CF 130 (High Strength Carbon Fiber Fabric)	9 oz. Unidirectional	0.165 (0.0065)	3800 (550)	227 (33,000)	1.67%
CF 530 (High Modulus Carbon Fiber Fabric)	9 oz. Unidirectional	0.165 (0.0065)	3500 (510)	373 (54,000)	0.94%
AK 60 (Aramid Fiber fabric)	18 oz. Unidirectional	.279 (00.0110)	2000 (290)	120 (17,400)	1.67%
EG 900 (E-Glass Fiber fabric)	27 oz. Unidirectional	0.353 (0.0139)	1520 (220)	724 (10,500)	2.10%

Table I-7-2- Mechanical properties for carbon fibers

-Tensile and Compressive Behaviour

When loaded in tension, FRP materials do not exhibit any plastic behavior (yielding) before rupture. The tensile behavior of FRP materials consisting of one type of fiber material is characterized by a linearly elastic stress-strain relationship until failure.

The tensile strength and stiffness of an FRP material is dependent on several factors. Because the fibers in an FRP material are the main load-carrying constituent, the type, , the orientation and the quantity of fibers primarily govern the tensile properties of the FRP material. Due to the primary role of the fibers and methods of application, the properties of an FRP repair system are sometimes reported based on the net-fiber area. In other instances, the reported properties are based on the gross-laminate area.

The gross-laminate area of an FRP system is calculated using the total cross-sectional area of the cured FRP system, including all fibers and resin. Gross-laminate area is typically used for reporting precured laminate properties where the cured thickness is constant and the relative proportion of fiber and resin is controlled.

The net-fiber area of an FRP system is calculated using the known area of fiber, neglecting the total width and thickness of the cured system; thus, resin is excluded. Net-fiber area is typically used for reporting properties of wet lay-up systems that use manufactured fiber sheets and

field-installed resins. The wet lay-up installation process leads to a controlled fiber content and a variable resin content.

System properties reported using the gross-laminate area have higher relative thickness dimensions and lower relative strength and modulus values; while system properties reported using the net-fiber area have lower relative thickness dimensions and higher relative strength and modulus values. Regardless of the basis for the reported values, the load-carrying capacity ($f_{fu}A_f$) and stiffness (A_fE_f) remain constant. Properties reported based on the net-fiber area are not the properties of the bare fibers. The properties of an FRP system should be characterized as a composite, recognizing not just the material properties of the individual fibers but also the efficiency of the fiber-resin system and fabric architecture. The mechanical properties of all FRP systems, regardless of form, should be based on the testing of laminate samples with a known fiber content.

Tests on FRP laminates used for repair on concrete have shown that the compressive strength is lower than the tensile strength (Wu 1990). The mode of failure of FRP subjected to longitudinal compression can include transverse tensile failure, fiber microbuckling, or shear failure. The mode of failure depends on the type of fiber, the fiber volume fraction, and the type of resin. In general, compressive strengths are higher for materials with higher tensile strengths, except in the case of AFRP where the fibers exhibit non-linear behavior in compression at a relatively low level of stress.

The modulus of elasticity is usually smaller than the tensile modulus of elasticity of FRP materials as well. Test reports on samples containing 55

to 60% volume fraction of continuous E-glass fibers in a matrix of vinyl ester or isophthalic polyester resin have reported a compressive modulus of elasticity of 34000 to 48000 MPa (5000 to 7000 kip/in.²) (Wu 1990). According to reports, the compressive modulus of elasticity is approximately 80% for GFRP, 85% for CFRP, and 100% for AFRP of the tensile modulus of elasticity for the same product (Ehsani 1993).

- Time-dependent behaviour

FRP materials subjected to a constant load over time can suddenly fail after a time period referred to as the endurance time. This failure is known as creep-rupture and is similar to fatigue in metals except that the stresses are sustained instead of cycled. As the ratio of the sustained tensile stress to the short-term strength of the FRP laminate increases, endurance time decreases.

The endurance time also decreases under adverse environmental conditions, such as high temperature, ultraviolet-radiation exposure, high alkalinity, wet and dry cycles, or freezing-thawing cycles. In general, carbon fibers are the least susceptible to creep-rupture; aramid fibers are moderately susceptible, and glass fibers are most susceptible. Creep rupture tests have been conducted on 0.25 in.(63.5 mm) diameter FRP bars reinforced with glass, aramid, and carbon fibers. The bars were tested at different load levels at room temperature. Results indicated that a linear relationship exists between creep-rupture strength and the logarithm of time for all load levels. The ratios of stress level at creep-rupture after 500000 hours (about 50 years) to the initial ultimate strength

of the GFRP, AFRP and CFRP bars were extrapolated to be 0.3, 0.47, and 0.91, respectively (*Yamaguchi et al.* 1997). Similar values have been determined elsewhere (*Malvar* 1998).

-Installation techniques: Manual Lay-Up

The *Manual Lay-Up* technique for the installation of FRP laminates is described.

FRP laminates are formed by manual lay-up onto the surface of the member being strengthened.

Prior to installing the composite strengthening system the concrete substrate must be prepared to accept the system. The integrity of system depends on the quality and strength of the concrete as well as the bond between the FRP and the concrete. Cracks, spalls and corroding reinforcing steel need to be addressed prior to installing the strengthening. Spalls and other types of damage should be removed and patched with suitable repair mortars. All cracks greater than 0.01 inch (0.25 mm.) in width and subject to movement (thermal, vibration, etc.) should be epoxy injected, corroding reinforcing steel should be cleaned (or replaced). FRP system, like conventional strengthening techniques are not intended to resist or arrest the enormous and incalculable expansive forces generated by continuing corrosion of the reinforcing steel. The surface of concrete should be free of loose and unsound materials. All laitance, dust, dirt, oil, curing compound, should be removed. Mechanical abrasion techniques (e. g. abrasive blasting,

grinding, water blasting or other approved methods should be used to open the pore structure of the concrete prior to applying the primer.

Once restored the damaged area, the sequential procedure is as follows:

1)Application of primer: a layer of epoxy-based primer is applied to the prepared concrete surface using a short or medium nap roller to penetrate the concrete pores and to provide an improved substrate for the saturant.



(1)Application of primer

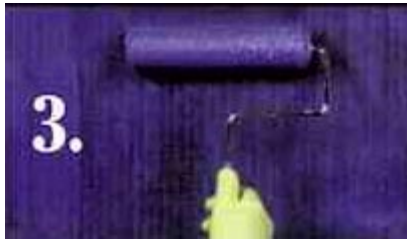
2)Application of putty: the putty is applied to the primed surface using a trowel. The putty should be used to fill any surface defects; complete coverage is not necessary. The putty may be applied to a freshly primed surface without waiting for the primer to cure.



(2)Application of putty

3)Application of first layer of saturant: the saturant is applied to the primed and puttied surface with a medium nap roller. The saturant is blue in color and should be applied to a thickness of 15 to 20 mils. The volume of saturant used depends on the FRP sheet used. The functions of

the saturant are: to impregnate the dry fibers, to maintain the fibers in their intended orientation, to distribute stress to the fibers, and to protect the fibers from abrasion and environmental effects.



(3) Application of first layer of saturant

4) Application of fiber sheet: the fiber sheets should be measured and pre-cut prior to installing on the surface. The sheet is placed on the concrete surface and gently pressed into the saturant. Prior to removing the backing paper, a squeegee or trowel may be used to remove any air bubbles. After the backing paper is removed a ribbed roller is rolled in the direction of the fibers to facilitate impregnation by separating the fibers. The ribbed roller should never be used in a direction transverse to the fibers since fibers could be damaged.

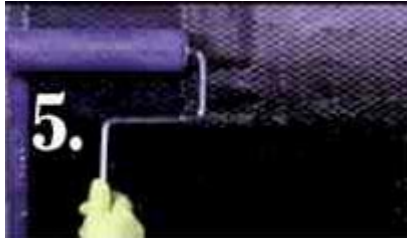
Streaks of blue colored saturant should be visible on the fiber sheet after rolling.



(4) Application of fiber sheet.

5) Application of second layer of saturant: a second is applied 30 minutes after placing and rolling the fiber sheet. This period of time allows the first coat of saturant to be completely adsorbed by the sheet.

The second coat of saturant is applied to the FRP sheet with a medium nap roller to a thickness of 15 to 20 mils.



(5) Application of second coat saturant

At this time if required, additional fiber plies may be installed by re-saturating the surface 30 minutes after the second saturant coat is applied and repeating steps 3, 4 and 5. This process should be repeated for as many plies as are necessary. After completion of this step, the fiber sheet layers are encapsulated in laminate form.

6) Application of optional topcoat: where required, the high solids, high gloss, corrosion-resistant topcoat provides a protective/aesthetic outer layer.



(6) Application optional topcoat.

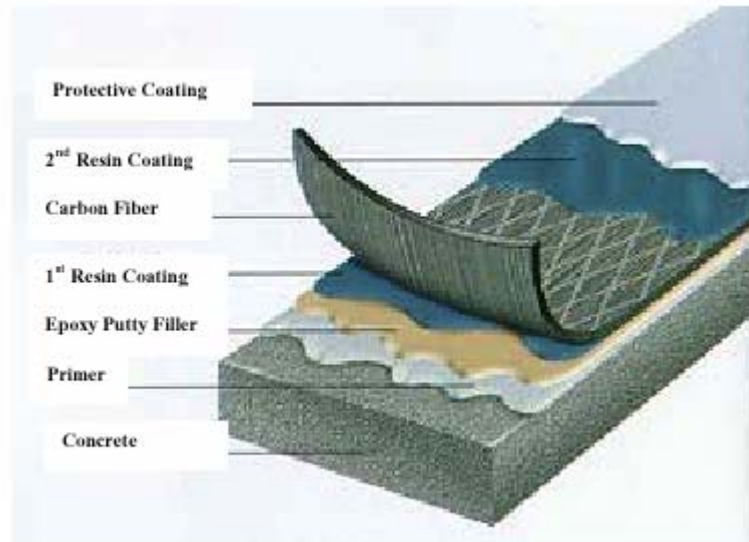


Figure I-7-2 - Installation step by step

-Pre-Cured Systems

They consist of a wide variety of composite shapes manufactured in the system supplier's facility and shipped to the job site. They are typically in the form of thin ribbon strips or grids that may be delivered in a roiled coil. Normally strips are pultruded. Typically, an adhesive (e.g. epoxy) is used to bond the precured shapes to the concrete surface.

-Hand Lay-UP systems

The most interesting types related to this technique are the following:

- Dry unidirectional fiber sheet and semi-unidirectional fabric, where fibers run predominantly in one direction partially or fully covering the structural element, and dry multidirectional fabric,

where fibers run in at least two directions. Installation on the concrete surface requires saturating resin usually after a primer has been applied. Two different processes can be used to apply the fabric:

- The fabric can be applied directly into the resin usually after a primer has been applied uniformly onto the concrete surface
- The fabric can be impregnated with the resin in a saturator machine and then applied wet to the sealed substrate
- Resin pre-impregnated uncured unidirectional or multidirectional sheet or fabric, where fibres run predominantly in one direction. Installation may be done with or without additional resin
- Dry fibre tows (untwisted bundles of continuous fibres) that are wound or otherwise mechanically placed onto the concrete surface. Resin is applied to the fibre during winding

Pre impregnated fibre tows that are wound or otherwise mechanically placed onto the concrete surface. Product installation may be executed with or without additional resin.

-Near Surface Mounted Bars

This FRP-based strengthening technique is a valid alternative to externally bonded FRP laminates. Although the use of FRP rods for this application is very recent, Near Surface Mounted (NSM) steel rods have been used in Europe for strengthening of RC structures since the early 50's.

Nowadays, FRP rods (GFRP and CFRP) are used in place of steel and epoxy paste replaces cementitious mortar. The advantage is primarily the resistance of FRP to corrosion. This property is particularly important in this case due to the position of the rods very close to the surface, which exposes them to the environmental attacks (De Lorenzis, L., Nanni, A. – 1999).

The use of NSM FRP rods is an attractive method for increasing the flexural and the shear strength of deficient RC members and masonry walls and, in certain cases, can be more convenient than using FRP laminates. Furthermore, this technique becomes particularly attractive for strengthening in the negative moment regions of slabs and decks, where external reinforcement would be subjected to mechanical and environmental damage and would require protective cover which could interfere with the presence of floor finishes. Examples for the application of NSM bars are shown in Figure I-7-33.



Figure I-7-3 -*Near Surface Mounted Bars*

8. INTERNAL REINFORCEMENT

Members internally reinforced with composite rebars need a thinner concrete cover; such reinforcement can be also used for structures in high chloride environments. Due to its non-magnetic properties, FRP is used as reinforcement in hospitals and in free-access floors, as well as in sensitive structures such as scientific laboratories and observatories. Relating to one/two/three-dimensional features of the composite, there are three different typologies of products:

- Rebars
- Grids
- Cages
- Prestressing Tendons

-Rebars

They are fabricated in the Pultrusion process. Hereby, the fibers are pulled through a resin bath, the forming guide and cured in the heated die. The most important issue to be addressed is the bond between the rebars and the concrete. Bars fabricated in the pultrusion process have a smooth surface. Nowadays two different surface treatments are used to give rebars the necessary grip.

One is to wrap the rebar with an additional resin impregnated fiber strand while the resin of the bar is still uncured to obtain a profile. Furthermore, a sand coating is applied. The other possibility is to stamp ribs on the

rebar. Rebars with an untreated surface require special anchoring devices. They are mainly used in prestressing applications.

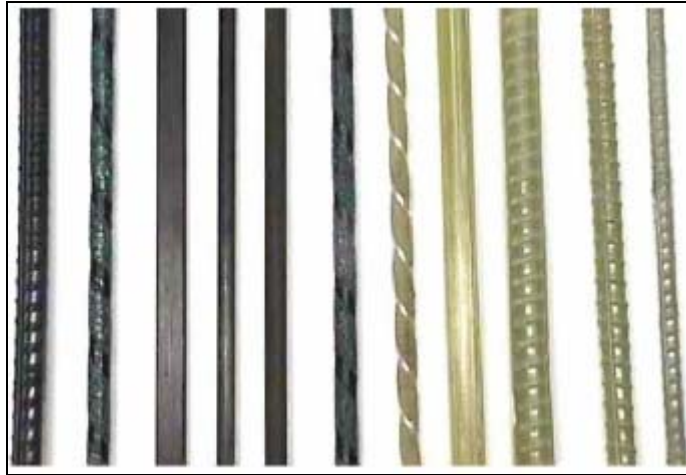


Figure I-8-1 - Rebars with different surfaces

The mains aspects of rebars are below described:

-Mechanical properties

FRP rods used in civil engineering are unidirectional composites. The direction parallel to the fibers is called the longitudinal direction, in which the mechanical properties are controlled by the fibers strength. The transversal direction, perpendicular to the fibers, presents lower mechanical properties, controlled by resin and fiber/matrix interface properties. It means that the mechanical properties depend on the nature and content of fibers in the longitudinal direction.

It is commonly assumed that the use of FRP rods in concrete structures is concerned with the longitudinal properties of these materials, but in durability studies, like those performed recently at University of

Missouri-Rolla (*Micelli* 2001), resin properties are significant too, because of the load is transferred to the fibers by means of the matrix, and because the resin constitute a chemical and physical protection to the fibers. Therefore, the damage and cracking of the resin do not allow the desired stress distribution, and open a preferential way for degradation of fibers. This reflects to longitudinal properties in ultimate strength and stiffness lower than assumed for design purposes.

GFRP rebars of fiberglass rebars are manufactured from E-glass fibers encapsulated in a vinyl ester resin matrix. (why you detail only on GFRP. Either you add something on CFRP, or cut this)

It features a deformed and sand-coated surface to facilitate bond with the concrete, mortar or epoxy-based paste. Deformations are slight undulations that take best advantage of the glass fiber structural element, constituting a minimum of 70% volume by weight of the end product.

-Tensile and compressive behaviour

When loaded in tension, FRP bars do not exhibit any plastic behavior (yielding) before rupture. The tensile behavior of FRP bars consisting of one type of fiber material is characterized by a linearly elastic stress-strain relationship until failure.

The tensile strength and stiffness of an FRP bar are dependent on several factors.

Because the fibers in an FRP bar are the main load-carrying constituent, the ratio of the volume of fiber to the overall volume of the FRP (fiber-volume fraction) significantly affects the tensile properties of an FRP bar.

Strength and stiffness variations will occur in bars with various fiber-volume fractions, even in bars with the same diameter, appearance, and constituents. The rate of curing, the manufacturing process, and the manufacturing quality control also affect the mechanical characteristics of the bar.

The tensile properties of a particular FRP bar should be obtained from the bar manufacturer. Usually, a normal (Gaussian) distribution is assumed to represent the strength of a population of bar specimens.

An FRP bar cannot be bent once it has been manufactured (an exception to this would be an FRP bar with a thermoplastic resin that could be reshaped with the addition of heat and pressure). FRP bars can be fabricated with bends. In FRP bars produced with bends, a strength reduction of 40 to 50% compared to the tensile strength of a straight bar can occur in the bend portion due to fiber bending and stress concentration (*Nanni et al.* 1998).

Tests on FRP bars with a length to diameter ratio from 1:1 to 2:1 have shown that the compressive strength is lower than the tensile strength (*Wu* 1990). The mode of failure for FRP bars subjected to longitudinal compression can include transverse tensile failure, fiber microbuckling, or shear failure. The mode of failure depends on the type of fiber, the fiber-volume fraction, and the type of resin. Compressive strengths of 55%, 78% and 20% of the tensile strength have been reported for GFRP, CFRP and AFRP respectively (*Mallick* 1998 and *Wo* 1990). In general, compressive strengths are higher for bars with higher tensile strengths, except in the case of AFRP where the fibers exhibit nonlinear behavior in compression at a relatively low level of stress.

The compressive modulus of elasticity of FRP reinforcing bars appears to be smaller than its tensile modulus of elasticity. Standard test methods are not yet established to characterize the compressive behavior of FRP bars. If the compressive properties of a particular FRP bar are needed, these should be obtained from the bar manufacturer.

-Bond behaviour

Bond performance of an FRP bar is dependent on the design, manufacturing process, mechanical properties of the bar itself, and the environmental conditions (*Al-Dulaijan et al. 1996, Nanni et al. 1997, Bakis et al. 1998, Bank et al. 1998, Freimanis et al. 1998*). When anchoring a reinforcing bar in concrete, the bond force can be transferred by:

- adhesion resistance of the interface, also known as chemical bond;
- Frictional resistance of the interface against slip;
- Mechanical interlock due to irregularity of the interface

In FRP bars, it is postulated that bond force is transferred through the resin to the reinforcement fibers, and a bond-shear failure in the resin is also possible. When a bonded deformed bar is subjected to increasing tension, the adhesion between the bar and the surrounding concrete breaks down and deformations on the surface of the bar cause inclined contact forces between the bar and the surrounding concrete. The stress at the surface of the bar resulting from the force component in the direction of the bar can be considered the bond stress between the bar and

the concrete. Unlike reinforcing steel, the bond of FRP rebars appears not to be significantly influenced by the concrete compressive strength provided adequate concrete cover exists to prevent longitudinal splitting. (Nanni *et al.* 1995, Benmokrane *et al.* 1996, Kachlakev and Lundy 1998). The bond properties of FRP bars have been extensively investigated by numerous researchers through different types of tests, such as, pullout tests, splice tests, and cantilever beams, to determine an empirical equation for embedment length (Faza and GangaRao 1990, Ehsani *et al.* 1996, Benmokrane 1997).

-Time-dependent behaviour

Creep rupture is not an issue with steel bars in reinforced concrete except in extremely high temperatures such as those encountered in a fire. An investigation of creep rupture in GFRP bars in room temperature laboratory conditions was reported by Seki *et al.* in 1997. The molded E-glass/vinyl ester bars had a small (4.4 mm^2 , 0.0068 in^2) rectangular cross-section and integral GFRP tabs. The percentage of initial tensile strength retained followed a linear relationship with logarithmic time, reaching a value of 55% at an extrapolated 50-yr endurance time.

Creep rupture data characteristics of a 12.5-mm. diameter (0.5 in.) commercial CFRP twisted strand in an indoor environment is available from the manufacturer (Tokyo Rope 2000). The rupture strength at a projected 100 yr endurance time is reported to be 85% of the initial strength. An extensive investigation of creep deformation (not rupture) in one commercial AFRP and two commercial CFP bars tested to 3000 hr

has been reported (*Saadatmanesh and Tannous 1999*). The bars were tested in laboratory air and in room-temperature solutions with pH equal to 3 and 12. The bars had diameters between 8-10 mm (0.313-0.375 in.) and the applied stress was fixed at 40% of initial strength. The results indicated a slight trend towards higher creep strain in the larger diameter bars and in the bars immersed in the acidic solution. Bars tested in air had the lowest creep strains of the three environments. Considering all environments and materials, the range of strains recorded after 3000 hr was 0.002%-0.037%. Creep strains were slightly higher in the AFRP bar than in the CFRP bars.

-Durability

FRP bars are susceptible to varying amounts of strength and stiffness changes in the presence of environments prior to, during, and after construction.

These environments can include water, ultraviolet exposure, elevated temperature, alkaline or acidic solutions, and saline solutions. Strength and stiffness may increase, decrease, or remain the same, depending on the particular material and exposure conditions. Tensile and bond properties of FRP bars are the primary parameters of interest for reinforced concrete construction.

The environmental condition that has attracted the most interest by investigators concerned with FRP bars is the highly alkaline pore water found in outdoor concrete structures (*Gerritse 1992, Takewaka and Khin 1996, Rostasy 1997, Yamaguchi et al. 1997*).

Aqueous solutions with high values of pH are known to degrade the tensile strength and stiffness of GFRP bars (*Porter and Barnes 1998*), although particular results vary tremendously according to differences in test methods. Higher temperatures and longer exposure times exasperate the problem. Most data have been generated using temperatures as low as slightly sub-freezing and as high as a few degrees below the T_g of the resin. The degree to which the resin protects the glass fibers from the diffusion of deleterious hydroxyl (OH⁻) ions figures prominently in the alkali resistance of GFRP bars (*Bank and Puterman 1997, Coomarasamy and Saadatmanesh 1999, Uomoto 2000*). Most researchers are of the opinion that vinyl ester resins have superior resistance to moisture ingress in comparison with other commodity resins. The type of glass fiber also appears to be an important factor in the alkali resistance of GFRP bars (*Devalapura et al. 1996*). Tensile strength reductions in GFRP bars ranging from zero to 75% of initial values have been reported in the cited literature. Tensile stiffness reductions in GFRP bars range between zero and 20% in many cases. Tensile strength and stiffness of AFRP rods in elevated temperature alkaline solutions either with and without tensile stress applied have been reported to decrease between 10-50% and 0-20% of initial values, respectively (*Takewaka and Khin 1996, Rostasy 1997, Sen et al. 1998*). In the case of CFRP, strength and stiffness have been reported to each decrease between 0-20% (*Takewaka and Khin 1996*).

Some results from combined ultraviolet and moisture exposure tests with and without applied stress applied to the bars have shown tensile strength reductions of 0-20% of initial values in CFRP , 0-30% in AFRP and 0-

40% in GFRP (*Sasaki et al. 1997, Uomoto 2000*). An extensive study of GFRP, AFRP and CFRP bars kept outdoors in a rack by the ocean showed no significant change of tensile strength or modulus of any of the bars (*Tomosowa and Nakatsuji 1996,1997*).

Adding various types of salts to the solutions in which FRP bars are immersed has been shown to not necessarily make a significant difference in the strength and stiffness of many FRP bars, in comparison to the same solution without salt (*Rahman et al. 1996*). Most studies do not separate the effects of water and salt added to water, however. One study found a 0-20% reduction of initial tensile strength in GFRP bars subjected to a saline solution at room-temperature and cyclic freeze/thaw temperatures (*Vijay and GangaRao 1999*) and another has found a 15% reduction in the strength of AFRP bars in a marine environment (*Sen et al. 1998*).

Studies of the durability of bond between FRP and concrete have been mostly concerned with the moist, alkaline environment found in concrete. Bond of FRP reinforcement relies upon the transfer of shear and transverse forces at the interface between bar and concrete and between individual fibers within the bar. These resin-dominated mechanisms are in contrast to the fiber-dominated mechanisms that control properties such as longitudinal strength and stiffness of FRP bars. Environments that degrade the polymer resin or fiber/resin interface are thus also likely to degrade the bond strength of an FRP bar. Numerous bond test methods have been proposed for FRP bars, although the direct pullout test remains rather popular due to its simplicity and low cost (*Nanni et al. 1995*). Pullout specimens with CFRP and GFRP bars have been subjected to

natural environmental exposures and have not indicated significant decreases in bond strength over periods of time between one and two years (*Clarke and Sheard 1998, Sen et al. 1998*). Positive and negative trends in pullout strength with respect to shorter periods of time have been obtained with GFRP bars subjected to wet elevated-temperature environments in concrete, with or without artificially added alkalinity (*Al-Dulaijan et al. 1996, Bakis et al. 1998, Bank et al. 1998, Porter and Barnes 1998*). Longitudinal cracking in the concrete cover can seriously degrade the apparent bond capability of FRP bars and sufficient measures must be taken to prevent such cracking in laboratory tests and field applications (*Sen et al. 1998*). The ability of chemical agents to pass through the concrete to the FRP bar is another important factor thought to affect bond strength (*Porter and Barnes 1998*).

-Grids

FRP composites are nowadays widely used to form 2-D reinforcing systems such as panels, grids or gratings. The method of production is a batch process. A series of continuous fibers is dispensed from individual creels by a mechanical system through a wet-bath to be deposited by two orthogonal traveling (winding) heads in a grid pattern. The heads move at synchronized speeds that define the size of the grid. Successive movement of the heads results in fiber cross-over and the placement of interlocking layers until the desired content/cross-sectional area is achieved. 2-D FRP reinforcing systems are available in various surfaces patterns, thickness and colors (see Figure I-8-2)



Figure I-8-2 - FRP grids

Grids are used in tunnels, runways and aprons for airstrips/tarmacs, roads, buildings, channels, rehabilitation, and for general architectural elements. They are often used as lightweight reinforcement in building fascia and curtain walls, where the lower requirements for cover applications result in thinner and lighter panels. Grids can be used in the construction of floating foundation slabs, columns and column bases, walls and floors. Due to their excellent corrosion resistance, 2-D grids, especially carbon fiber reinforced, have been used extensively in marine structures and reinforcements in systems for slope protections and stability. Some applications can be seen in Figure I-8-3.



Figure I-8-3- Applications of FRP grids

-Cages

They are ideal to reinforce complex concrete structures. Through the prefabrication, the installation time on the construction site is considerably decreased. Cages are made as a combination of pultrusion and filament winding: first the 2-D trusses are fabricated then these are combined into a 3-D cage by filament winding. Further complex shapes can be assembled by combining these elements. Fiber material, number of filaments and distance between rovings can be varied easily. Figure I-8-2 shows an example for a GFRP cage.



Figure I-8-2- *GFRP cage*

-Prestressing Tendons

The interest in the use of FRP composites in prestressed concrete is mainly based on durability issues. Corrosion of prestressing steel tendons caused serious deterioration of infrastructure. Properties like high tensile strength and high resistance to corrosion would appear to make FRP composites good candidates for prestressing tendons. A problem is that FRP materials are very time dependent. Under constant load they show varying degrees of creep deformation:

- CFRP does not creep
- GFRP shows a negligible creep
- AFRP is showing long-term deformations due to creep.

Furthermore, GFRP tendons exhibit premature tensile rupture under sustained loading. Carrying permanent tension, the tensile strength of GFRP drops to values as low as 20% what causes stress rupture. Because of these reasons CFRP seems to be the most suitable FRP for prestressing applications. Another problem, which needs to be addressed, is the anchorage of the tendons. Special devices are necessary due to the low transverse strength of the tendons. Examples for on the market available anchorage systems are shown in Figure I-8-5. An advantage is that FRP reinforcement has high tensile strength with moderate modulus of elasticity less sensitive to fluage of concrete



Figure I-8-3- *Anchorage systems for prestressing tendons*

9. CONCLUSIVE REMARKS

The main properties of FRP composites can be summarized as follows:

- **High Strength-** composites can be designed to provide a wide range of mechanical properties including tensile, flexural, impact and compressive strengths. And, unlike traditional materials, composites can have their strength oriented to meet specific design requirements of an application.
- **Light Weight/Parts Consolidation** FRP composites deliver more strength per unit of weight than most metals. In fact, FRP composites are generally 1/5th the weight of steel. The composite can also be shaped into one complex part, often times replacing assemblies of several parts and fasteners. The combination of these two benefits makes FRP composites a powerful material system, structures can be partially or completely pre-fabricated, delivered on-site and installed.
- **Creep (Permanent Deflection Under Long Term Loading) -** The addition of the reinforcement to the polymer matrix increases the creep resistance of the properly designed FRP part.
- **Resistance to Environmental Factors -** Composites display excellent resistance to the corrosive effects of:
 - **Freeze-thaw:** because composites are not attacked by galvanic corrosion and have low water absorption, they resist the destructive expansion of freezing water

- **Weathering and Ultra-Violet Light:** FRP composite structures designed for weather exposure are normally fabricated with a surface layer containing a pigmented gel coat or have an ultraviolet (UV) inhibitor included as an additive to the composite matrix.
- **Chemicals and Temperature:** Composites do not rust or corrode and can be formulated to provide long-term resistance to nearly every chemical and temperature environment. Of particular benefit, is composites ability to successfully withstand the normally destructive effects of de-icing salts and/or saltwater spray of the ocean
- **Fire Performance of FRP Composites** - FRP composites can burn under certain conditions. Composites can be designed to meet the most stringent fire regulations by the use of special resins and additives. (add a note on how the ACI documents address this issue)

In any case it is necessary to note that there are significant gaps in durability data that need to be addressed. However, there is an important collection of studies to suggest that if the appropriate materials-process-design aspects are considered, FRP composite components can provide almost maintenance-free service in very harsh environments over extended periods of time.

It is also acknowledged that environments, which are typical in civil infrastructure, can cause significant degradation in FRP composites, and that there is in reality a lack of validated data and a comprehensive knowledge of lifetime durability related to some materials systems likely to be used in civil infrastru

CHAPTER II

STRENGTHENING OF IMPACT-DAMAGED BRIDGE GIRDER USING FRP LAMINATES

1. INTRODUCTION

Strengthening of reinforced and prestressed concrete (RC and PC) structures using externally bonded composite laminates has proven to be an effective method for increasing or restoring structural capacity. In the case of highway structures, this repair option provides an effective and fast alternative to conventional repair methods.

Bridges throughout the U.S.A. are falling into a state of disrepair caused by deterioration, vehicular impact, poor maintenance and pollution. It is estimated that out of half million existing bridges, nearly 105,000 are rated critically deficient. Since the nation's economy depends on an adequate transportation system, upkeep of structures is of primary importance. When a bridge is designed, it calls for a serviceable life span of at least 50 years. However, the majority of these bridges shows some

kind of deficiency within a few years of their construction. The strengthening or retrofitting of existing concrete structures to resist higher design loads, correct deterioration-related damage, or increase ductility has traditionally been accomplished using conventional materials and construction techniques. Externally bonded steel plates, steel or concrete jackets, and external post-tensioning are some of the most traditional available techniques.

These strengthening and repair methods are expensive and time consuming and the results are most often disappointing.

When a bridge girder is significantly damaged due to impact the repair alternative is to replace the damaged girders. The full replacement of damaged bridge elements, although it could be effective, is typically an expensive solution. Also, this method requires the closure of at least one traffic lane as well as the road under the bridge during the girder replacement. FRP have emerged as an alternative to traditional materials and techniques.

The feasibility of using advanced composite material for bridge rehabilitation has been assessed from a National Cooperative Highway Research Program (NCHRP) with two publications (Shanafelt and Horn 1980 and 1985) addressing this topic. Researchers at Iowa State University have recently published a comprehensive report (Klaiber et al. 1999). This study includes an extensive annotated bibliography as well as from field and laboratory experiments. With respect to US experience, in addition to Iowa, Departments of Transportation Georgia (Aboutaha et al. 1997), Minnesota (Olson et al. 1992), and Texas (Zobel et al. 1997) have supported work in this area. Under the repetitive nature of highway

loading, repair methods such as internal strand splices and external post-tensioning were found to be only partially satisfactory because they could not restore the ultimate strength to the damaged member(Olson et al. 1992 Zobel and Jirsa 1998).

At this time some bridges have been retrofitted to examine the feasibility of accepting such repair method. A project involving the strengthening of a damaged bridge girder has been conducted on the impacted bridge of highway Appia, near Rome (Nanni 1997).(see Figure II-1-1)

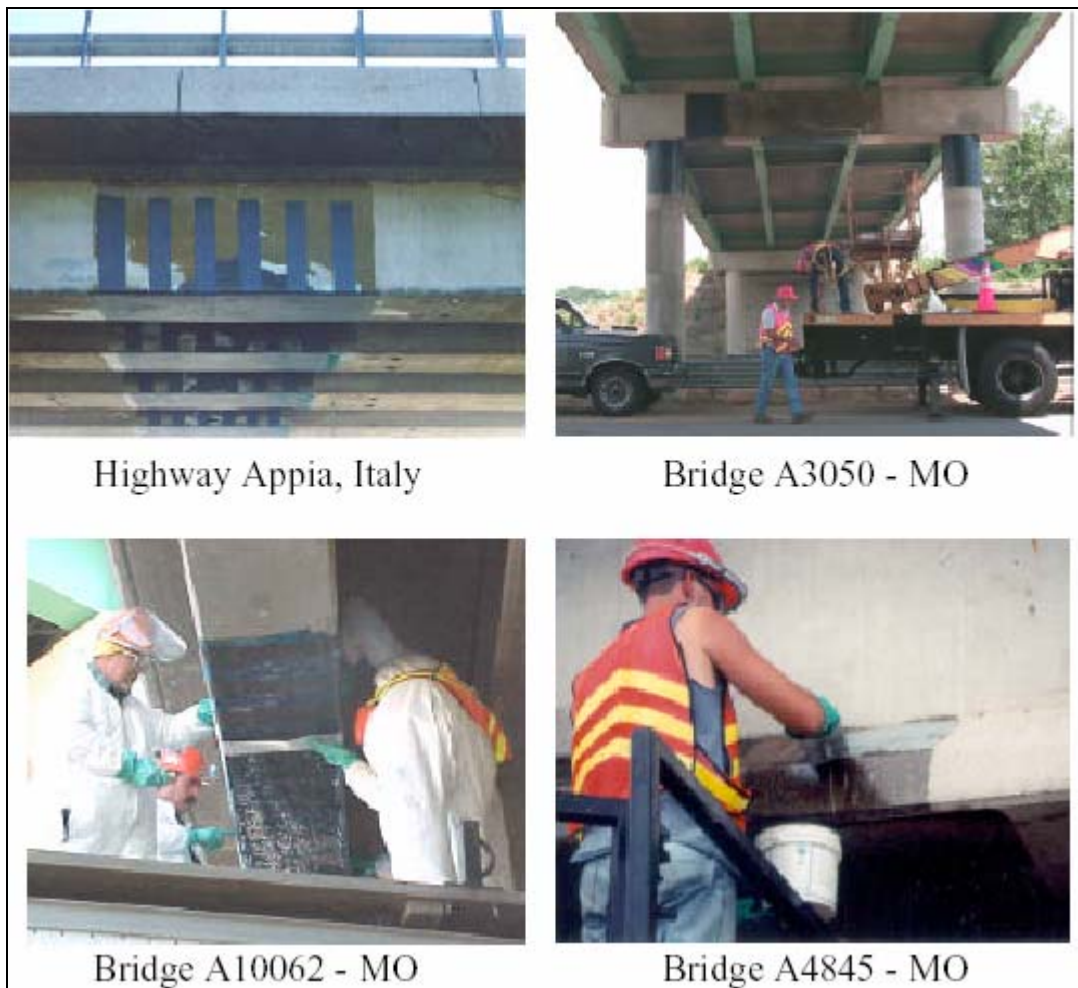


Figure II-1-1- Accidental Damage Repair Using FRP Technology

Advanced composites technology has already been explored and used for three more bridges under MoDOT sponsorship

2. A CASE OF STUDY

The A5657 Bridge, on Route 28 over the Gasconade River, South of Dixon, Missouri, U.S.A., 291.2m (955.2 ft) long consists of 8 spans, each 36.4 m. (119.4 ft) long, as Figure II-2-2 and Figure II-2-2 depicts. Construction works were completed on July 2002. The bridge is owned by the Missouri Department of Transportation (MoDot).



Figure II-2-1- *Bridge A5657 side view*



Figure II-2-2– Bridge A5657

The central of the five PC girders of the North span that compose the bridge was accidentally damaged during the construction by the contractor; removal of lost concrete showed that two prestressing tendons were fractured due to the impact (see Figure II-2-3). This resulted in approximately 5% reduction in flexural capacity.



Figure II-2-3– Damaged Area in the girder

Such fact induced the owner to replace the girder; the contractor proposed to strengthen the damaged girder in order to restore its original capacity. After negotiation, both parts agreed to the following: MODOT would subtract from the payments owed to the contractor five times the cost of the strengthening to cover possible future replacements.

In order to find the best upgrade technique, the University of Missouri-Rolla was consulted. CFRP laminates were proposed for installation by manual lay up to restore the original ultimate capacity of the impacted girder. The choice took into account that, due to the repetitive nature of highway loading, repair methods such as internal strand splices and external post-tensioning were found to be questionable because they could not restore the ultimate strength of the damaged member.

The A5657 Bridge case underlined the need for the scientific validation of the FRP technique for the strengthening of PC structures. By confirming its effectiveness, it could be possible to show the reliability of such technique and then help preventing similar cases in the future. An experimental campaign was developed to that aim and it is discussed in Chapter III.

3. MATERIAL PROPERTIES

-PC Girder and deck

The damaged girder is prestressed by 38 low-relaxation steel strands with a tensile strength of 1862 MPa (270 ksi). It is assumed that a portion of the bridge deck with dimension of $20 \times 270 \text{ cm}$ ($8 \times 106 \text{ in.}$) provides composite action with the girder.

The cross section of the damaged girder is shown in Figure II-3-1.

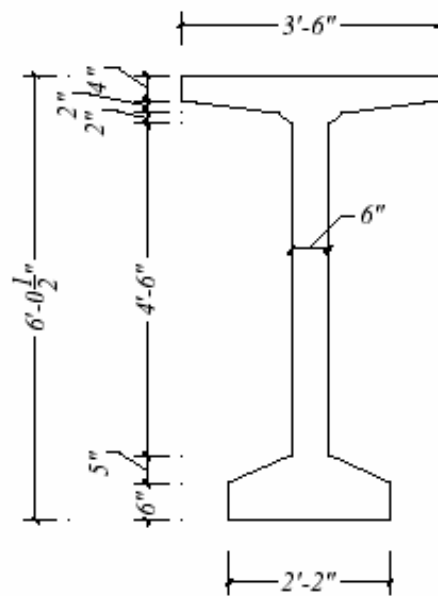


Figure II-3-1- Girder Dimensions ($1 \text{ in.} = 2.54 \text{ cm}$)

In Figure II-3-2 cross-section with strands configurations is reported.

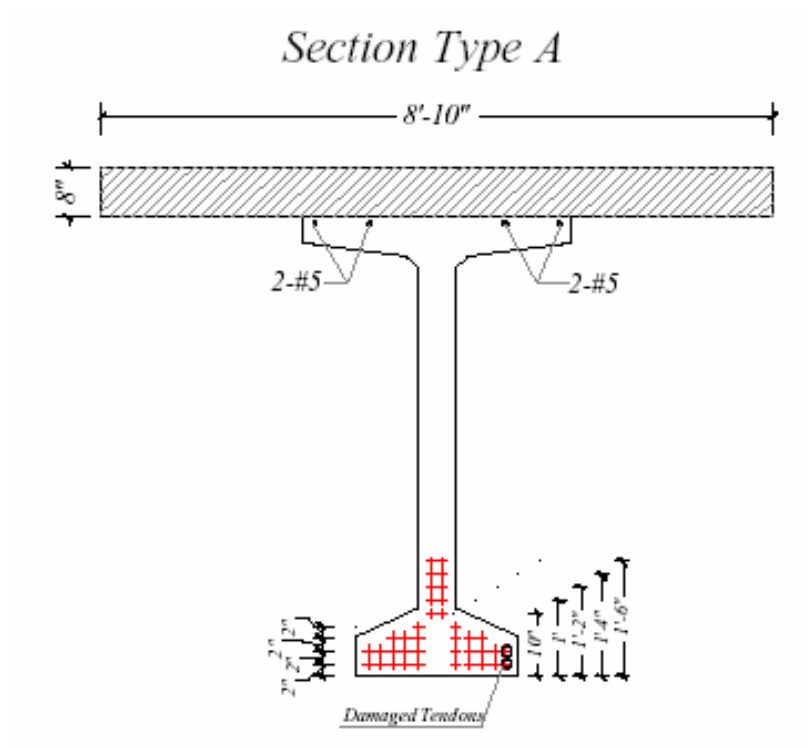


Figure II-3-2- Prestressing Details(1 in.=2.54 cm)

Material properties used in the analysis are shown in Table II-3-1

PRESTRESSING TENDONS	Strand Type	Low relaxation
	Strand Tensile Strength, MPa (ksi)	1,862 (270)
	Nominal Diameter, mm. (in.)	12.7 (0.5)
	Strand Area, mm ² (in ²)	98.7 (0.153)
	Modulus of Elasticity, GPa (ksi)	196.5 (28,500)
MILD STEEL	Tensile strength, MPa (ksi)	413 (60)
	Modulus of Elasticity, GPa (ksi)	200 (29,000)
CONCRETE	Concrete deck, MPa (psi)	27.6 (4,000)
	PC Girder, MPa (psi)	41.4 (6,000)

Table II-3-1- Material Properties

-FRP Laminate

A commercially available FRP strengthening system is selected for its high strength and excellent performance under sustained and cyclic loading. The system includes primer, putty, CFRP sheets, and impregnating resin (i.e., saturant). Considering an environmental reduction factor CE of 0.85 corresponding to exterior exposure condition (see provisional ACI design guidelines) the design ultimate tensile strength and elongation at failure can be expressed as follows:

$$f_{fu} = C_E f_{fu}^*$$

$$\varepsilon_{fu} = C_E \varepsilon_{fu}^*$$

where f_{fu}^* and ε_{fu}^* are the manufacturer guaranteed maximum tensile strength and elongation, respectively. FRP laminate properties are calculated and reported (see Table II-3-2) using the net fiber area.

Ultimate Strength, MPa (ksi), f_{fu}^*	3,800 (550)
Design Strength, MPa (ksi), f_{fu}	3,220 (467)
Tensile Modulus, GPa (ksi), E_f	227 (33000)
Thickness, mm (in.), t_f	0.165 (0.0065)
Ultimate Design Strain, %, ε_{fu}	1.4

Table II-3-2- Properties of Carbon FRP (MBT, 1998)

4. CFRP DESIGN CALCULATIONS

-Strengthening Design

The ultimate limit state analysis calculates the capacity of the section at failure by combining force equilibrium, strain compatibility, and the constitutive materials laws. Figure II-4-1 shows stress distribution at ultimate and forces needed to satisfy the equilibrium condition.

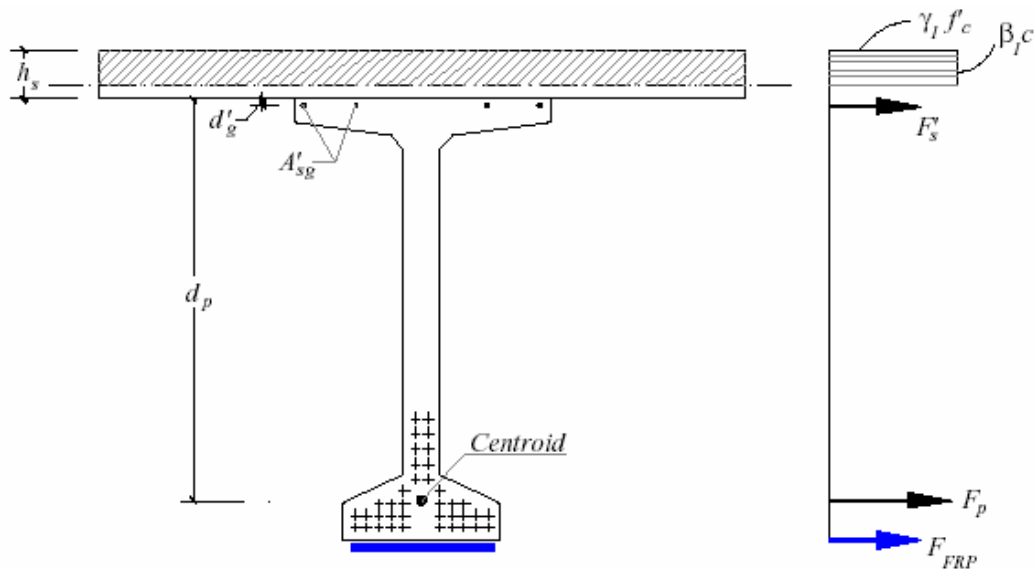


Figure II-4-1- *Stress Distribution in a PC Section at Ultimate*

The general equation for the nominal moment capacity of a PC section strengthened with FRP flexural reinforcement is given in this equation :

$$M_n = F_{FRP} \left(h - \frac{\beta_1 c}{2} \right) + F_p \left(d_p + h_s - \frac{\beta_1 c}{2} \right) + F'_s \left(d'_g + h_s - \frac{\beta_1 c}{2} \right)$$

where F_{FRP} , F_p , and F_s represent tensile forces in the FRP laminate, prestressing tendons, and top mild steel, respectively.

The stresses in each of the materials will depend on the strain distribution and the governing failure mode. (TELL THE STORY!!!)

-Design criteria

The nominal moment capacity of the PC girder and concrete deck was determined by the conventional rectangular stress block approach. The stress in the tendons at ultimate was determined according to standard equations as shown . The computed factored moment capacity of the virgin member before damage, of the member being impacted, and of the member after the repair strengthening is performed is reported in Table II-4-1 for cross section types A.

	Section type A	
	d_p cm (in.)	ΦM_n kN-m (kips-ft)
Virgin	167 (65.9)	10,901 (8,040.5)
Impacted	65.7 (166)	10,328 (7,617.3)
Repaired	65.7 (166)	10,929 (8,061.0)

Table II-4-1– Moment Capacity of the Cross-Section

It is assumed that the FRP laminate is externally bonded to the concrete surface when the concrete surface itself is subjected to a given level of strain and that perfect bond exists between FRP and concrete.

The rehabilitation of this impact-damaged girder calls for concrete repair and application of CFRP laminates as shown in Figure II-4-2.

The flexural strengthening consists of three. 60 cm (24 in) wide plies with lengths of 3.00, 3.35, and 3.65 m (10 ft, 11 ft, and 12 ft), respectively, applied to the bottom of the girder with fibers aligned along its longitudinal axis. The triple-ply laminate is centered over the damaged area.

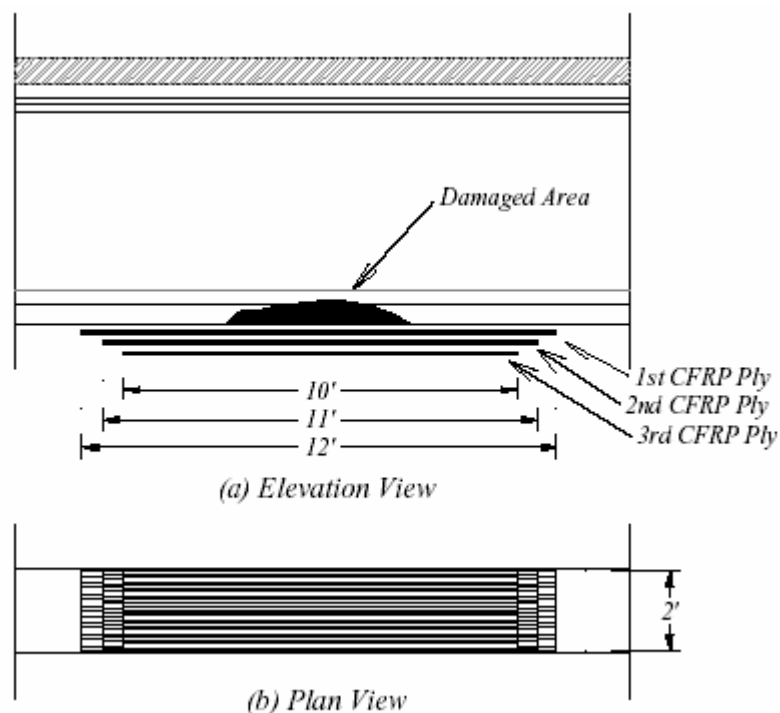


Figure II-4-2- *Three-Ply CFRP Laminate (1 in.=2.54cm)*

Ten strips, . 20 cm (8 in) wide and spaced at. 40 cm (16 in) on centers, are then U-wrapped around the bulb of the girder over the previous installation (see Figure II-4-3). The purpose of the U-wrap is to prevent the delamination of the FRP plies applied to the bottom surface of the girder.

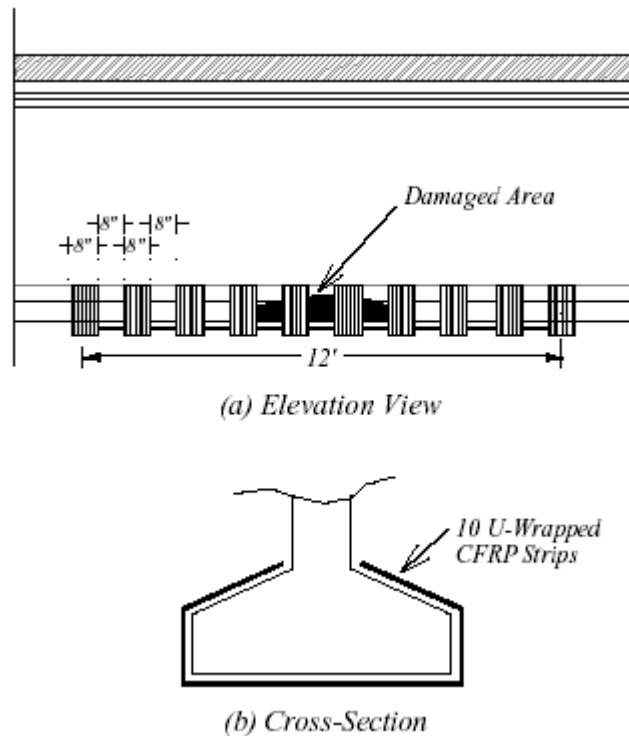


Figure II-4-3 - CFRP Strips U-Wrapped around the Girder Bulb (1 in.=2.54 cm)

-Development length

FRP reinforcement is no longer needed at the cross section where the damaged strands become effective. For the damaged strands it is reasonable to assume a linear transition between the point of zero and full bond over their development length. The development length, l_d , where the damaged strands can be considered fully bonded is expressed as follows:

$$l_d = \left(f_{ps} - \frac{2}{3} f_{se} \right) d_b$$

where d_b is the strand diameter (in cm (*in.*)), f_{ps} is the stress in the prestressed reinforcement at nominal strength of member (in MPa (*ksi*)),

and f_{se} represents the effective stress in prestressed steel after losses (in Mpa (ksi)). In turn, f_{ps} and f_{se} are given as follows:

$$f_{ps} = f_{pu} \left\{ 1 - \frac{\gamma_p}{\beta_1} \left[\rho_p \frac{f_{pu}}{f} + \frac{d}{d_p} (\omega - \omega') \right] \right\}$$

$$f_{se} = \frac{P_f / 36}{0.153} = \frac{1004 / 36}{0.153} = 182 \text{ksi} (1255 \text{ Mpa})$$

where f_{pu} is the specified tensile strength of prestressing strands, γ_p is the factor for type of prestressing strand equal to 0.28, ρ_p is the ratio of prestress reinforcement, $\beta_1 = 0.75$, $\omega = \rho f_y / f'_c$, $\omega' = \rho' f_y / f'_c$, $\rho = A_s / bd$, $\rho' = A'_s / bd$, and P_f represents the final prestressing force after losses.

The term in the square bracket in equation of f_{ps} shall not be less than 0.17, as suggested by ACI 318. Using this controlling value one can get

$$f_{ps} = 1744 \text{ MPa} (253 \text{ ksi}). \text{ From equation } l_d = \left(f_{ps} - \frac{2}{3} f_{se} \right) d_b = 1.7 \text{ m} (5.5 \text{ ft}).$$

The development length is 1.7 m (5.5 ft). (see Figure II-4-4)

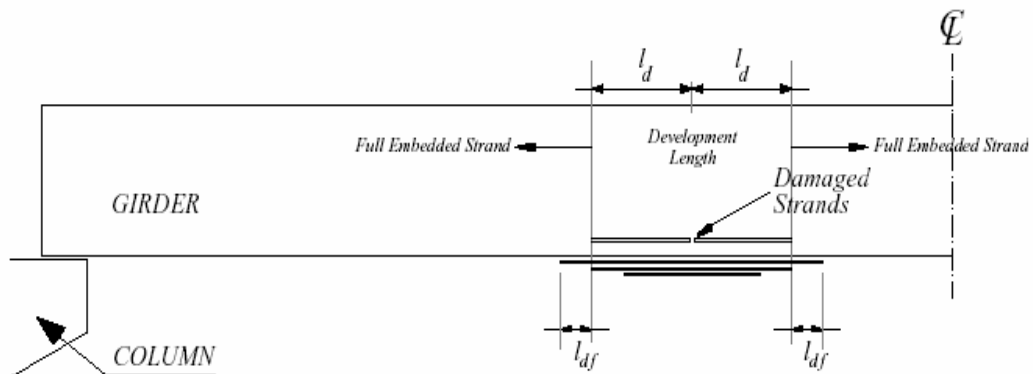


Figure II-4-4- Strand and FRP Development Length

-Redistribution of stresses due to strands rupture

If one were to consider that the effect of the two-strand rupture be limited to the bulb portion of the girder (conservative assumption), than the differential stress at each extremity would be equal to:

$$\sigma_{inc} = \frac{M}{W} = \frac{2(P_f / 38)(b_1 / 2 - 2")}{h_1 b_1^2 / 6} = \frac{2(1,004,000lb / 38)(13" - 2")}{(9")(26")^2 / 6} = 573 \text{ psi } (3965 \text{ kPa})$$

where b_1 is the bottom wide of the girder, and h_1 represent the height of an equivalent rectangular section having the same area of the girder's bulb.

Since the stress differential is small and extremely localized, the effect of the unbalanced prestress force about the girder's vertical axis of symmetry due to two strands being severed on one side of the girder is negligible.

5. -INSTALLATION

Before carrying out the CFRP laminate installation, the damaged area of the girder needs to be restored with a rapid setting, no-shrinkage, cementitious mortar. The sequential installation procedure is as follows:

Surface Preparation: the bottom edges of the girder are rounded for proper wrapping. Next, the concrete surface is sandblasted until the aggregate is exposed and the surface of the concrete is free of loose and unsound materials. (see Figure A-7 and Figure A-8)

Application of primer: a layer of epoxy-based primer is applied to the prepared concrete surface using a short nap roller to penetrate the concrete pores and to provide an improved substrate for the saturant. (see Figure A-9, Figure A-10 and A-11)

Application of putty: after the primer became tack-free, a thin layer of putty is applied using a trowel to level the concrete surface and to patch small holes.

Application of first layer of saturant: the first layer of saturant is rolled on the putty using a medium nap roller. The functions of the saturant are: to impregnate the dry fibers, to maintain the fibers in their intended orientation, to distribute stress to the fibers, and to protect the fibers from abrasion and environmental effects. (see Figure A-12, Figure A-13)

Application of fiber sheet: after the fiber sheet is measured and pre-cut, it is placed on the concrete surface and gently pressed into the saturant. Prior to removing the backing paper, a trowel is used to remove any air void. After the backing paper is removed, a ribbed roller is rolled in the fiber direction to facilitate impregnation by separating the fibers. (see Figure A-14)

Application of second layer of saturant: a second layer of saturant is applied and worked into the fibers with a ribbed roller. After this, the second and third fiber sheet can be installed by repeating the described procedure. (see Figure A-14)

U-wrap installation: a thin layer of putty is applied using a trowel to level the concrete surface and to patch small holes; after that the same procedure up described is followed in order to apply carbon fiber strips

In Appendix A each installation step on Bridge A 5657 on Route 28 over Gasconade River, South of Dixon, Missouri (Mo), U.S.A. is reported.

-Inspection and maintenance

Based on current experience, FRP strengthening of impacted girders is a longterm reliable repair procedure, and no special maintenance should be necessary.

However, the continuing long-term evaluation of the strengthening system being applied

is recommended. As a first step, on the same girder and close to the abutment to facilitate operations, one FRP strip should be installed in the same fashion, modality, and number of plies of that adopted during the strengthening system installation. The area for inspection should be 20” wide and 2’ long. MoDOT inspector should tap this area when inspecting the bridge and if any doubt arises, perform a bond test. The tests (i.e., bond pull-off and torsion tests – see Khataukar, 2001) can be used to evaluate the performance of the installed strengthening system over time.

CHAPTER III

RESEARCH PROGRAM

1. INTRODUCTION

Every year, numerous prestressed concrete (PC) girder bridges are accidentally damaged by over height vehicles or sometimes during very site clean up and when this happens numerous questions occur relative to the behavior and strength of the bridge.

In order to make practicable the bridge besides the most traditional available techniques (i.e. externally bonded steel plates, steel or concrete jackets, and external post-tensioning) are nowadays strengthening using FRP laminates in continuous development.

Therefore an experimental confirmation about the effectiveness of this upgrade technique, already realized in a few practical applications, it is an urgent need.

In this research program four PC girder have been designed, constructed and two of them, one undamaged and one intentionally damaged and CFRP upgraded, tested.

2. THEORETICAL BACKGROUND

-Nominal moment strength of undamaged beam

Unlike the case of reinforced concrete (RC) members, various loading stages can be pointed out for a PC member. These loading stages are summarized as follows:

- Initial prestress P_i is applied and then the concrete is cast. Once concrete is cured, the anchors of the strands are released and the force is transmitted from the prestressing strands to the concrete.
- The full self weight w_D acts on the member together with the initial prestressing force.
- Once the top deck is poured, the full superimposed dead load w_{SD} is applied to the member.
- Short term losses in the prestressing force occur, leading to a reduced prestressing force P_{f0} .
- The member is subjected to the full service load, with long term losses due to creep, shrinkage, and strand relaxation taking place and leading to a net prestressing force P_f .
- Overloading of the member occurs under certain conditions up to the limit state at failure.

A typical loading history and corresponding stress distribution across the depth of the critical section are shown in Figure III-2-1, while a schematic plot of load versus deformation (camber or deflection) is

shown in Figure III-2-2 for the various loading stages from the self weight effect up to rupture.

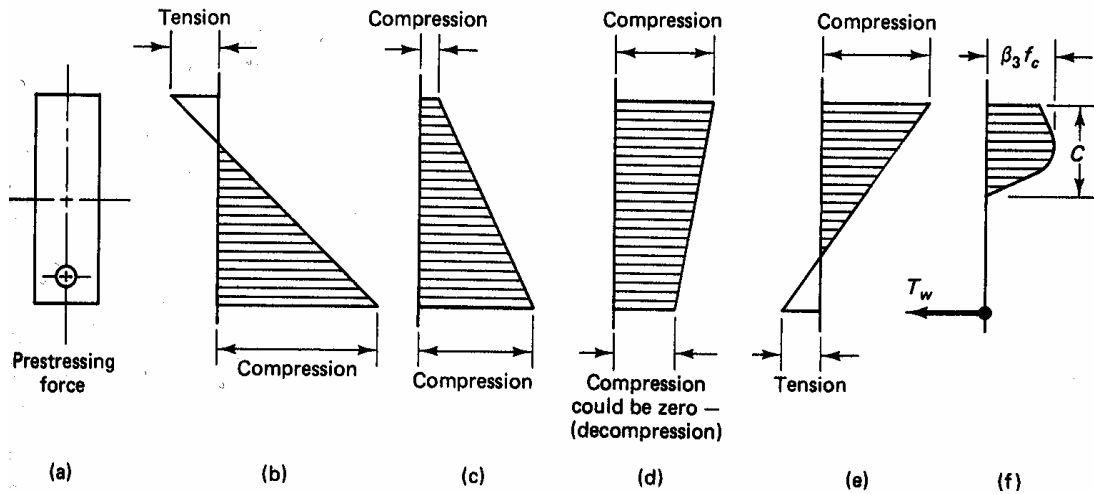


Figure III-2-1- *Stress distribution throughout loading history for a PC beam. (a) Beam section. (b) Initial prestressing stage. (c) Self-weight and effective prestress. (d) Full dead load plus effective prestress. (e) Full service load plus effective prestress. (f) Limit state of stress at ultimate load for underreinforced beam. (Edward G. Navy, Prestressed concrete)*

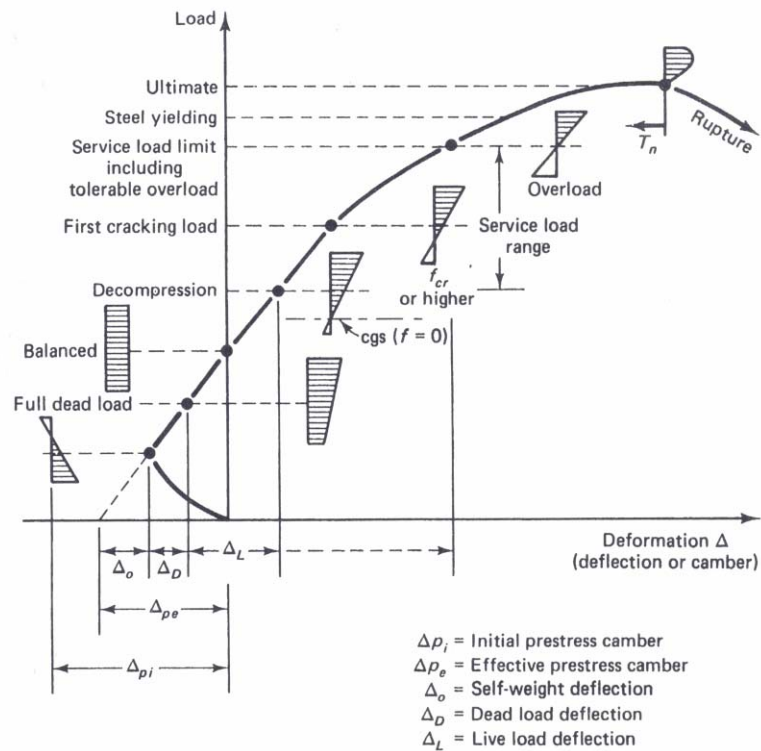


Figure III-2-2- Load-deformation curve of typical prestressed beam.
(Edward G. Navy, *Prestressed concrete*)

The following assumptions are made in defining the behavior of the cross-section at ultimate:

1. The strain distribution is assumed to be linear, assuming that that plane sections remain plane (Bernoulli's hypothesis).
2. The strain in the steel and the surrounding concrete is the same prior to cracking of the concrete or yielding of the steel as after such cracking or yielding.
3. Concrete is weak in tension. It cracks at an early stage of loading at about 10 percent of its compressive strength limit. Consequently, concrete in the tension zone of the section is

neglected in the flexural analysis and design computations, and the tension reinforcement is assumed to take the total tensile force.

The actual distribution of the compressive stress in a section at failure has the form of a rising parabola (see Figure III-2-4). It is time consuming to evaluate the volume of the compressive stress block if it has a parabolic shape. An equivalent rectangular stress block due to Whitney can be used with ease and without loss of accuracy to calculate the compressive force and hence the flexural moment strength of the section. This equivalent stress block has a depth a and an average compressive strength $0.85f'_c$. The value of $a=\beta_1c$ is determined by using a coefficient β_1 so that the area of the rectangular block is equivalent to that of the parabola (same compressive force C in both cases).

Factor β_1 shall be taken as 0.85 for concrete strengths f'_c up to and including 27.58 MPa (4000 psi). For strengths above 27.58 MPa (4000 psi), β_1 shall be reduced continuously at a rate of 0.05 for each 6.89 MPa (1000 psi) of strength in excess of 27.5 MPa (4000 psi), but β_1 shall not be taken less than 0.65.

The value $0.85f'_c$ for the average stress of the equivalent compressive block is based on the core test results of concrete in the structure at a minimum age of 28 days.

Based on exhaustive experimental tests, a maximum allowable strain of 0.003 cm/cm (in./in.) was adopted by ACI as a safe limiting value. Even though several forms of stress blocks, including the trapezoidal, have been proposed to date, the simplified equivalent rectangular block is accepted as the standard in the analysis and design. The behavior of the steel is assumed to be elastoplastic. In following Figure III-2-3 it is possible to

see the total strain diagram due to self-weight and effective prestress plus full service load, while in

Figure III-2-4 is reported strain and stress at ultimate state.

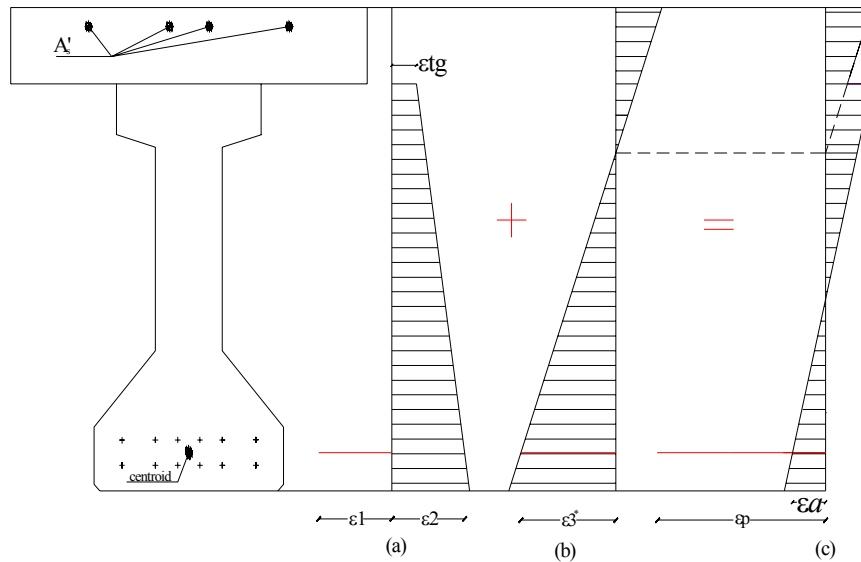


Figure III-2-3-(a) strain distribution due to self weight and effective prestress-(b) strain distribution due to full service load-(c) strain distribution due to (a) plus (b).

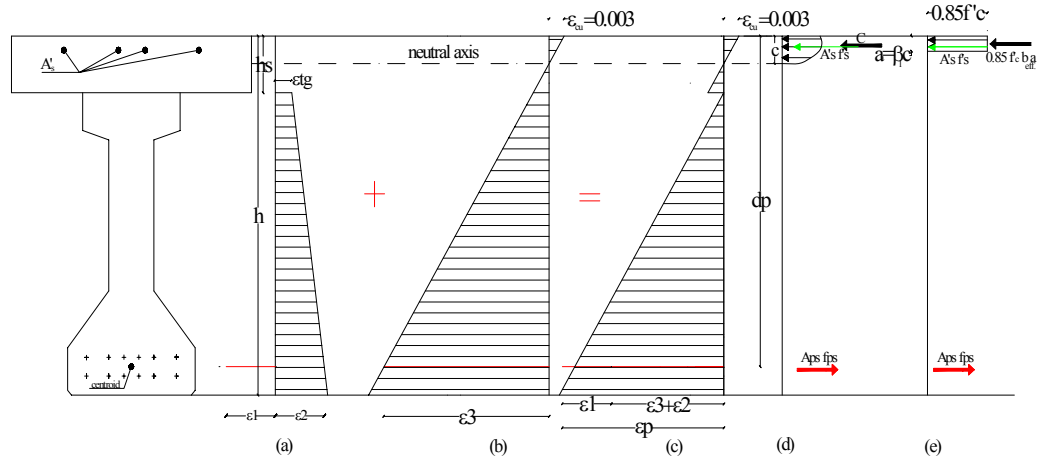


Figure III-2-4- Stress and strain distribution across beam depth at ultimate load . (a) strain distribution due to self weight and effective prestress; (b) strain distribution due to external load; (c) strain distribution at failure[(a) plus (b)];(d) actual stress block;(e) assumed equivalent stress block

In order to evaluate the nominal moment of the section is necessary to solve the following equilibrium equation in which the unknown is c (depth of neutral axis).

$$f_{ps} A_p = 0.85 f'_c \beta_1 c b + A'_s \epsilon'_s E_s$$

where :

A_p : Area of prestressing steel, cm^2 (in^2)

A'_s : Area of compression reinforcement, cm^2 (in^2)

b = deck wide, cm ($\text{in}.$)

ϵ'_s : strain in compression steel, in/in , from strain

compatibility = $\epsilon_{cu} \left(\frac{c - d'}{c} \right)$ where

ϵ_{cu} : concrete maximum strain allowable=0.003 cm/cm (in/in)

d' : distance from extreme compression fiber to centroid of compression reinforcement, cm (in.)

f_{ps} : nominal failure stress of prestressing steel, MPa (ksi).

The value of the stress f_{ps} is not readily available. However, it can be determined by *strain compatibility* through the various loading stages up to the limit state at failure. Such a procedure is required if:

$$f_{pe} = \frac{P_f}{A_p} < 0.50 f_{pu}$$

Approximate determination by the ACI 318 building code provided that

$$f_{pe} = \frac{P_f}{A_p} \geq 0.50 f_{pu}$$

with separate equations for f_{ps} given for bonded and nonbonded members.

The empirical expression for bonded members (as in this research) is

$$f_{ps} = f_{pu} \left(1 - \frac{\gamma_p}{\beta_1} \left[\rho_p \frac{f_{pu}}{f'_c} + \frac{d}{d_p} (\omega - \omega') \right] \right)$$

where

f_{pu} : specified tensile strength of prestressing strands,psi

γ_p : $\gamma_p=0.55$ for f_{py}/f_{pu} not less than 0.80

$\gamma_p=0.40$ for f_{py}/f_{pu} not less than 0.85

$\gamma_p=0.28$ for f_{py}/f_{pu} not less than 0.90

ρ_p : is the ratio of prestress reinforcement = $A_p/[b(z)d_p]$

f'_c : specified compressive strength of concrete, MPa (psi)

d : distance from extreme compression fiber to centroid of non prestressed tension reinforcement, cm (in.)

d_p : distance from extreme compression fiber to centroid of prestressed reinforcement, cm (in.)

$$\omega = \rho f_y / f'_c$$

$$\omega' = \rho' f_y / f'_c$$

$$\rho = A_s / bd$$

$$\rho' = A'_s / bd,$$

If the compression reinforcement is taken into account when calculating

f_{ps} , the term $\left(\rho_p \frac{f_{pu}}{f'_c} + \frac{d}{d_p} (\omega - \omega') \right)$ should not be less than 0.17. Since that

equation assumes that the compression reinforcement is yielding than d' , the distance from extreme compression fiber to the centroid of the compression steel, should not be greater than $0.15d_p$.

If d' is greater than $0.15d_p$, then ω' is taken as zero.

The value of the factor γ_p is based on the criterion that $f_{py} = 0.80f_{pu}$ for high-strength prestressing bars, 0.85 for stress-relieved strands, and 0.90 for low-relaxation strands.

Once solved this system, known c , will be possible evaluate the nominal moment of the section by following equation:

$$M_n = A_p f_{ps} \left(d_p - \frac{\beta_1 c}{2} \right) + A'_s f'_s \left(\frac{\beta_1 \cdot c}{2} - d' \right)$$

In order to evaluate the nominal moment capacity with a more sophisticated method is possible to determine the nominal failure stress

of prestressing steel f_{ps} evaluating for each load step the strain in the tendons. The final value of strain will be:

$\epsilon_p = \epsilon_1 + \epsilon_2 + \epsilon_3$ where

$$\epsilon_1 = \frac{P_f}{E_p A_p}$$

$$\epsilon_2 = \frac{P_f}{A_{cg} E_{cg}} + \frac{P_f e^2}{E_{cg} I_g} - \frac{M_g e}{E_{cg} I_g}$$

where: A_p : Area of prestressing steel, cm^2 (in^2)

A_{cg} : Area concrete girder, cm^2 (in^2)

E_p : Modulus of elasticity of prestressing steel, MPa (ksi)

E_{cg} : Modulus of elasticity of concrete girder, MPa (ksi)

e : eccentricity, cm (in.)

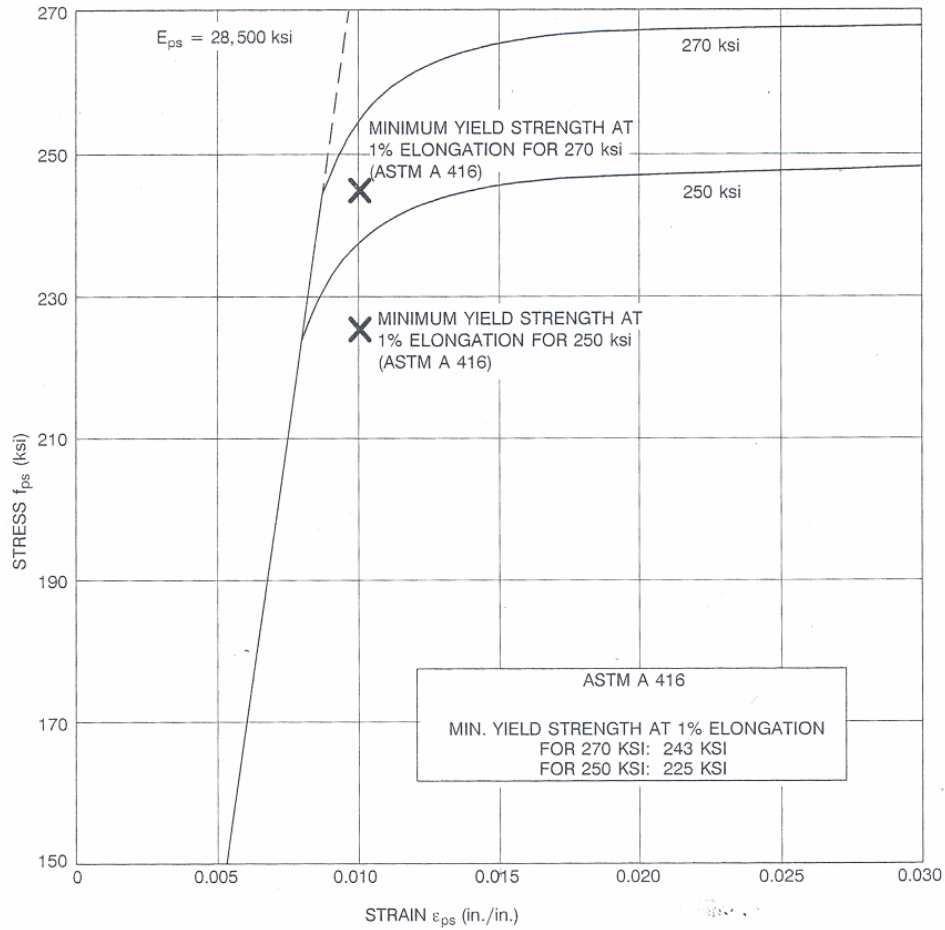
I : Moment of inertia of girder, cm^4 (in^4)

M_g : Moment due to self weight of the girder, kN-m (kips-ft)

$$\epsilon_3 = \epsilon_{cu} \frac{(d_p - c)}{c}$$

where h_s is the deck high.

and once known the final strain value, f_{ps} is available from stress-strain diagram of tendon reported in Figure III-2-5.



These curves can be approximated by the following equations:

<p>250 ksi</p> $\varepsilon_{ps} \leq 0.0076 : f_{ps} = 28,500\varepsilon_{ps} \text{ (ksi)}$ $\varepsilon_{ps} > 0.0076 : f_{ps} = 250 - \frac{0.04}{\varepsilon_{ps} - 0.0064} \text{ (ksi)}$	<p>270 ksi</p> $\varepsilon_{ps} \leq 0.0086 : f_{ps} = 28,500\varepsilon_{ps} \text{ (ksi)}$ $\varepsilon_{ps} > 0.0086 : f_{ps} = 270 - \frac{0.04}{\varepsilon_{ps} - 0.007} \text{ (ksi)}$
---	--

Figure III-2-5- Typical stress-strain curve, 7 wire low-relaxation prestressing strand.

-Nominal moment strength of CFRP upgraded beam

This chapter presents guidance on the calculation of the flexural strengthening effect of adding longitudinal FRP reinforcement to the tension face of a reinforced concrete member

The following assumptions are made in calculating the flexural resistance of a section strengthened with an externally applied FRP system:

- Design calculations are based on the actual dimensions, internal reinforcing steel arrangement, and material properties of the existing member being strengthened;
- The strains in the reinforcement and concrete are directly proportional to the distance from the neutral axis, that is, a plane section before loading remains plane after loading;
- The maximum usable compressive strain in the concrete is 0.003;
- The tensile strength of concrete is neglected;
- The FRP reinforcement has a linear elastic stress-strain relationship to failure;
- Perfect bond exists between the concrete and external FRP reinforcement.

Unless all loads on a member, including self-weight and any prestressing forces, are removed before installation of FRP reinforcement, the substrate to which the FRP is applied will be strained. These strains should be considered as initial strains and should be excluded from the strain in the FRP (Arduini and Nanni 1997; Nanni et al. 1998). The initial strain level on the bonded substrate, ε_{bi} , can be determined from an

elastic analysis of the existing member, considering all loads that will be on the member, during the installation of the FRP system. It is recommended that the elastic analysis of the existing member be based on cracked section properties. The value of strain level in the concrete substrate at the time of FRP installation ε_{bi} is given in the case of prestressed concrete (where the section remains uncracked at the time of FRP installation) from following equation:

$$\varepsilon_{bi} = \frac{M_{ip} \cdot c_b}{I_g \cdot E_{cg}} - \frac{P_f}{A_{cg} \cdot E_{cg}} \cdot \left(1 + \frac{e \cdot c_b}{r_g^2} \right) \text{ where}$$

M_{ip} : Moment due to loads in place at the time of FRP installation (mainly dead loads) not including moments caused by eccentric prestressing forces, kN-m (kips-ft.)

c_b : Distance from the neutral axis of the gross concrete section to the bonded substrate, cm (in.)

I_g : Moment of inertia of the gross concrete section, cm^4 (in.^4)

E_{cg} : Elastic modulus of elasticity of the girder in compression, MPa (psi)

P_f : Effective prestress force at the time of FRP installation, kN (lb.)

A_{cg} : Area of gross concrete girder section, cm^2 (in.^2)

e : Eccentricity of prestressing force with respect to the neutral axis of the gross concrete girder section. Positive eccentricities cause compression on the bonded substrate, cm. (in.)

r_g : radius of gyration of the gross concrete girder section = $\sqrt{I_{cg} / A_{cg}}$, cm (in.)

The flexural capacity of a section depends on the controlling failure mode. The following flexural failure modes should be investigated for an FRP-strengthened section (GangaRao and Vijay 1998):

- Crushing of the concrete in compression before yielding of the reinforcing steel;
- Yielding of the steel in tension followed by rupture of the FRP laminate;
- Yielding of the steel in tension followed by concrete crushing;
- Shear/tension delamination of the concrete cover (cover delamination);
- Debonding of the FRP from the concrete substrate (FRP debonding).

Concrete crushing is assumed to occur if the compressive strain in the concrete reaches its maximum usable strain ($\epsilon_c = \epsilon_{cu} = 0.003$). Rupture of the FRP laminate is assumed to occur if the strain in the FRP reaches its design rupture strain ($\epsilon_f = \epsilon_{fu}$) before the concrete reaches its maximum usable strain.

Cover delamination or FRP debonding can occur if the force in the FRP cannot be sustained by the substrate. In order to prevent debonding of the FRP laminate, a limitation should be placed on the strain level developed in the laminate. The following equations gives an expression for a bond dependent coefficient, κ_m .

$$\kappa_m = \begin{cases} \frac{1}{60\varepsilon_{fu}} \left(1 - \frac{nE_f t_f}{2,000,000} \right) \leq 0.90 & \text{for } nE_f t_f \leq 1,000,000 \\ \frac{1}{60\varepsilon_{fu}} \left(\frac{500,000}{nE_f t_f} \right) \leq 0.90 & \text{for } nE_f t_f > 1,000,000 \end{cases} \quad \text{US}$$

customary units

$$\kappa_m = \begin{cases} \frac{1}{60\varepsilon_{fu}} \left(1 - \frac{nE_f t_f}{360,000} \right) \leq 0.90 & \text{for } nE_f t_f \leq 180,000 \\ \frac{1}{60\varepsilon_{fu}} \left(\frac{90,000}{nE_f t_f} \right) \leq 0.90 & \text{for } nE_f t_f > 180,000 \end{cases} \quad \text{SI}$$

customary units

The term κ_m , expressed is a factor no greater than 0.90 that may be multiplied by the rupture strain of the FRP laminate to arrive at a strain limitation to prevent debonding. The number of plies, n , used in this equation is the number of plies of FRP flexural reinforcement at the location along the length of the member where the moment strength is being computed. This term recognizes that laminates with greater stiffness are more prone to delamination. Thus, as the stiffness of the laminate increases, the strain limitation becomes more severe. For laminates with a unit stiffness, $n E_f t_f$, greater than . 180,000 N/mm (1,000,000 lb/in), κ_m limits the force in the laminate as opposed to the strain level. This effectively places an upper bound on the total force that can be developed in an FRP laminate, regardless of the number of plies.

The κ_m term is only based on a general recognized trend and on the experience of engineers practicing the design of bonded FRP systems. Further research into the mechanics of bond of FRP flexural reinforcement should result in more accurate methods for predicting

delamination. Further development of the equation will likely account not only for the stiffness of the laminate but also for the stiffness of the member to which the laminate is bonded. In the interim, the committee recommends the use of these equations to limit the strain in the FRP and prevent delamination.

It is important to determine the strain level in the FRP reinforcement at the ultimate-limit state. Because FRP materials are linearly elastic until failure, the level of strain in the FRP will dictate the level of stress developed in the FRP. The maximum strain level that can be achieved in the FRP reinforcement will be governed by either the strain level developed in the FRP at the point at which concrete crushes, the point at which the FRP ruptures, or the point at which the FRP debonds from the substrate. This maximum strain or the effective strain level in the FRP reinforcement at the ultimate-limit state can be found from the following equation.

$$\epsilon_{fe} = \epsilon_{cu} \left(\frac{h-c}{c} \right) - \epsilon_{bi} \leq \kappa_m \epsilon_{fu}$$

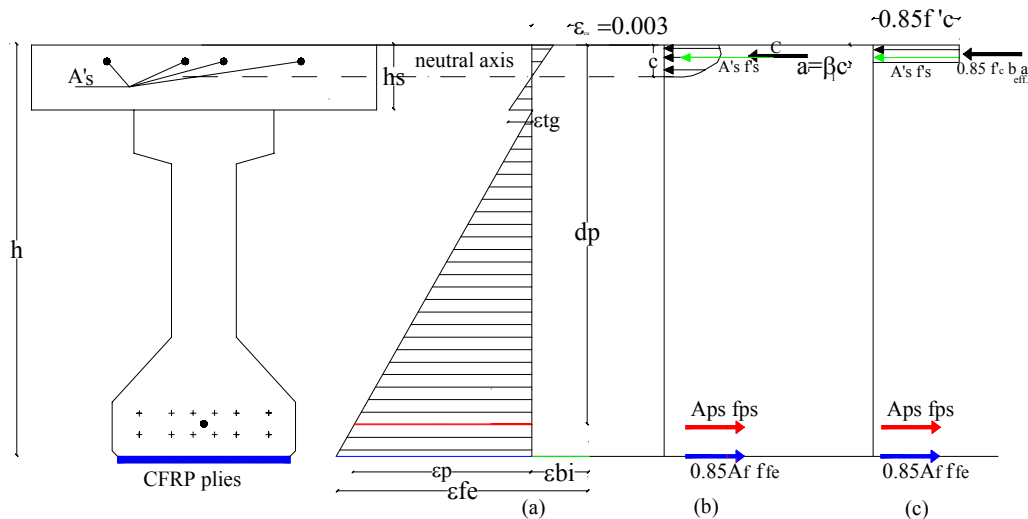


Figure III-2-6 illustrates the internal strain and stress distribution on PC beam section strengthened with FRP under flexure at the ultimate limit state

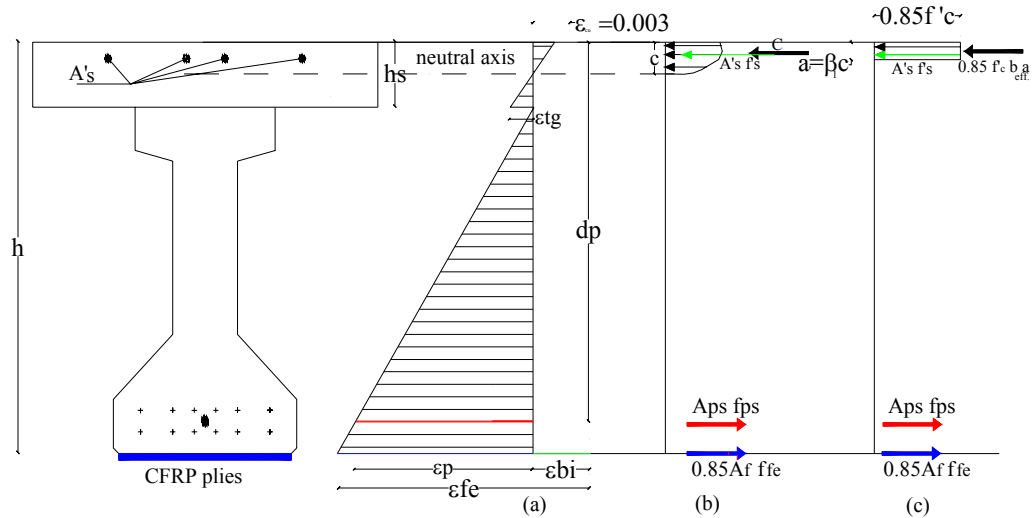


Figure III-2-6- *Internal strain and stress distribution under flexure at ultimate stage*

The calculation procedure used to arrive at the ultimate strength should satisfy strain compatibility and force equilibrium and should consider the governing mode of failure. Several calculation procedures can be derived to satisfy these conditions. The calculation procedure described herein is one such procedure that illustrates a trial and error method. The trial and error procedure involves selecting an assumed depth to the neutral axis, c ; calculating the strain level in each material using strain compatibility; calculating the associated stress level in each material; and checking internal force equilibrium. If the internal force resultants do not equilibrate, the depth to the neutral axis must be revised and the procedure repeated.

For any assumed depth to the neutral axis, c , the strain level in the FRP reinforcement can be computed from following equation:

$$\varepsilon_{fe} = \varepsilon_{cu} \left(\frac{h-c}{c} \right) - \varepsilon_{bi}$$

This equation considers the governing mode of failure for the assumed neutral axis depth. If the first term in the equation controls, concrete crushing controls flexural failure of the section. If the second term controls, FRP failure (rupture or debonding) controls flexural failure of the section.

The effective stress level in the FRP reinforcement can be found from the strain level in the FRP, assuming perfectly elastic behavior.

$$f_{fe} = E_f \varepsilon_{fe}$$

Based on the strain level in the FRP reinforcement, the strain level in the non prestressed tension steel can be found from following equation using strain compatibility.

$$\varepsilon'_s = \varepsilon_{cu} \left(\frac{c-d'}{c} \right) \text{ for failure by concrete crushing}$$

$$\varepsilon'_s = (\varepsilon_{fu} + \varepsilon_{bi}) \left(\frac{c-d'}{h-c} \right) \text{ for failure by FRP rupture}$$

The stress in the steel is calculated from the strain level in the steel assuming elastic-plastic behaviour.

$$f'_s = E_s \varepsilon'_s \leq f_y$$

The total strain in the tendons is due to strains at three load stages , prestress alone, decompression of the prestressing steel and ultimate load:

$\varepsilon_p = \varepsilon_{p1} + \varepsilon_{p2} + \varepsilon_{p3}$ where:

$$\varepsilon_{p1} = \frac{P_f}{A_p E_p}$$

$$\varepsilon_{p2} = \frac{P_f}{A_{cg} \cdot E_{cg}} \cdot \left(1 + \frac{e \cdot c_b}{r_g^2} \right)$$

$$\varepsilon_{p3} = \left(\varepsilon_{fe} + \varepsilon_{bi} \right) \left(\frac{d_p - c}{h - c} \right)$$

The stress in the tendons f_{ps} should be determined from stress-strain diagram of tendon reported in Figure III-2-5.

With the strain and stress level in the FRP and steel reinforcement determined for the assumed neutral axis depth, internal force equilibrium may be checked using following equation

$$c = \frac{A_f f_{fe} + A_p f_{ps} - A'_s f'_s}{\gamma f'_c \beta_1 b}$$

The terms γ and β_1 in the last equation are parameters defining a rectangular stress block in the concrete equivalent to the actual nonlinear distribution of stress. If concrete crushing is the controlling mode of failure (before or after steel yielding), γ and β_1 can be taken as the values associated with the Whitney stress block ($\gamma = 0.85$ and β_1 from Section 10.2.7.3 of ACI 318). If FRP rupture, cover delamination, or FRP-debonding control failure, the Whitney stress block will give reasonably accurate results. A more accurate stress block for the actual strain level

reached in the concrete at the ultimate-limit state may be used. Because the concrete does not reach its ultimate strain in compression, the Whitney stress block (used by ACI 318) is not appropriate. The stress resultant for concrete should be determined from an appropriate non-linear stress –strain relationship or by a rectangular stress block suitable for the particular level of strain in the concrete.

Parameters for such a stress block are given in following equations:

$$\beta_1 = 2 - \left[4 \cdot \frac{(\varepsilon_c / \varepsilon'_c) - \tan^{-1}(\varepsilon_c / \varepsilon'_c)}{(\varepsilon_c / \varepsilon'_c) \ln(1 + \varepsilon_c^2 / \varepsilon'^2_c)} \right]$$

$$\gamma = \frac{0.90 \ln(1 + \varepsilon_c^2 / \varepsilon'^2_c)}{\beta_1 \varepsilon_c / \varepsilon'_c}$$

where $\varepsilon'_c = \frac{1.71 f'_c}{E_c}$, and $\tan^{-1}(\varepsilon_c / \varepsilon'_c)$ is computed in radians.

The actual depth to the neutral axis, c , is found by simultaneously satisfying of equation shown, thus establishing internal force equilibrium and strain compatibility.

The nominal flexural capacity of the section with FRP external reinforcement can be computed from next equation. An additional reduction factor, ψ_f , is applied to the flexural-strength contribution of the FRP reinforcement. A factor $\psi_f = 0.85$ is recommended.

$$M_n = A_p f_{ps} \left(d_p - \frac{\beta_1 c}{2} \right) + \psi_f A_f f_{fe} \left(h - \frac{\beta_1 c}{2} \right) - A'_s f'_s \left(\frac{\beta_1 c}{2} - d' \right)$$

- Length of FRP reinforcement

FRP reinforcement is no longer needed at the cross section where the damaged strands become effective. For the damaged strands it is reasonable to assume a linear transition between the point of zero and full bond over their development length. The development length, l_d , where the damaged strands can be considered fully bonded is expressed as follows

$$l_d = \left(f_{ps} - \frac{2}{3} f_{se} \right) d_b$$

where db is the strand diameter (in $cm(in.)$), f_{ps} is the stress in the prestressed reinforcement at nominal strength of member (in MPa (ksi)), and f_{se} represents the effective stress in prestressed steel after losses (in MPa (ksi)). In turn, f_{ps} and f_{se} are given as follows:

$$f_{ps} = f_{pu} \left\{ 1 - \frac{\gamma_p}{\beta_1} \left[\rho_p \frac{f_{pu}}{f} + \frac{d}{d_p} (\omega - \omega') \right] \right\}$$

$$f_{se} = \frac{P_f}{A_p}$$

where f_{pu} is the specified tensile strength of prestressing strands, γ_p is the factor for type of prestressing strand equal to 0.28, ρ_p is the ratio of prestress reinforcement, $\beta_1 = 0.85$,

$\omega = \rho f_y / f'_c$, $\omega' = \rho' f_y / f'_c$, $\rho = A_s / bd$, $\rho' = A'_s / bd$, and Pf represents the final prestressing force after losses.

The term in the square bracket in equation of f_{ps} shall not be less than 0.17, as suggested by ACI 318.

-Cracking –Load Moment

One of the fundamental differences between prestressed and reinforced concrete is the continuous shift in the prestressed beams of the compressive C-line away from the tensile line as the load increases. In other words, the moment arm of the internal couple continues to increase with the load without any appreciable change in the stress f_{pe} in the prestressing steel. As the flexural moment continues to increase when the full dead load and live load act, a loading stage is reached where the concrete compressive stress becomes zero. This stage of stress is called the limit state of decompression: any additional external load or overload results in cracking at bottom face, where the modulus of rupture of concrete f_r is reached due to the cracking moment M_{cr} caused by first cracking load. At this stage, a sudden increase in the steel stress takes place and the tension is dynamically transferred from the concrete to steel. It is important to evaluate the first cracking load, since the section stiffness is reduced and hence an increase in deflection has to be considered. Also, the crack width has to be controlled in order to prevent reinforcement corrosion.

The concrete fiber stress at tension face is:

$$f_b = -\frac{P_f}{A_{cg}} \left(1 + \frac{ec_b}{r^2} \right) + \frac{M_{cr.}}{S_b} = f_r$$

where the modulus of rupture $f_r = 7.5\sqrt{f'_c}$ and the cracking moment M_{cr} is the moment due to all loads at that load level. From the equation up reported is possible to know M_{cr} :

$$M_{cr.} = f_r S_b + P_f \left(e + \frac{r^2}{c_b} \right)$$

where:

f_r = modulus of rupture of concrete, MPa (psi.)

S_b = moduli of the complete section for the bottom fibers, cm^3 (in.^3)

c_b : Distance from the neutral axis of the gross concrete section to the bonded substrate, cm (in.)

P_f : Effective prestress force at the time of FRP installation, kN (lb.)

e : Eccentricity of prestressing force with respect to the neutral axis of the gross concrete girder section. Positive eccentricities cause compression on the bonded substrate, cm (in.)

r_g : radius of gyration of the gross concrete girder section = $\sqrt{I_{cg} / A_{cg}}$, cm (in.)

3. SPECIMEN DESCRIPTION

-Specimen 1 (undamaged)

First problem to tackle before starting the experimental campaign concerned the design of the cross section. The final choice was suggested essentially by two reasons: the similarity with a real case and the laboratory restrictions. In order to satisfy the first requirement, the girder section was designed with dimension normally used for bridge construction; concerning laboratory limitations, at first a specimen cross section without deck but with a larger equivalent height of concrete was designed; this choice, however, led to a specimen height too big so that test results probably would not have been valid. For this reason, this approach was neglected and the specimen cross section was designed with top deck and construction realized in two different steps. First, the PC girder was built in the factory; its total length was equal to 11m (36 ft) and the girder cross section is reported in Figure III-3-1. The shear reinforcement was designed so that shear failure was prevented during the test, while strands number and diameter were chosen with reference to maximum load applicable in the laboratory.

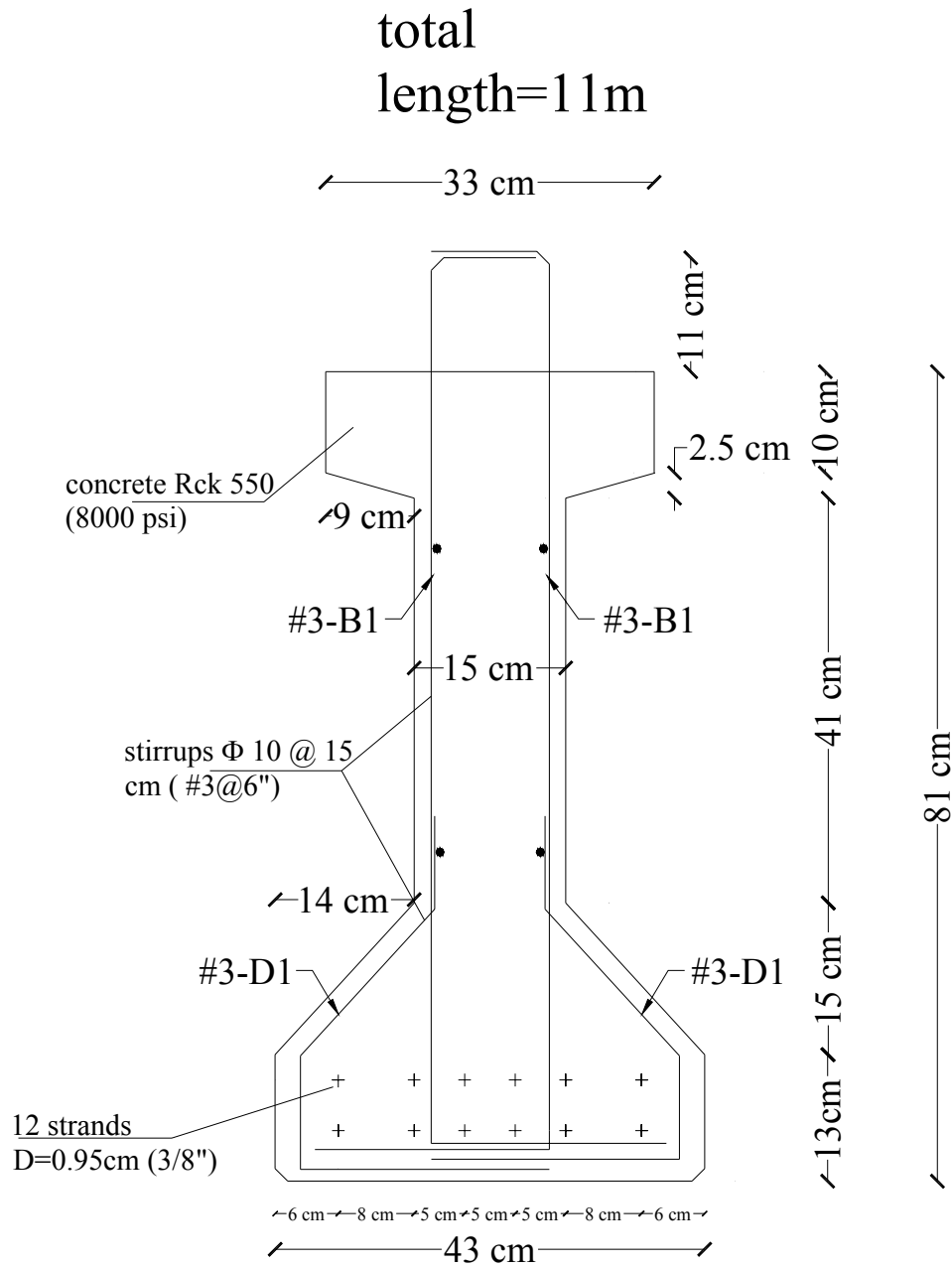


Figure III-3-1-Girder cross section (1 in.=2.54 cm)

Once this girder was conducted in the laboratory the deck was cast with a dimension of 81cm.x15cm (32 in. by 8 in.), so that the complete specimen cross section was realized (see Figure III-3-2)

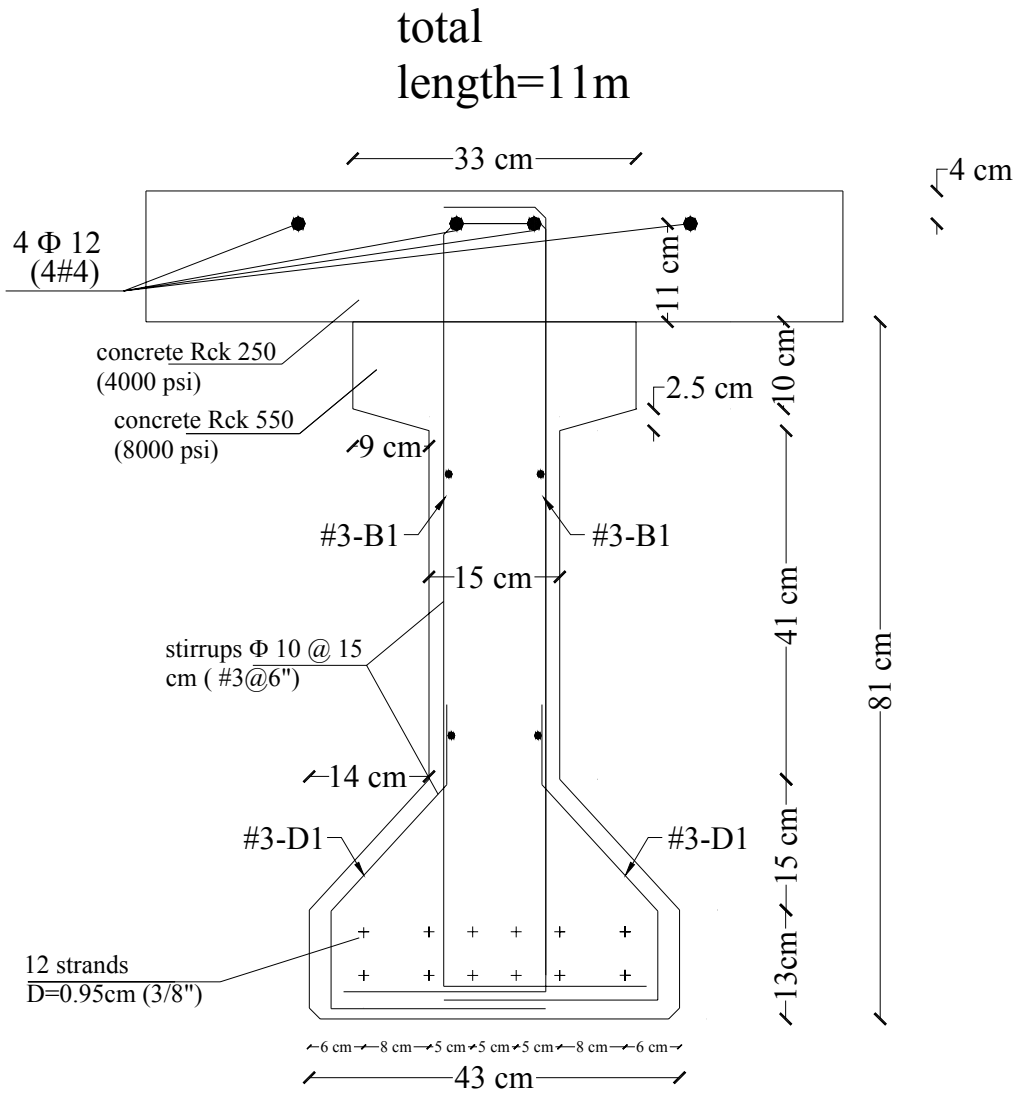


Figure III-3-2- Specimen 1 cross section (1 in.=2.54 cm)

Although for this research program only two specimen were tested (one undamaged and one damaged and then CFRP strengthened), four specimens were realized in order to use test results of this research program for futures researches.

The quantity and properties of deck, PC girder, mild steel and prestressing tendons are reported in Table III-3-1:

PRESTRESSING TENDONS	Strand Type	Low relaxation
	Strand Tensile Strength, MPa (ksi)	1,862 (270)
	Nominal Diameter, mm. (in.)	9.525 (0.375)
	Strand Area,(mm ² (in ²))	54.84 (0.085)
	Modulus of Elasticity, GPa (ksi)	200 (29,000)
	Number of strands	12
	Total strands Area , mm ² (in ²)	658.08 (1.02)
MILD STEEL	Reinforcing bar type	#4
	Tensile strength, MPa (ksi)	413 (60)
	Diameter, mm. (in.)	12.7 (0.59)
	Area, mm ² (in ²)	129 (0.20)
	Modulus of Elasticity, GPa (ksi)	200 (29,000)
	Number of bars	4
	Total Area , mm ² (in ²)	516 (0.80)
CONCRETE	Concrete deck, MPa (psi)	27.6 (4,000)
	Deck Total Area, cm ² (in ²)	1238.8 (1929)
	PC Girder, MPa (psi)	55.16 (8,000)
	Girder Total Area, cm ² (in ²)	2009.8 (311.5)

Table III-3-1-Material quantity and properties

The first specimen analyzed in this research program was used as control.

-Specimen 2 (intentionally damaged and upgraded)

For the second one another construction step was necessary. In order to evaluate the effectiveness of CFRP laminates retrofit, the specimen was intentionally damaged in mid-span by a length of 25.4 cm (10 in.) (12.7 cm (2.5 in.) on the left and right from mid-span respectively). The damage was achieved by removing the concrete cover and cutting two tendons (see Figure III-3-3).



Figure III-3-3 – *Tendons cut and intentionally damaged area on specimen 2*

After that, in order to upgrade the flexural capacity of the specimen, a flexural strengthening design was considered according to ACI 318 and ACI 440. The calculations showed that flexural strengthening consisted of two 43 cm (14 in.) wide plies with lengths of 3.0 and 3.5, m (10 ft, 11 ft), respectively, applied to the bottom of the girder with fibers aligned along its longitudinal axis. The double-ply

laminates are centered over the damaged area at mid-span (see Figure III-3-4).

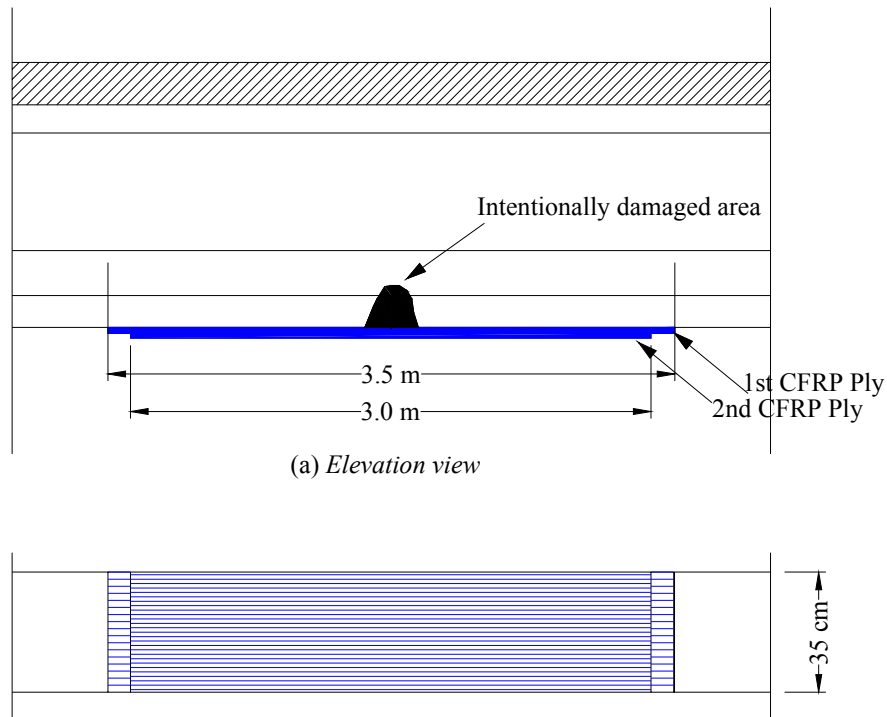
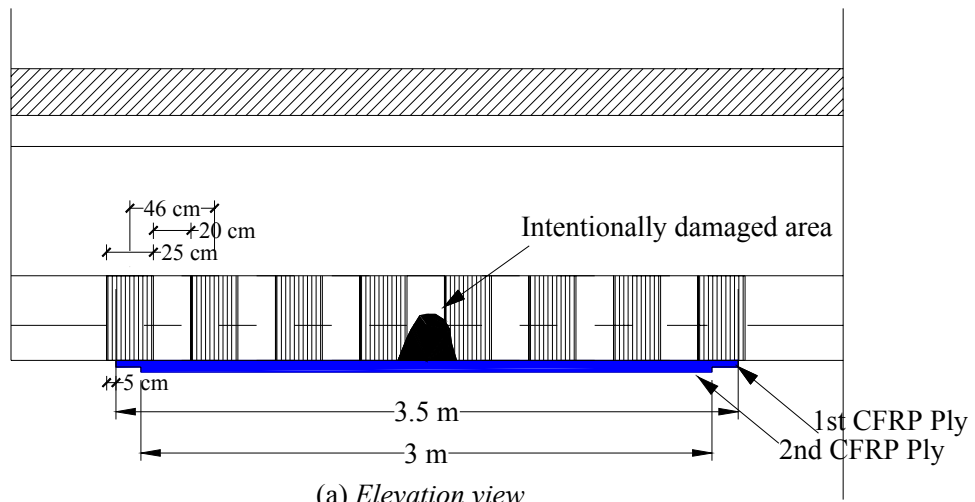
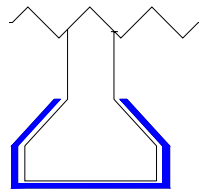


Figure III-3-4 - Two plies of CFRP laminate (1 in. = 2.54 cm)

Furthermore eight strips, 25.4 cm (10 in.) wide and spaced at 45.7 cm (18 in.) on centers, were then U-wrapped around the bulb of the girder over the previous installation (see Figure III-3-5). The purpose of the U-wrap is to prevent the delamination of the FRP plies applied to the bottom surface of the girder.



(a) Elevation view



(b) Cross section

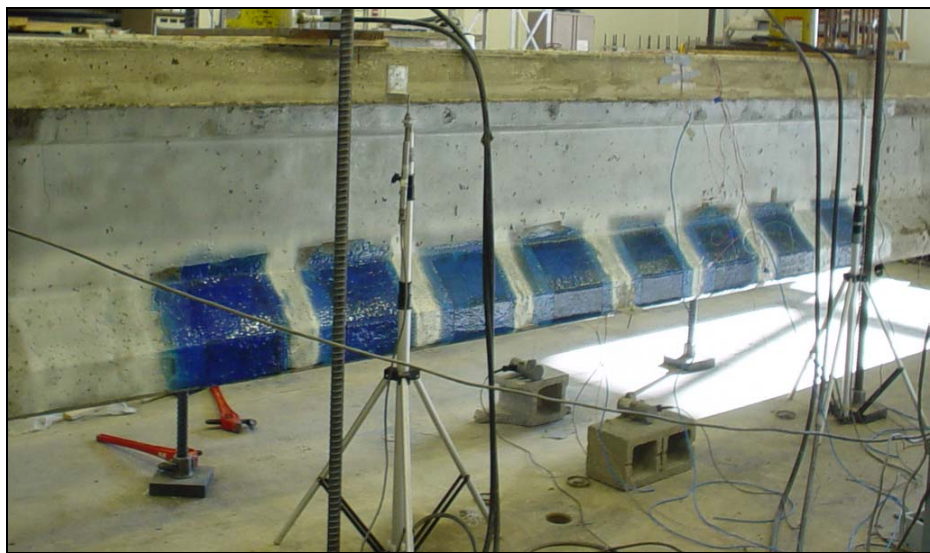


Figure III-3-5 – *CFRP Strips U-Wrapped around the Girder Bulb on specimen 2 (1 in.=2.54 cm)*

Final cross section of specimen 2 is depicted in Figure III-3-6; in Table III-3-2 the properties of CFRP 130 utilized to upgrade the specimen are summarized.

Type of fiber	CF 130 (High Strength Carbon Fiber Fabric)
Fabric Architecture	Unidirectional
Nominal Thickness mm per ply (in. per ply)	0.165mm/ply (0.0065 in./ply)
Ultimate tensile Strength MPa (ksi)	3800 MPa (550 ksi)
Tensile Modulus of elasticity GPa (ksi)	227 GPa (33,000 ksi)
Rupture strain	1.67%

Table III-3-2-CFRP 130 properties

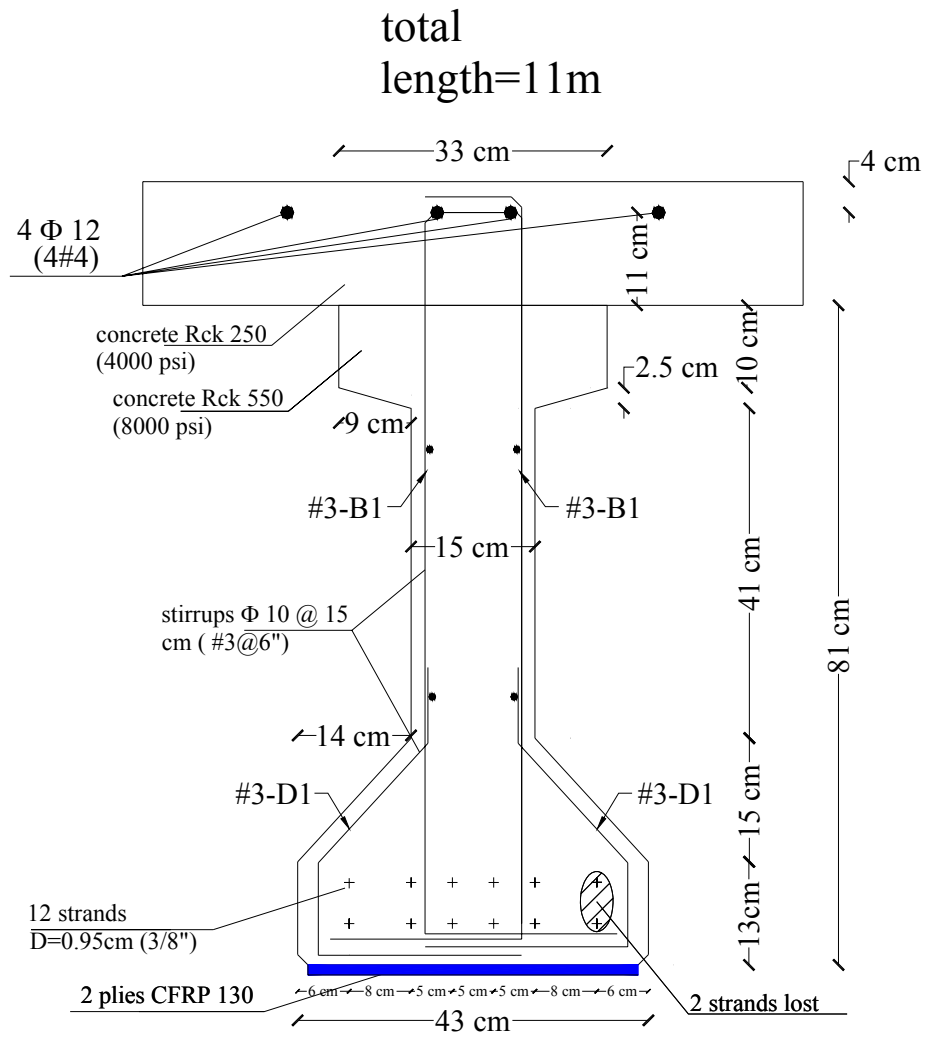


Figure III-3-6-Second Specimen mid-span cross section (1 in.=2.54 cm)

In Appendix B each construction step is documented by pictures.

4. MATERIALS CHARACTERIZATION

This chapter presents materials properties used in the experimental program. Compressive characterization through laboratory testing was performed for girder and deck concrete cylinders. In the case of steel rods and prestressed concrete strands data from the manufacturer are provided.

-Girder concrete

Six cylinders were manufactured in order to verify mechanical properties of girder concrete. Their dimensions were 102 by 203 mm (4 by 8 in.) (see Figure III-4-1). Compression tests were performed under a Tinius Olsen Test machine (Figure III-4-1). Test results are presented in Table III-4-1.



Figure III-4-1- *Girder Concrete cylinders*



Figure 4-2- *Compression test under a Tinius Olsen Test machine*

Days	Cylinder #	Compressive Strength
		f'_c MPa (psi)
28	G1	59.1 (8572)
28	G2	59.5 (8637)
28	G3	52.5 (7620)
28	G4	58.8 (8526)
28	G5	59.3 (8599)
28	G6	57.6 (8352)
	AVERAGE	57.8 (8381)

Table III-4-1- *Test results for girder concrete cylinders*

- Deck concrete

Ten cylinders were manufactured in order to verify mechanical properties of deck concrete. Their dimensions were 102 by 203 mm (4 by 8 in.) (see Figure III-4-3). Compression tests were performed under a Tinius Olsen Test machine as before. Test results are presented in Table III-4-2.



Figure III-4-3 -Deck concrete cylinders

Days	Cylinder #	Compressive Strength
		f'c MPa (psi)
6	D1	18.3 (2660)
6	D2	19.3 (2800)
6	AVERAGE	18.8 (2726)
20	D3	27.0 (3923)
20	D4	29.5 (4285)
20	AVERAGE	28.2 (4096)
28	D5	29.3 (4248)
28	D6	29.8 (4321)
28	D7	28.7 (4161)
28	D8	27.5 (3988)
28	D9	28.2 (4089)
28	D10	29.4 (4263)
28	AVERAGE	28.8 (4178)

Table III-4-2- Test results for deck concrete cylinders

-Prestressed concrete strands

The data concerning prestressing tendons are certified by “Insteel wire Products Company” conforms to ACI. Material properties are summarized in Table III-4-3.

Ultimate breaking strength, kN (lbs.)	1080 (24300)
Load @ 1% extension, MPa (lbs)	98.3 (221009)
Ultimate elongation, %	6.1
Representative area , cm ² (in. ²)	0.54 (0.085)
Actual area, cm ² (in. ²).	0.55(0.08579)
Modulus of elasticity, ksi	128990 (29000)

Table III-4-3- Prestressed concrete strands properties

-Mild steel

The data concerning mild steel #4 grade 60 used as deck reinforcement are certified by the manufacturing source conforms to ACI. Material properties are summarized in Table III-4-4.

Type	Grade 60
Yield strength, kN (lbs)	267 (60000)
Ultimate strength, lbs	400 (90000)
Weight per foot, N (lb)	3 (0.668)
Diameter, mm. (in)	13 (0.5)
Actual area, cm ² in ² .	1.30 (0.20)
Modulus of elasticity,MPa (ksi)	200 (29.0)

Table III-4-4- Mild steel properties

5. THEORETICAL PREDICTIONS

According to the above theoretical assumptions, analytical results with reference to undamaged, virgin damaged and damaged and CFRP upgraded specimen are expressed as follows:

-Undamaged beam

First is necessary to compute the effective prestress force:

$$P_f = P_i - (ES + CR + SH + RE)$$

where:

P_f = Effective prestress force considering total losses

P_i = Initial prestress force

ES = elastic shortening

CR = creep of concrete

SH = shrinkage of concrete

RE = relaxation of tendon

The terms CR and RE are long time losses so that they are not include in this case of study. Therefore:

$$P_f = P_i - (ES + SH) = 845 \text{ kN (190 kips)}$$

$$P_i = 0.75 f_{pu} A_p = 916 \text{ kN (206 kips)}$$

$$f_{pu} = 1862 \text{ MPa (270 ksi)}$$

$$A_p = 0.548 \cdot 12 = 6.58 \text{ cm}^2 (1.02 \text{ in.}^2)$$

$$ES = k_{es} E_{ps} f_{ci} / E_{ci} = 62 \text{ Mpa (10.8 ksi)}$$

$$K_{es} = 1.0$$

$$E_{ps} = 200 \text{ GPa (29000 ksi)}$$

$$f_{cir} = k_{cir} \left(\frac{P_i}{A_{cg}} + \frac{P_i e^2}{I_{cg}} \right) - \left(\frac{M_g e}{I_{cg}} \right) = 8.60 \text{ Mpa (1.248 ksi)}$$

$$E_{ci} = 35 \text{ Gpa (5098 ksi)}$$

$$SH = (8.2 \cdot 10^{-6}) k_{sh} E_s (1 - 0.06 V/S) (100 - R.H.) = 35.8 \text{ Mpa (5.2 ksi)}$$

In order to evaluate the nominal moment of the section is necessary to solve the following equilibrium equation in which the unknown is c (depth of neutral axis).

$$f_{ps} A_p = 0.85 f'_c \beta_1 c b + A'_s \varepsilon_s E_s$$

where:

$$f_{ps} = f_{pu} \left(1 - \frac{\gamma_p}{\beta_1} \left[\rho_p \frac{f_{pu}}{f'_c} + \frac{d}{d_p} (\omega - \omega') \right] \right) = 255 \text{ ksi (1758 MPa) (ACI}$$

according)

$$f_{pu} = 1862 \text{ MPa (270 ksi)}$$

$$\beta_1 = 0.85$$

$$f_{py} = 1675 \text{ MPa (243 ksi)}$$

$$\gamma_p = 0.28 \quad (\text{considering that } f_{py} / f_{pu} = 0.9)$$

$$\rho_p = A_p / A_{cs} = 0.002$$

$$d = d_p = 89 \text{ cm (35 in.)}$$

$$\omega = \rho f_y / f'_c = (A_s / bd) (f_y / f'_c) = 0$$

$$\omega' = \rho' f'_y / f'_c = (A'_s / bd') (f'_y / f'_c) = 0.25$$

$$d' = 3.81 \text{ cm. (1.5 in.)}$$

$$f_{ps} = 270 - \frac{0.04}{\varepsilon_p - 0.007} = 1855 \text{ MPa (269 kips) (more sophisticated analysis)}$$

$$\varepsilon_p = \varepsilon_1 + \varepsilon_2 + \varepsilon_3 = 0.044$$

$$\varepsilon_1 = \frac{P_f}{E_p A_p} = 0.0057$$

$$\varepsilon_2 = \frac{P_f}{A_{cg} E_{cg}} + \frac{P_f e^2}{E_{cg} I_g} - \frac{M_g e}{E_{cg} I_g} = -0.000208$$

$$\varepsilon_3 = \varepsilon_{cu} \frac{(d_p - c)}{c} = 0.038$$

$$A_p = 0.548 \cdot 12 = 6.58 \text{ cm}^2 (1.02 \text{ in.}^2)$$

$$f'_c = (\text{deck}) = 27.58 \text{ MPa (4000 psi)}$$

$$\beta_1 = 0.85$$

$$b = 81.3 \text{ cm (32 in.)}$$

$$A'_s = 1.29 \cdot 4 = 5.16 \text{ cm}^2 (0.80 \text{ in.}^2)$$

$$\varepsilon'_s = (\varepsilon_{cu} (c - d'))/c$$

$$E_s = 200 \text{ GPa (29000 ksi)}$$

Therefore from equilibrium equation:

$$c = 6.37 \text{ cm (2.509 in.) (ACI according)}$$

$$c = 6.70 \text{ cm. (2.640 in.) (more sophisticated analysis)}$$

$$M_n = A_p f_{ps} \left(d_p - \frac{\beta_1 c}{2} \right) + A'_s f'_s \left(\frac{\beta_1 \cdot c}{2} - d' \right) = 995 \text{ kN-m (734 kips-ft) (ACI$$

according)

$$M_n = A_p f_{ps} \left(d_p - \frac{\beta_1 c}{2} \right) + A'_s f'_s \left(\frac{\beta_1 \cdot c}{2} - d' \right) = 1048 \text{ kN-m (773 kips-ft) (more$$

sophisticated analysis)

Cracking moment M_{cr} is compute as follows:

$$M_{cr} = f_r S_b + P_f \left(e + \frac{r^2}{c_b} \right) = 627 \text{ kN-m (463 kips - ft)}$$

$$f_r = 7.5 \sqrt{f'_c} = 4.6 \text{ MPa (0.67 ksi)}$$

$$S_b = 69920 \text{ cm}^3 (4266 \text{ in.}^3)$$

$$c_b = 90.2 \text{ cm (35.5 in.)}$$

$$P_f = 845.1 \text{ kN (190000 lb.)}$$

$$e = 31.0 \text{ cm (12.24 in.)}$$

$$r_g = \sqrt{I_{cg} / A_{cg}} = 21.0 \text{ cm (8.3 in.)}$$

- Virgin damaged beam

First is necessary to compute the effective prestress force:

$$P_f = P_i - (ES + CR + SH + RE)$$

The terms CR and RE are long time losses so that they are not include in this case of study. Therefore:

$$P_f = P_i - (ES + SH) = 690 \text{ kN (155 kips)}$$

$$P_i = 0.75 f_{pu} A_p = 765 \text{ kN (172 kips)}$$

$$f_{pu} = 1862 \text{ MPa (270 ksi)}$$

$$A_p = 0.548 \cdot 10 = 5.48 \text{ cm}^2 (0.85 \text{ in.}^2)$$

$$ES = k_{es} E_{ps} f_{cir} / E_{ci} = 67.5 \text{ Mpa (9.8 ksi)}$$

$$SH = (8.2 \cdot 10^{-6}) k_{sh} E_s (1 - 0.06 V/S) (100 - R.H.) = 49.6 \text{ Mpa (7.2 ksi)}$$

In order to evaluate the nominal moment of the section is necessary to solve the following equilibrium equation in which the unknown is c (depth of neutral axis).

$$f_{ps} A_p = 0.85 f'_c \beta_1 c b + A'_s \varepsilon_s E_s$$

where:

$$f_{ps} = f_{pu} \left(1 - \frac{\gamma_p}{\beta_1} \left[\rho_p \frac{f_{pu}}{f_c} + \frac{d}{d_p} (\omega - \omega') \right] \right) = 1758 \text{ MPa (255 ksi) (ACI}$$

according)

$$f_{pu} = 1862 \text{ MPa (270 ksi)}$$

$$\beta_1 = 0.85$$

$$f_{py} = 1675 \text{ MPa (243 ksi)}$$

$$\gamma_p = 0.28 \quad (\text{considering that } f_{py} / f_{pu} = 0.9)$$

$$\rho_p = A_p / A_{cs} = 0.00076$$

$$d = d_p = 89 \text{ cm (35 in.)}$$

$$\omega = \rho f_y / f_c = (A_s / bd) (f_y / f_c) = 0$$

$$\omega' = \rho' f_y' / f_c = (A_s' / bd') (f_y' / f_c) = 0.25$$

$$d' = 3.81 \text{ cm (1.5 in.)}$$

$$f_{ps} = 270 - \frac{0.04}{\varepsilon_p - 0.007} = 1860 \text{ MPa (269.7 kips) (more sophisticated}$$

analysis)

$$\varepsilon_p = \varepsilon_1 + \varepsilon_2 + \varepsilon_3 = 0.052$$

$$\varepsilon_1 = \frac{P_f}{E_p A_p} = 0.0056$$

$$\varepsilon_2 = \frac{P_f}{A_{cg} E_{cg}} + \frac{P_f e^2}{E_{cg} I_g} - \frac{M_g e}{E_{cg} I_g} = -0.0000036$$

$$\varepsilon_3 = \varepsilon_{cu} \frac{(d_p - c)}{c} = 0.046$$

$$A_p = 0.548 \cdot 10 = 5.48 \text{ cm}^2 (0.85 \text{ in.}^2)$$

$$f_c = (\text{deck}) = 27.58 \text{ MPa (4000 psi)}$$

$$\beta_1 = 0.85$$

$$b = 81.3 \text{ cm (32 in.)}$$

$$A'_s = 1.29 \cdot 4 = 5.16 \text{ cm (0.80 in.}^2)$$

$$\varepsilon'_s = (\varepsilon_{cu} (c-d'))/c$$

$$E_s = 200 \text{ GPa (29000 ksi)}$$

Therefore from equilibrium equation:

$$c = 5.38 \text{ cm (2.122 in.) (ACI according)}$$

$$c = 5.66 \text{ cm (2.230 in.) (more sophisticated analysis)}$$

$$M_n = A_p f_{ps} \left(d_p - \frac{\beta_1 c}{2} \right) + A'_s f'_s \left(\frac{\beta_1 \cdot c}{2} - d' \right) = 834 \text{ kN-m (615 kips-ft) (ACI}$$

according)

$$M_n = A_p f_{ps} \left(d_p - \frac{\beta_1 c}{2} \right) + A'_s f'_s \left(\frac{\beta_1 \cdot c}{2} - d' \right) = 880 \text{ kN-m (649 kips-ft) (more}$$

sophisticated analysis)

- Intentionally damaged and CFRP upgraded beam

P_f is the same of virgin damaged specimen:

$$P_f = P_i - (ES+SH) = 690 \text{ kN (155 kips)}$$

In this case is necessary to compute:

$$\varepsilon_{bi} = \frac{M_{ip} \cdot c_b}{I_g \cdot E_{cg}} - \frac{P_f}{A_{cg} \cdot E_{cg}} \cdot \left(1 + \frac{e \cdot c_b}{r_g^2} \right) = 0.0002$$

$$M_{ip} = 111.28 \text{ kN-m (82.08 kips-ft)}$$

$$I_g = 3583540 \text{ cm}^4 (86380 \text{ in.}^4)$$

$$E_{cg} = 35150 \text{ MPa (5098} \cdot 10^3 \text{ psi)}$$

$$c_b = 71.1 \text{ cm (28 in.)}$$

$$A_{cg} = 2009.8 \text{ cm}^2 (311.5 \text{ in.}^2)$$

$$e = 31.3 \text{ cm (12.32 in.)}$$

$$I_g = 1464718.3 \text{ cm}^4 \text{ (35190 in.}^4\text{)}$$

$$k_m = 0.8$$

$$\varepsilon_{fe} = \varepsilon_{fu} k_m = 0.8 \cdot 0.0167 = 0.014$$

Using the trial and error procedure is possible to determine the depth to the neutral axis: $c = 3.226 \text{ in. (8.19 cm)}$

$$\varepsilon_{cu} \left(\frac{h-c}{c} \right) - \varepsilon_{bi} = 0.0298$$

Therefore because $\varepsilon_{fe} < \varepsilon_{cu} \left(\frac{h-c}{c} \right) - \varepsilon_{bi}$ FRP failure (rupture or debonding) controls flexural failure of the section.

Finally the nominal flexural capacity of the section with FRP external reinforcement can be computed from next equation

$$M_n = A_p f_{ps} \left(d_p - \frac{\beta_1 c}{2} \right) + \psi_f A_f f_{fe} \left(h - \frac{\beta_1 c}{2} \right) - A'_s f'_s \left(\frac{\beta_1 c}{2} - d' \right)$$

$$f_{ps} = f_{pu} \left(1 - \frac{\gamma_p}{\beta_1} \left[\rho_p \frac{f_{pu}}{f'_c} + \frac{d}{d_p} (\omega - \omega') \right] \right) = 1758 \text{ MPa (255 ksi) (ACI}$$

according)

$$f_{pu} = 1862 \text{ MPa (270 ksi)}$$

$$\beta_1 = 0.85$$

$$f_{py} = 1675 \text{ MPa (243 ksi)}$$

$$\gamma_p = 0.28 \quad (\text{considering that } f_{py} / f_{pu} = 0.9)$$

$$\rho_p = A_p / A_{cs} = 0.00076$$

$$d = d_p = 89 \text{ cm (35 in.)}$$

$$\omega = \rho f_y / f'_c = (A_s / bd) (f_y / f'_c) = 0$$

$$\omega' = \rho f_y' / f_c' = (A_s' / bd') (f_y' / f_c') = 0.25$$

$$d' = 3.81 \text{ cm (1.5 in.)}$$

$$f_{ps} = 270 - \frac{0.04}{\varepsilon_p - 0.007} = 1848 \text{ MPa (268 kips)} \text{ (more sophisticated}$$

analysis)

$$\varepsilon_p = \varepsilon_1 + \varepsilon_2 + \varepsilon_3 = 0.013$$

$$\varepsilon_1 = \frac{P_f}{E_p A_p} = 0.0056$$

$$\varepsilon_2 = \frac{P_f}{A_{cg} E_{cg}} + \frac{P_f e^2}{E_{cg} I_g} - \frac{M_g e}{E_{cg} I_g} = -0.0000036$$

$$\varepsilon_3 = \varepsilon_{cu} \frac{(d_p - c)}{c} = 0.046$$

$$A_p = 0.548 \cdot 10 = 5.48 \text{ cm}^2 \text{ (0.85 in.}^2\text{)}$$

$$d_p = 88.9 \text{ cm (35 in.)}$$

$$\beta_1 = 2 - \left[4 \cdot \frac{(\varepsilon_c / \varepsilon_c') - \tan^{-1}(\varepsilon_c / \varepsilon_c')}{(\varepsilon_c / \varepsilon_c') \ln(1 + \varepsilon_c^2 / \varepsilon_c'^2)} \right] = 0.72$$

$$\varepsilon_c = \varepsilon_{fe} \frac{c}{h - c} = 0.0014$$

$$\varepsilon_c' = \frac{1.71 f_c'}{E_c} = 0.0019$$

$$\psi_f = 0.85$$

$$A_f = 0.1651 \cdot 35.6 = 5.87 \text{ cm}^2 \text{ (0.91 in.}^2\text{)}$$

$$f_{fe} = E_f \cdot \varepsilon_{fe} = 227000 \cdot 0.014 = 3178 \text{ MPa (462 ksi)}$$

$$h = 96.5 \text{ cm (38 in.)}$$

$$A_s' = 1.29 \cdot 4 = 5.16 \text{ cm}^2 \text{ (0.80 in.}^2\text{)}$$

$$\varepsilon'_s = (\varepsilon_{fu} + \varepsilon_{bi}) \left(\frac{c - d'}{h - c} \right) = 0.00008$$

$$E_s = 200 \text{ GPa (29000 ksi)}$$

$$f_s = 137.9 \text{ MPa (20 ksi)}$$

$$d' = 3.81 \text{ cm (1.5 in.)}$$

$$M_n = A_p f_{ps} \left(d_p - \frac{\beta_1 c}{2} \right) + \psi_f A_f f_{fe} \left(h - \frac{\beta_1 c}{2} \right) - A'_s f'_s \left(\frac{\beta_1 c}{2} - d' \right) = 1171 \text{ kN-m (814}$$

kips-ft) (ACI according)

$$M_n = A_p f_{ps} \left(d_p - \frac{\beta_1 c}{2} \right) + \psi_f A_f f_{fe} \left(h - \frac{\beta_1 c}{2} \right) - A'_s f'_s \left(\frac{\beta_1 c}{2} - d' \right) = 1239 \text{ kN-m (914}$$

kips-ft) (More sophisticated analysis)

Cracking moment M_{cr} is compute as follows:

$$M_{cr} = f_r S_b + P_f \left(e + \frac{r^2}{c_b} \right) = 566 \text{ kN-m (417 kips - ft)}$$

$$f_r = 7.5 \sqrt{f'_c} = 4.6 \text{ MPa (0.67 ksi)}$$

$$S_b = 68872 \text{ cm}^3 \text{ (4197 in.}^3\text{)}$$

$$c_b = 90.2 \text{ cm (35.5 in.)}$$

$$P_f = 689.4 \text{ kN (155000 lb.)}$$

$$e = 31.0 \text{ cm (12.24 in.)}$$

$$r_g = \sqrt{I_{cg} / A_{cg}} = 21.0 \text{ cm (8.3 in.)}$$

In Table III-5-1 theoretical results in terms of nominal moment capacity, strain in the prestressing steel and in CFRP laminates with reference to undamaged, virgin damaged and CFRP upgraded beam are summarized:

BEAM TYPE	UNDAMAGED	VIRGIN DAMAGED	CFRP 130 UPGRADED
TOTAL TENDONS AREA cm ² (in. ²)	6.58 (0.085 · 12)=1.02	5.48 (0.085x10=0.85)	5.48 (0.085x10=0.85)
CRACKING MOMENT M _{cr} kN-m (kips-ft)	627 (463)	557 (410)	566 (417)
NOMINAL MOMENT M _n ACI approach kN-m (kips-ft)	995 (734) ACI 318	834 (615) ACI 318	1082 (798) ACI 440
ULTIMATE TENDONS STRAIN ε _p (in./in.)	0.0389	0.0465	0.012
FRP ULTIMATE STRAIN ε _{fe} (in./in.)	-	-	0.014
NOMINAL MOMENT M _n More sophisticated analysis kN-m (kips-ft)	1048 (773)	880 (649)	1171 (814)

Table III-5-1-Theoretical results

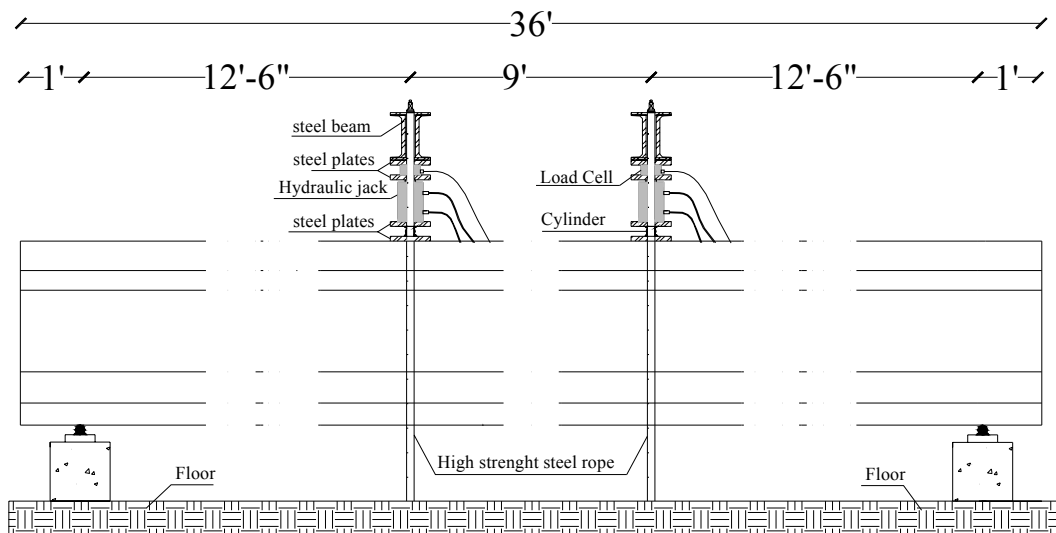
The table shows that ACI approach is, in terms of nominal moment capacity, more conservative than a sophisticated analysis .

6. TEST SETUP AND INSTRUMENTATION

Both specimens were tested utilizing a four point bending configuration with a distance between supports of 10.36 m (34 ft). The constant moment region was 2.8 m (9 ft) long.

Two hydraulic jacks with capacity of 890 kN (200 kips) were used to apply the load, recorded by load cells placed on each jack. A real time measurement of the structural response was achieved using an electronic data acquisition system. (see Figure III-6-1).

The load was applied by cycles of loading and unloading. An initial cycle based on a low load was performed in each specimen to verify that both the mechanical and electronic equipment worked properly (see Table III-6-1)



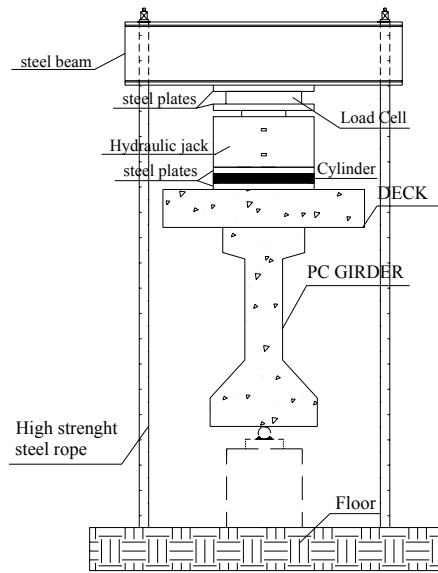


Figure III-6-1- Test Set up

Cycle	Load Range kN (kips)
0	0-3.1-0 (0-0.7-0)
1	0-134.4-44.6 (0-30-10)
2	22.3-271.2-44.6 (10-60-10)
3	22.3-406.8-44.6 (10-90-10)
4	22.3-542.4-44.6 (10-120-10)
5	22.3- failure (10-failure)

Table III-6-1- Load cycles

-Instrumentation Specimen 1 (undamaged)

In order to evaluate the strain in the tendons, two strain gages were applied on them before casting the girder; one on tendon 3 and one on tendon 9, both at mid-span. In Table III-6-1 strain recorded on these tendons before and after prestressing stage are reported:

SPECIMEN 1: UNDAMAGED				
	ε_o (load=2.4kips)[$\mu\varepsilon$]	ε_f (full load=17.2kips)[$\mu\varepsilon$]	$\Delta\varepsilon$ [$\mu\varepsilon$]	f_p MPa [ksi]
Tendon#3	2732	7860	5128	1011.5 (146.7)
Tendon#9	1486	6250	4764	939.8 (136.3)

Table III-6-2 – Strain on tendons due to prestress

Initial prestress applied on each strand by manufacturer was 76.5 kN (17.2 kips) that gave a total initial prestress:

$P_i = 12 \cdot 76.5 = 918 \text{ kN (206 ksi)}$ exactly as expected by theoretical prediction.

Two strain gages were applied at mid-span on the concrete top deck in order to measure the concrete strain in compression. Strain gages positions and details are shown in Figure III-6-2 and Figure III-6-3.

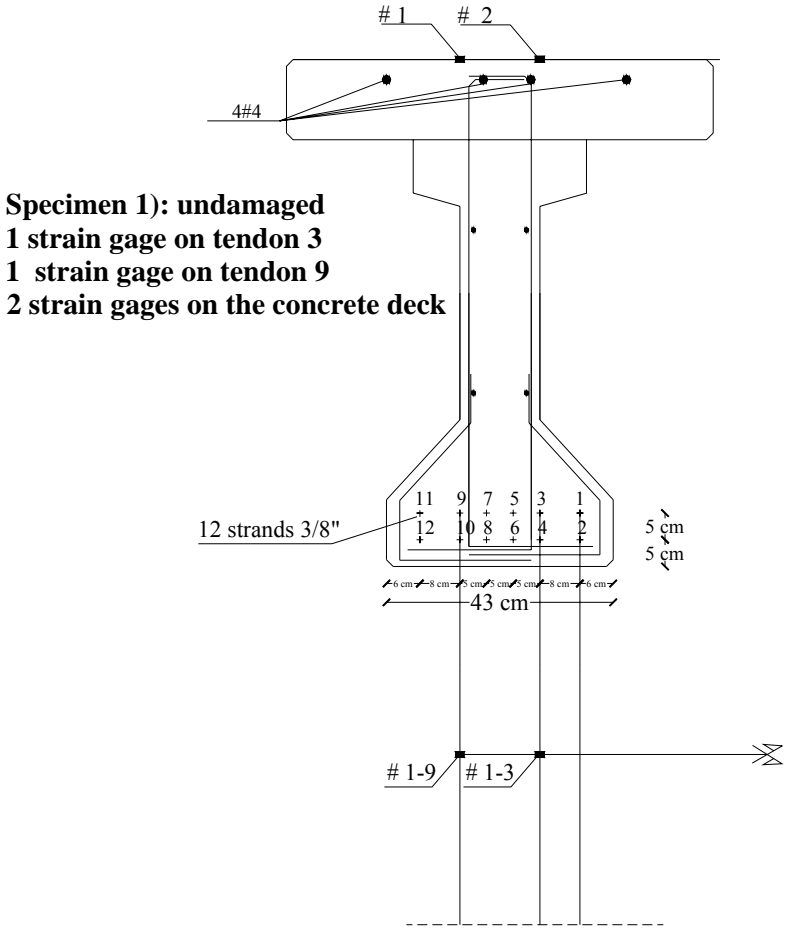


Figure III-6-2- *Strain gages on the specimen 1 (1 in. = 2.54 cm)*

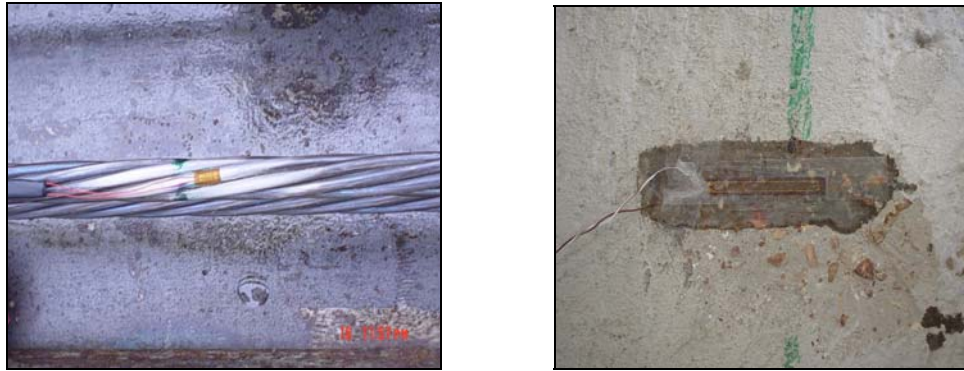


Figure III-6-3- *Detail strain gauges on the tendon and on the concrete*

Furthermore, two stringer LVDTs (stringer LVDTs #1 and stringer LVDTs #2) (linear variable displacement transducers) were placed at mid-span and four more were located along the specimen (two at 4.5 ft (1.37 m) from mid-span, LVDTs #3 and LVDTs #4 and two at support position LVDTs #5 and LVDTs #6) (see Figure III-6-4)

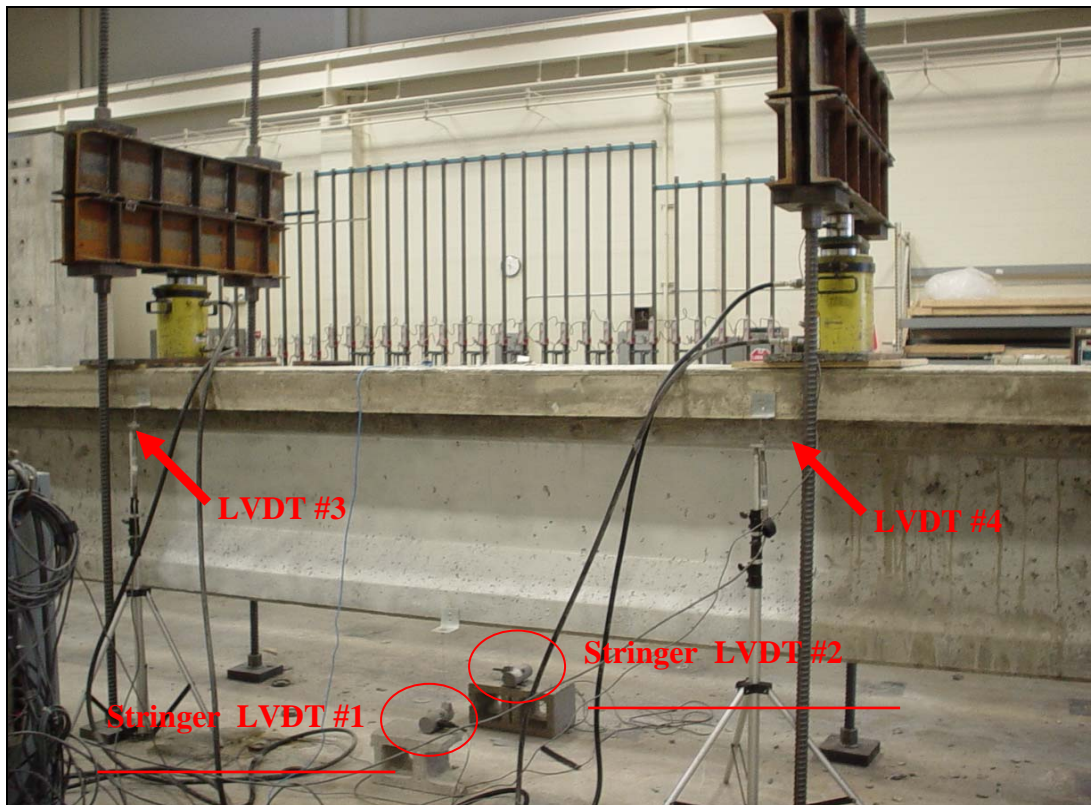


Figure III-6-4- Stringer LVDTs and LVDTs positions

-Instrumentation Specimen 2 (intentionally damaged and upgrade)

Specimen 2 was intentionally damaged and then upgraded by 2 CFRP plies 35.6 cm (14 in.); the double-ply laminate was centered over

the damaged area at mid-span. Furthermore eight strips, 25.4 cm (10 in.) wide and spaced at 45.7 cm (18 in.) on centers, were U-wrapped around the bulb of the girder.

In order to evaluate the strain in tendons, four strain gages were applied on tendons, one on tendon 3, one on tendon 9 at mid-span and other two on the intentionally cut tendon 1 at 20.32 cm (8 in.) and 66.04 cm (26 in.) from mid-span respectively. In Table III- 6-3 the strains recorded on tendon 1 (20.3 cm (8 in.) from mid-span) before and after prestressing stage is reported:

SPECIMEN 2: DAMAGED				
	ϵ_o (load=2.4kips) [$\mu\epsilon$]	ϵ_f (full load=17.2kips) [$\mu\epsilon$]	$\Delta\epsilon$ [$\mu\epsilon$]	f_p MPa [ksi]
Tendon#1 (20.3 cm, 8 in. from mid-span)	1894	6600	4706	928.0 (134.6)

Table III- 6-3 - Strain on tendons due to prestress

Initial prestress applied on each strand by manufacturer was 76.5 kN (17.2 kips) that gave a total initial prestress:

$P_i = 10 \cdot 76.5 = 765$ kN (172 ksi) exactly as expected by theoretical prediction.

Six strain gages were applied on concrete surface, two at mid-span and other four symmetrically disposed at 20.32 cm (8 in.) and 66.04 cm (26 in.) respectively from each side of mid-span in order to evaluate the concrete strain in compression and the moment curvature diagram. For this specimen were also applied six strain gages along the FRP

reinforcement, two at mid-span and other four symmetrically disposed at 10.16 cm (4 in.) and 55.88 cm (22 in) respectively from each side of mid-span. (see

Figure III-6-5)



Figure III-6-5 – Strain gage on CFRP detail

Strain gauges positions and details are shown in Figure III-6-6

Finally concerning stringer LVDTs and LVDTs t the same configuration utilized for first specimen was adopted.

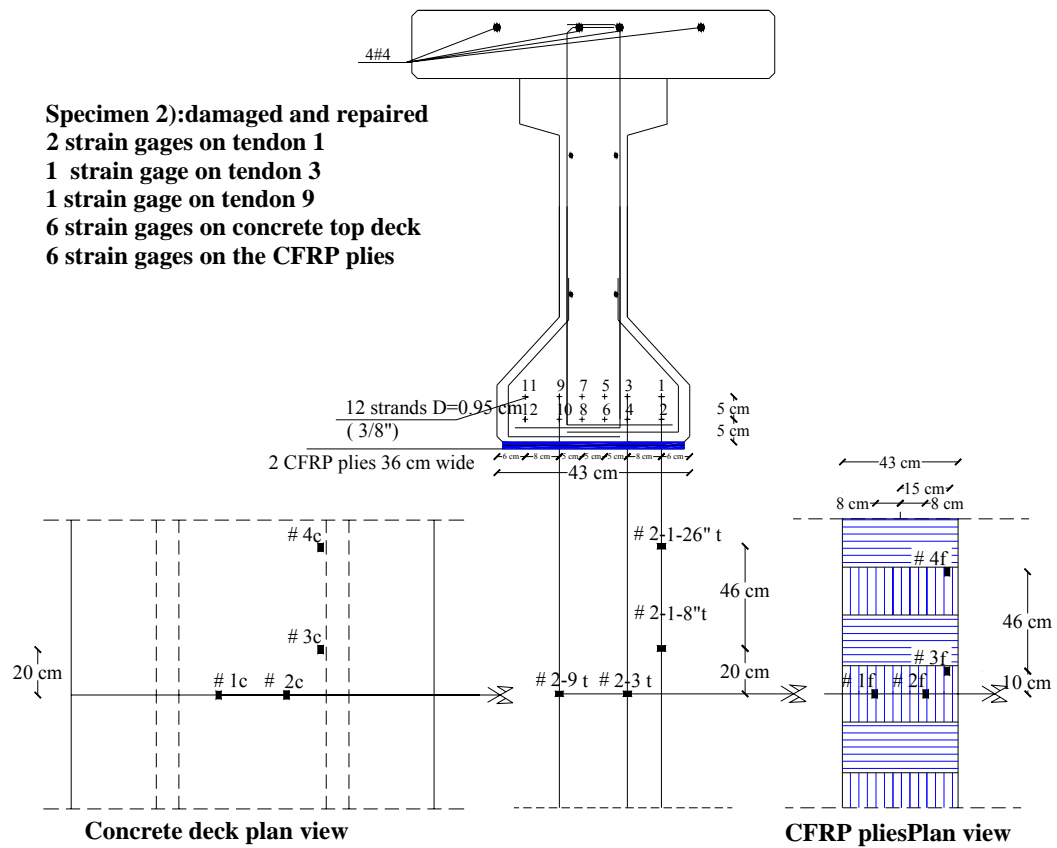


Figure III-6-6 – Strain gages on specimen 2(1 in.=)2.54 cm)

7. TEST RESULTS

-Specimen 1 (undamaged)

After a low load cycle to check the instrumentation applied on the PC girder, the specimen was subjected to five load cycles as above mentioned. No visible cracks were observed during the two initial load cycles while the first crack was observed in the third at 391.4 kN (88 kips) load (that give a $M_{cr}=745$ kN-m (550 kips-ft)) as was expected from analytical calculation. Increasing the external load others flexural cracks were opened along the girder especially near mid-span where a maximum constant flexural action was applied.(see Figure III-7-1)

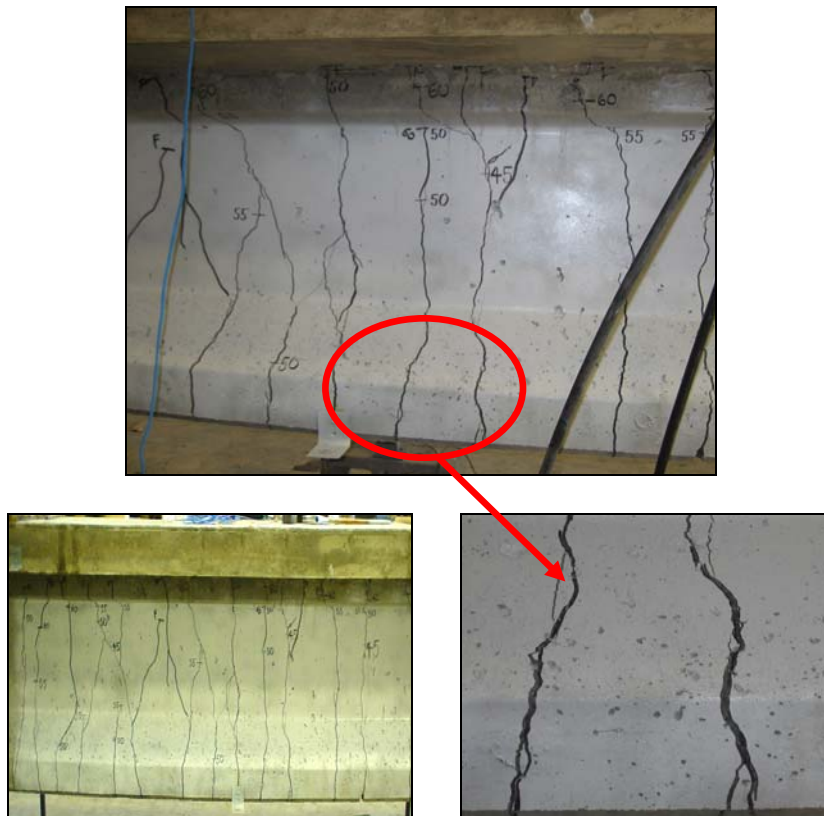


Figure III-7-1- Flexural cracks

It was not need to load this specimen until failure; the maximum load applied on it was 609.36 kN (137 kips) corresponding to a maximum moment of 1161 kN-m (856.25 kips-ft) that was already higher than theoretical moment of 1048.0 kN (773.0 kips-ft).

Load-displacement curves obtained by data provided from two stringer LVDT's placed at mid-span cross-section and LVDT #3 at 1.37 m (4.5 ft) from mid-span are below depicted (see Figure III-7-2 and Figure III-7-3)

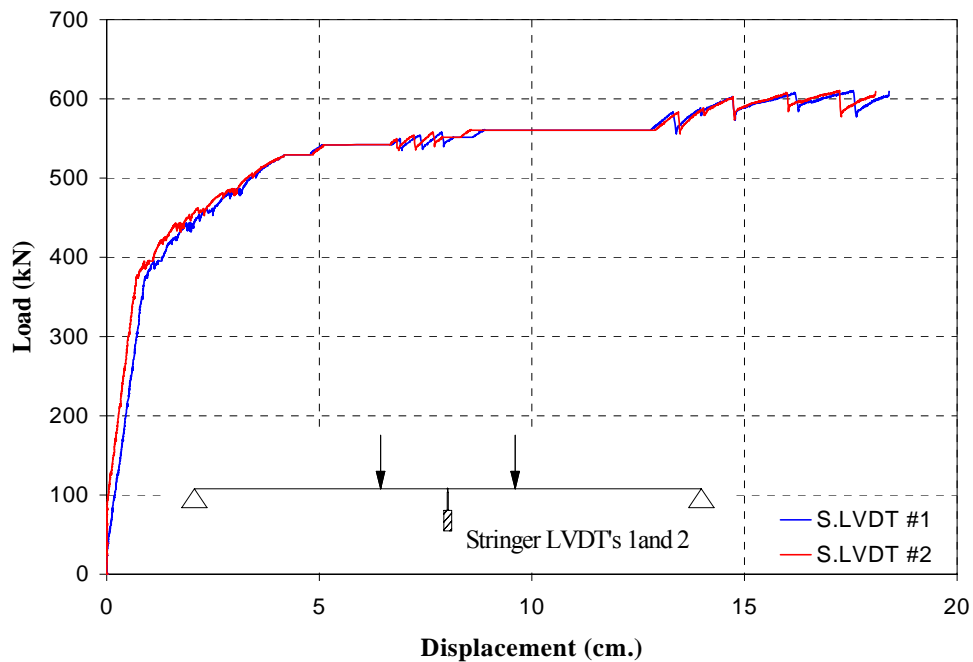


Figure III-7-2- Load-displacement stringer LVDTs #1 and #2

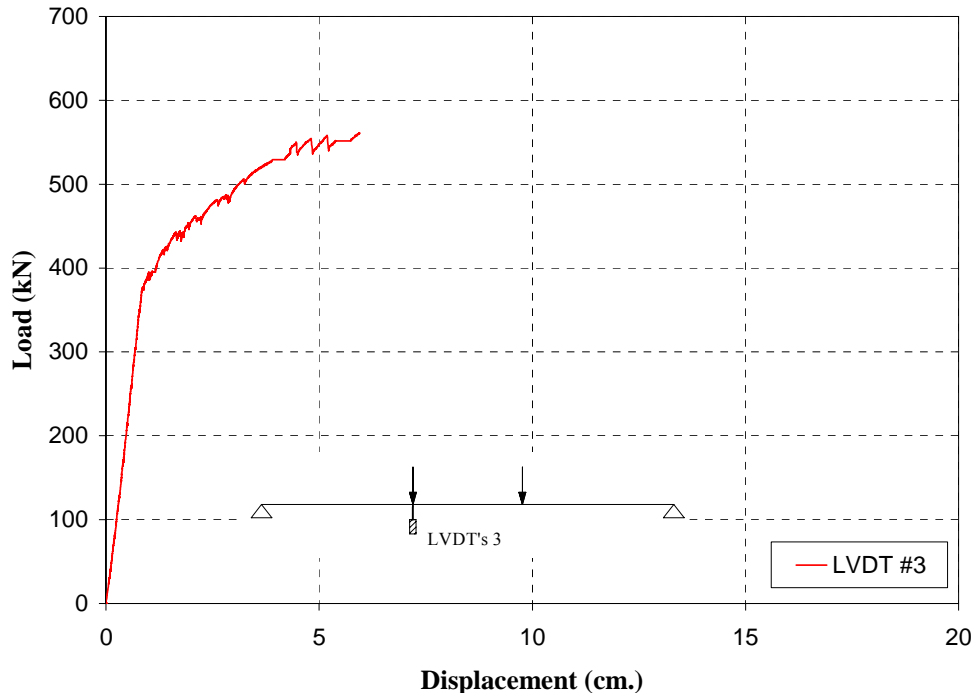


Figure III-7-3- Load-displacement LVDTs #3(1.37 m (4.5 ft) from mid-span)

In Table III-7-1 cracking and maximum load with corresponding displacement values for each diagram are summarized:

	Cracking load $P_{cr.} = 380 \text{ kN}$ (85.4 kips)	Maximum load $P_{max.} = 609.4 \text{ kN}$ (137.0 kips)
Stringer LVDT#1	1.1 (0.4)	18.4 (7.2)
Stringer LVDT#2	1.1 (0.4)	18.0 (7.1)
LVDT #3	0.9 (0.3)	6.0 (2.3)

Table III-7-1- Displacement cm (in.) at cracking and maximum load

In Figure III-7-4 and Figure III-7-5 load- strain curves obtained by data provided from strain gages applied on tendons 3 and 9, and on concrete at mid-span cross section, respectively, are depicted. The strain values on the tendons were read only for some load values, this is the reason for having only some points on the curves. Furthermore these curves are depicted until 534 kN (120 kips) load value because after that threshold the instruments were not working anymore.

Strain value of Figure III-7-4 are plotted starting from the strain value corresponding to that induced in the tendons by the prestressing force.

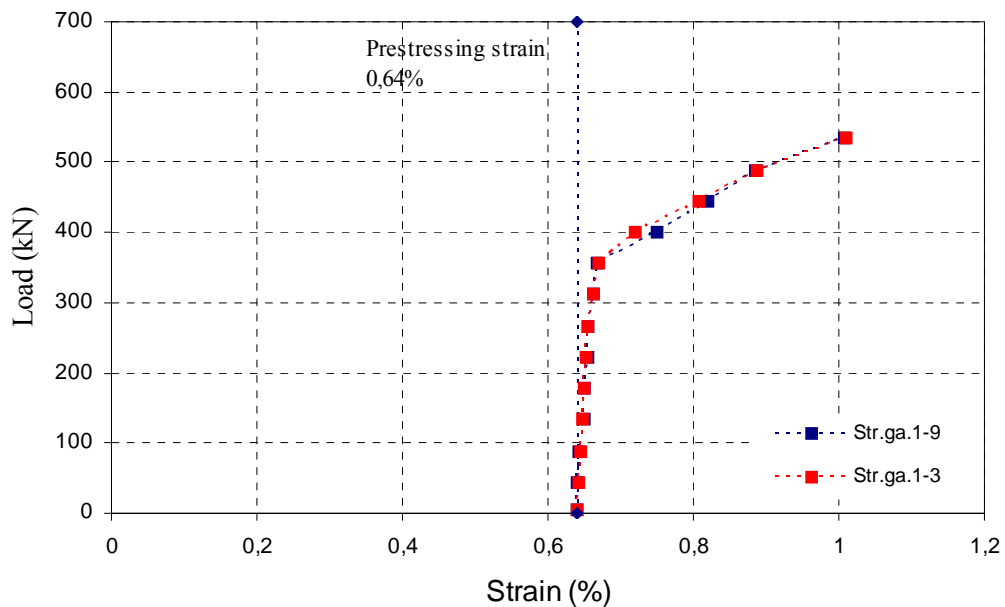


Figure III-7-4- *Strain on tendons placed at mid-span*

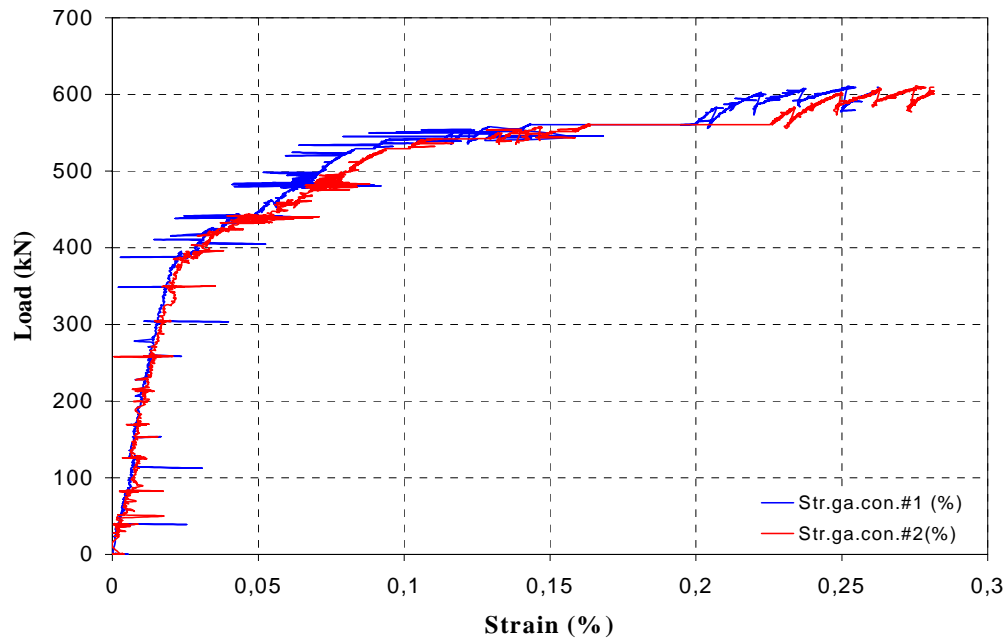


Figure III-7-5- Strain on concrete placed at mid-span

In * *Including strain due to prestress*

Table III-7-2 strain values at cracking load and at maximum load for each strain gage placed at mid-span on concrete and tendons are summarized:

Strain gage	Strain at Cracking load (%)	Strain at Maximum load (%)
#1 concrete	0.03	0.25
#2 concrete	0.03	0.28
#1-3 tendon*	0.67	1.0
#1-9 tendon*	0.67	1.0

* *Including strain due to prestress*

Table III-7-2 – Strain on concrete and tendons

Using strain data concerning strain gages applied on concrete and tendons located in the same position at mid-span cross-section, it was possible to represent two moment-curvature diagram each for every couple of strain gages. Both moment-curvature diagram are reported below: (see Figure III-7-6 and Figure III-7-7)

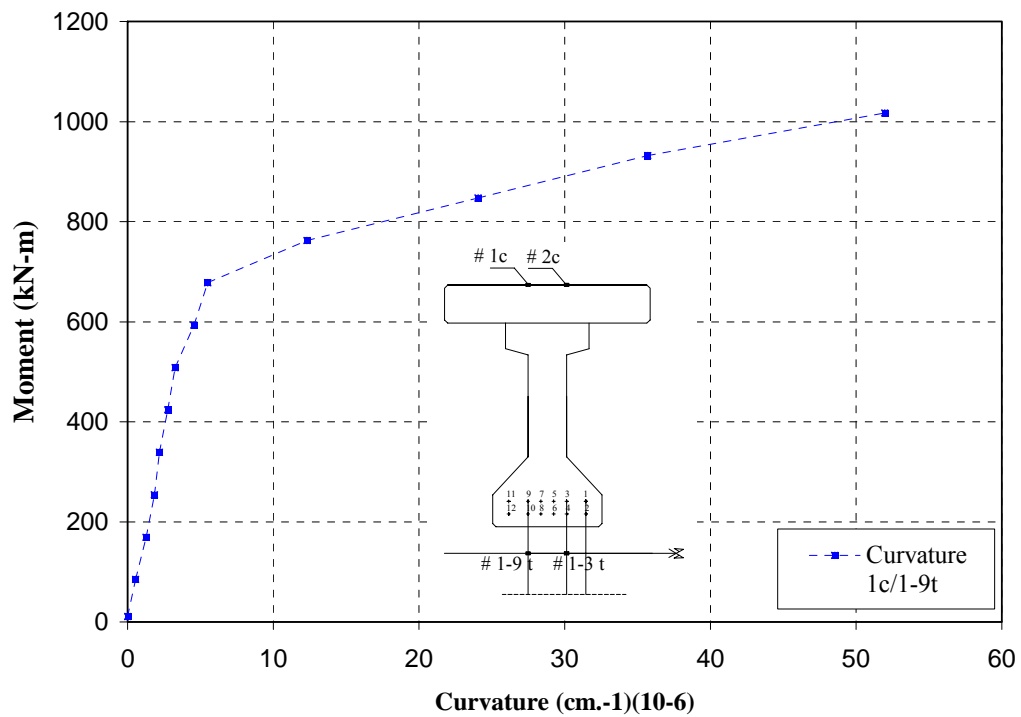


Figure III-7-6– *Moment-curvature (curvature 1c/ 1-9t)*

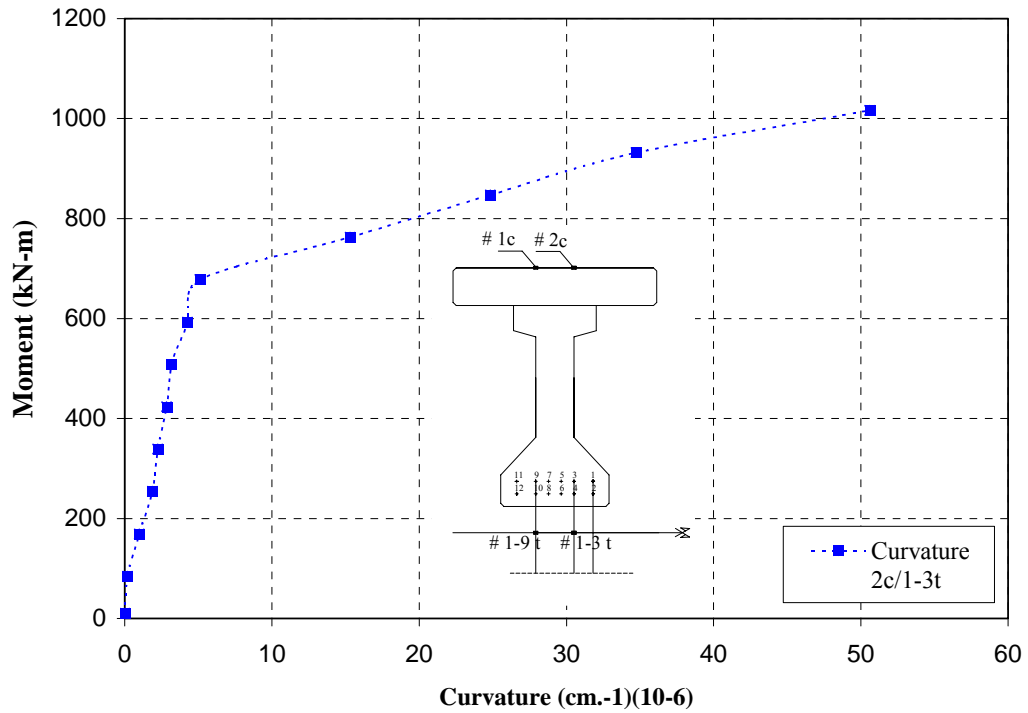


Figure III-7-7– Moment-curvature (2c/1-3t)

In Table III-7-3 experimental cracking and maximum moment with corresponding curvature values are summarized

	Cracking Moment $M_{cr.} = 678 \text{ kN-m (500 kips-ft)}$	Maximum Moment $M_{max.} = 1016 \text{ kN-m (750 kips-ft)}$
Curvature 1c/1-3t $\text{cm}^{-1} (\text{in.}^{-1})$	5.51	51.95
Curvature 2c/1-9t $\text{cm}^{-1} (\text{in.}^{-1})$	5.10	50.59

Table III-7-3– Curvature value at cracking and maximum load

-Specimen 2 (intentionally damaged and upgraded)

After a low load cycle to check the instrumentation applied on the PC girder, the specimen was subjected to five load cycles as above mentioned. No visible cracks were observed during the two initial load cycles while the first crack was observed in the third at 355.8 kN (80 kips) load (that gives a $M_{cr} = 678.0$ kN-m (500.0 kips-ft)). Once 524 kN (120 kips) load was achieved a problem with the two stringer LVDTs placed at mid-span occurred and imposed to stop the test (this test phase will be named step I) and to start it again the day after (step II). Therefore, considering that the cracking moment was already achieved, all curves, obtained by data provided by instrumentations used, are depicted using both data recorded.

Increasing the external load others flexural cracks opened along the girder especially in the constant moment region

A horizontal crack at top girder bulb was also observed.(see Figure III-7-8)



Figure III-7-8– *Cracks pattern*

Failure of CFRP reinforcement was observed at load value of 615.9 kN (138.5 kips) conducting to a failure moment of 1173.5 kN-m (865.6 kips-ft).(see Figure III-7-9)



Figure III-7-9 – *CFRP failure*

After that, once unloaded the specimen, another cycle of loading was applied (step III) in order to observe the mechanical behaviour of the virgin damaged (2 tendons cut) specimen.

The maximum load carried by this specimen was 500.0 kN (112.4 kips) corresponding to a maximum moment of 952.5 kN-m (702.5 kip-ft).

Load-displacement curves obtained by data provided from two stringer LVDTs placed at mid-span are below reported.(see Figure III-7-10 and Figure III-7-11). Since in the first cracking phase the stringer LVDTs did not record any values these curves represent the load displacement diagram obtained by loading and unloading cycles applied on the specimen already cracked. In each diagram two curves are shown: one represent the load-displacement until CFRP failure (step II) and one depict the load – displacement of virgin damaged specimen until rupture (step III).

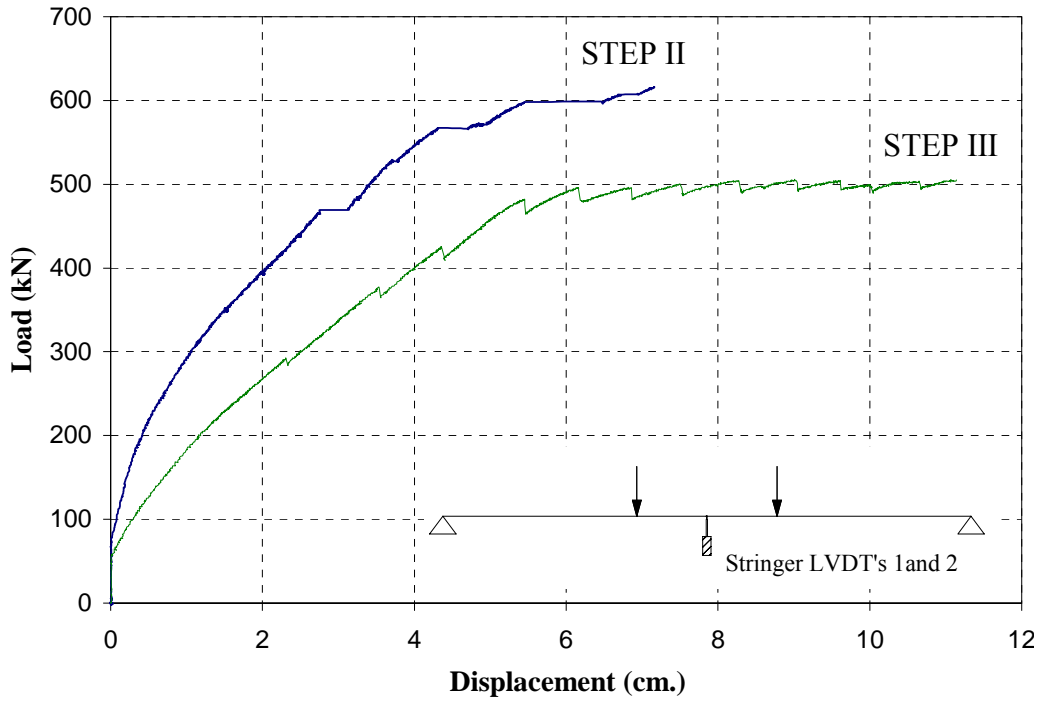


Figure III-7-10- Load-displacement stringer LVDTs #1 (mid-span)

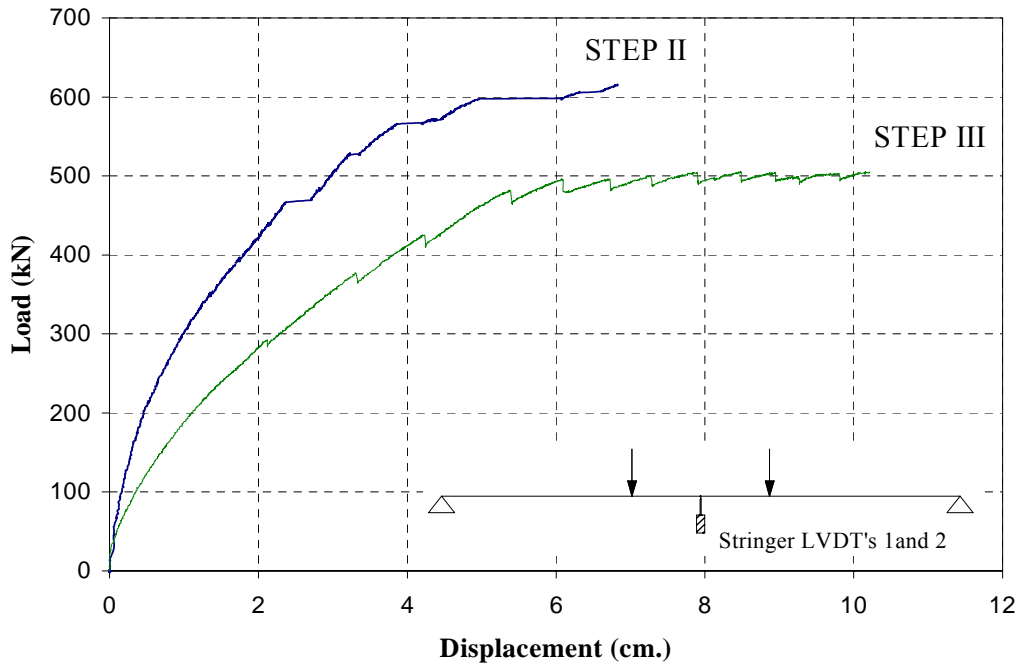


Figure III-7-11– Load-displacement stringer LVDTs #2 (mid-span)

In the diagram obtained by data provided by LVDTs #3 two curves are depicted, one with reference to upgraded specimen during first loading phase (step I) (until 523.6 kN (120 kips)) and another one until CFRP failure (615.92 kN (138.5 kips)) (step II).(see Figure III-7-12)

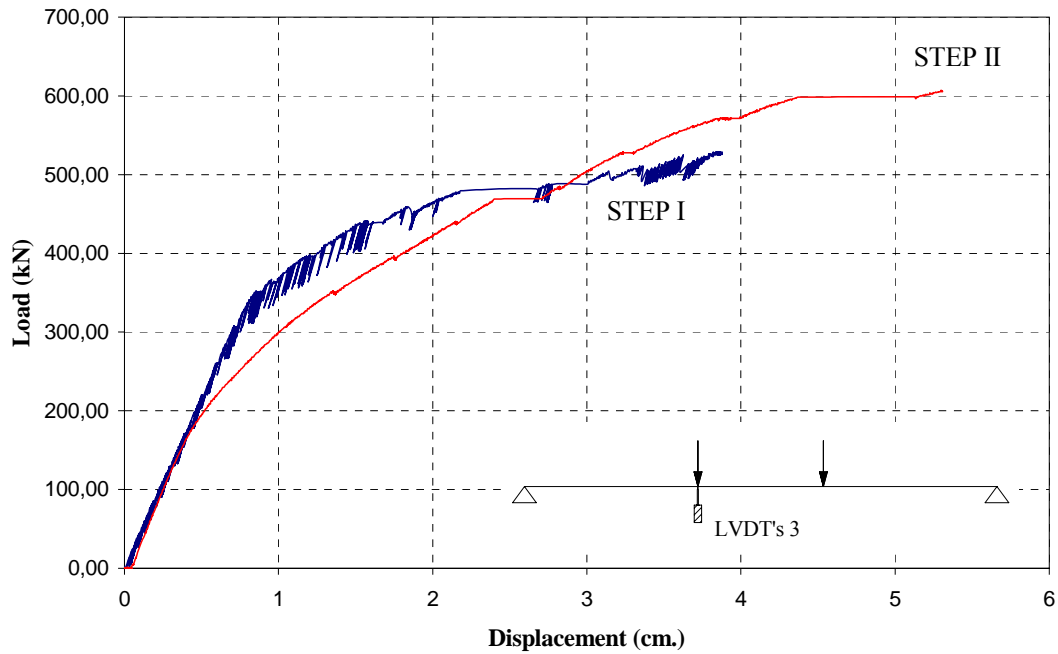


Figure III-7-12– Load-displacement LVDT #3 (1.4 m. (4.5 ft) from mid-span)

In Table III-7-4 cracking and ultimate load with corresponding displacement values for each graph are summarized:

	Cracking load $P_{cr.} = 346 \text{ kN}$ (77.8 kips)	Ultimate load (upgraded) $P_{max.} = 615.9 \text{ kN}$ (138.5 kips)	Ultimate load (virgin damaged) $P_{max.} = 500.0 \text{ kN}$ (112.4 kips)
Stringer LVDT#1	-	7.2 (2.8)	11.1 (4.4)
Stringer LVDT#2	-	6.8 (2.7)	10.2 (4.0)
LVDT #3	0.9 (0.3)	5.3 (2.0)	-

Table III-7-4—Displacement cm (in.) at cracking and maximum load

As concern the tendons, four strain gages were applied on them, two at mid-span cross-section (on tendon 3 and on tendon 9) and another two on tendon 20.3 cm. (8 in.) and 66.0 cm (26 in.) from mid-span respectively. The strain values on the tendons were read only for some load values, that's the reason for having only some points on their load-strain curves (see Figure III-7-13 Figure III-7-14 Figure III-7-13 and Figure III-7-14) .

In each diagram two curves are shown: one represent the load-strain with reference to first loading phase (step I) and one depict the load-strain until 616 kN (139 kips) load value when CFRP failure occurred (step II).

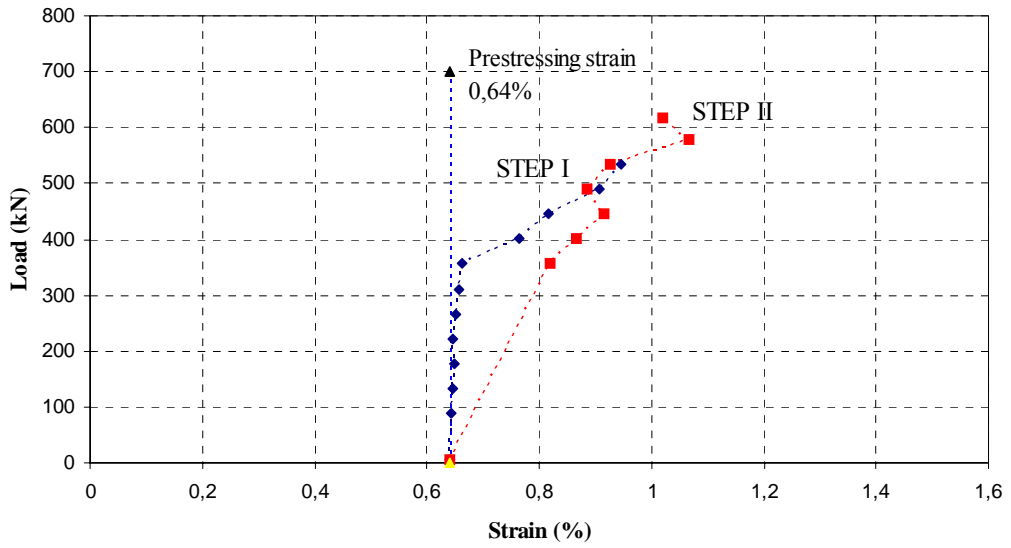


Figure III-7-13 – Load-strain on tendon 9 (mid-span cross-section)

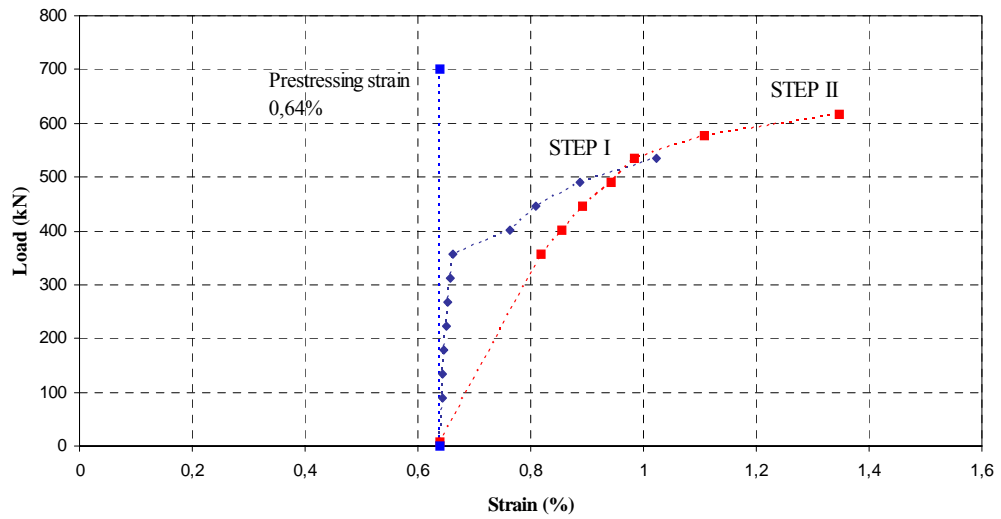


Figure III-7-14– Load-strain on tendon 3 (mid-span cross-section)

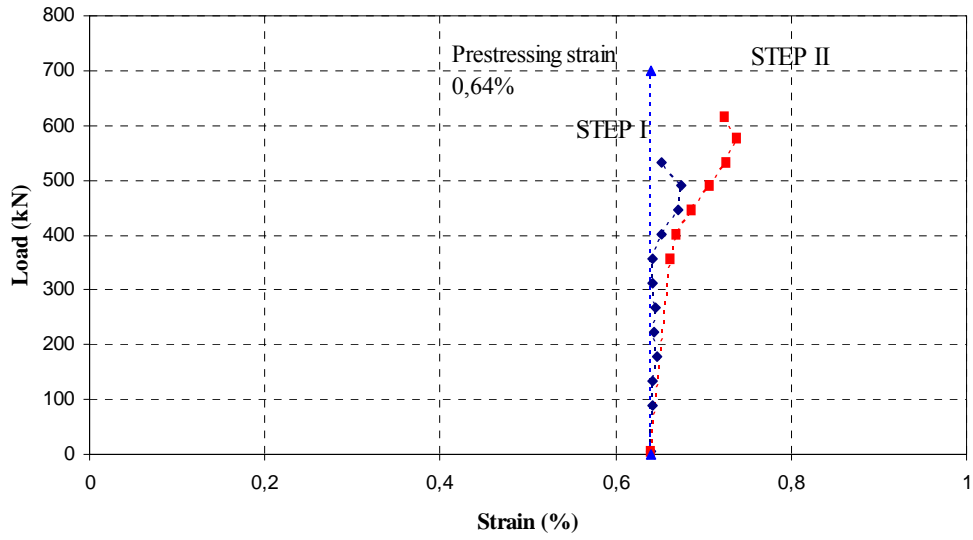


Figure III-7-15- – *Load-strain on tendon 1 (20.3cm (8 in.) from mid-span cross-section)*

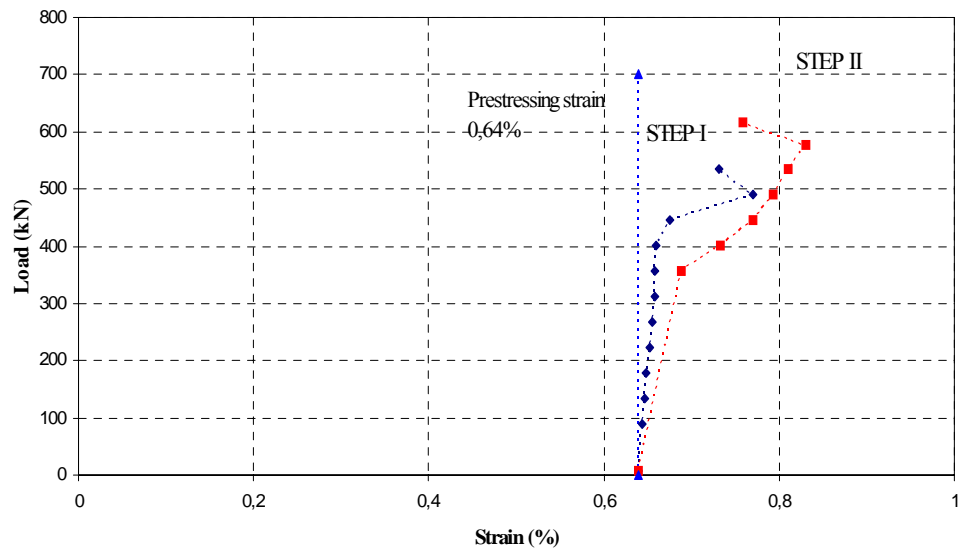


Figure III-7-16- *Load-strain on tendon 1 (66.0 cm (26 in.) from mid-span cross-section)*

Six strain gages were applied on concrete deck surface , two at mid-span cross-section, two 20.3 cm (8 in.) and two 66.0 cm (26 in.) symmetrically placed from mid-span. The curves obtained by data provided from these strain gages are below shown (see Figure III-7-17, Figure III-7-18, Figure III-7-17 and Figure III-7-18). Both curves concerning two strain gages placed at mid-span are reported considering that, due to the 2 tendons cut, the cross-section is asymmetrical; as concern the other four strain gages symmetrically placed from mid-span only two curves, one for each couple of symmetrical strain gages, are, instead, depicted .

In each diagram three curves are depicted: one represent the load-strain with reference to first loading phase (step I), the second one depict the load-strain until 616 kN (139 kips) load value when CFRP failure occurred (step II), finally the third one depict the load-strain recorded on virgin damaged specimen (step III).

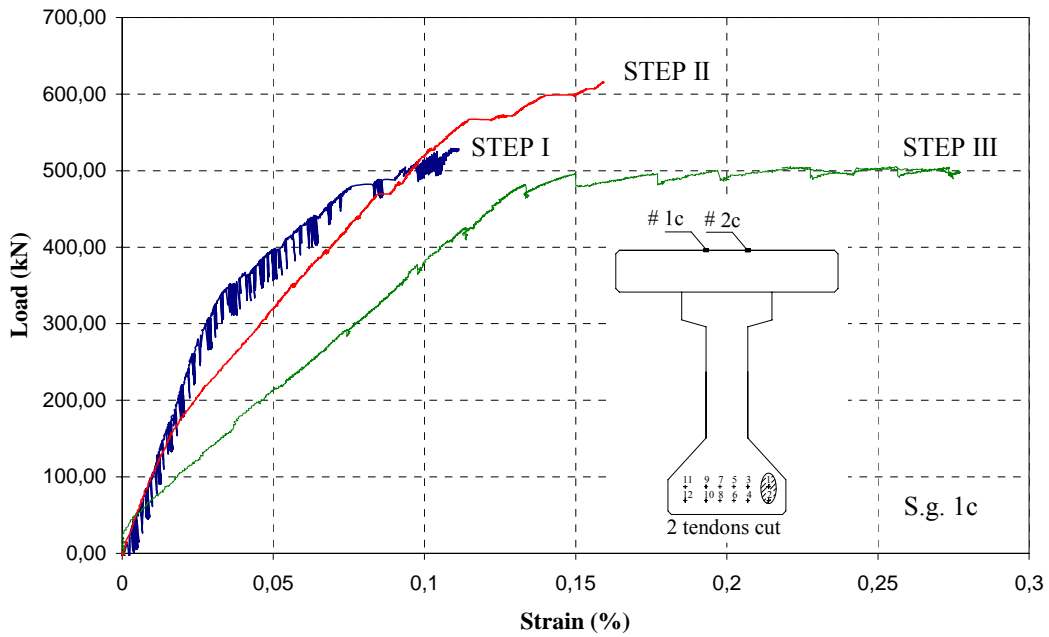


Figure III-7-17 – Load-strain on concrete deck (mid-span cross-section strain gage 1c)

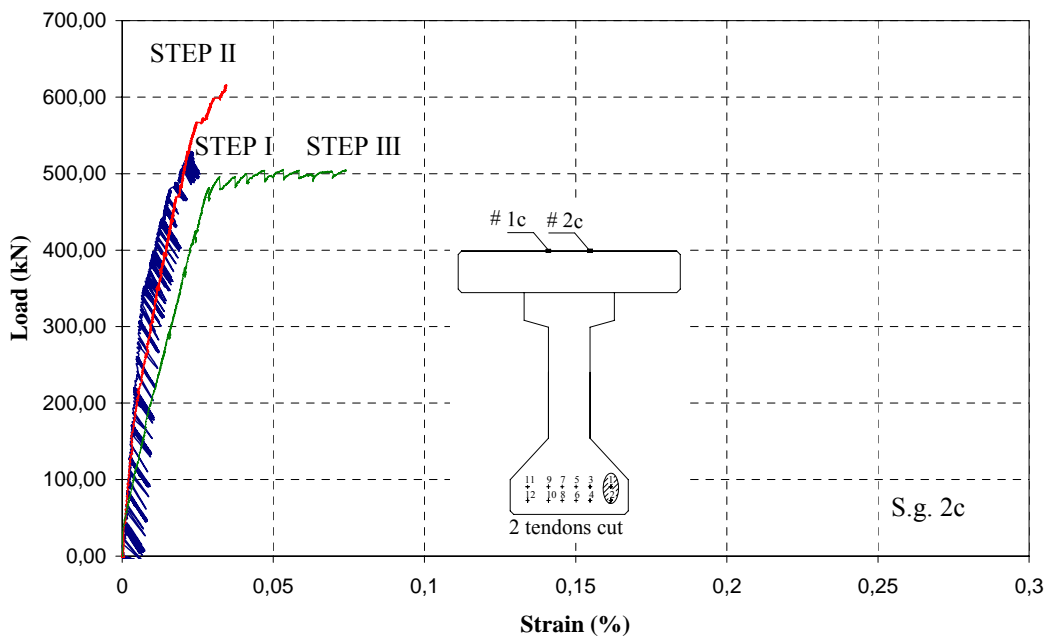


Figure III-7-18 - Load-strain on concrete deck (mid-span cross-section strain gage 2c)

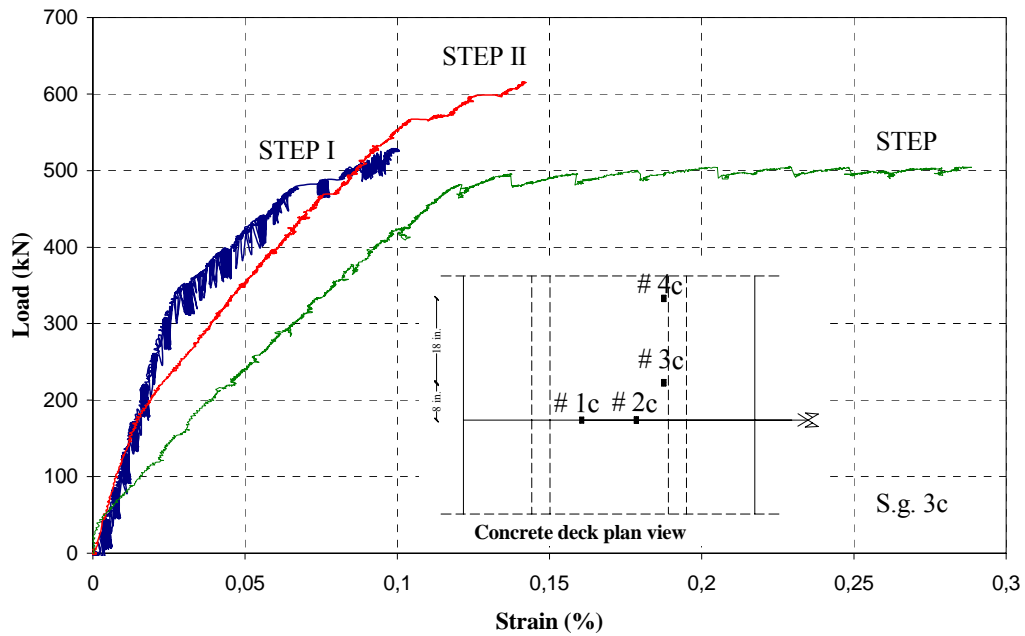


Figure III-7-19– Load-strain on concrete deck (20.3cm (8 in.) from mid-span cross-section strain gage 3c)

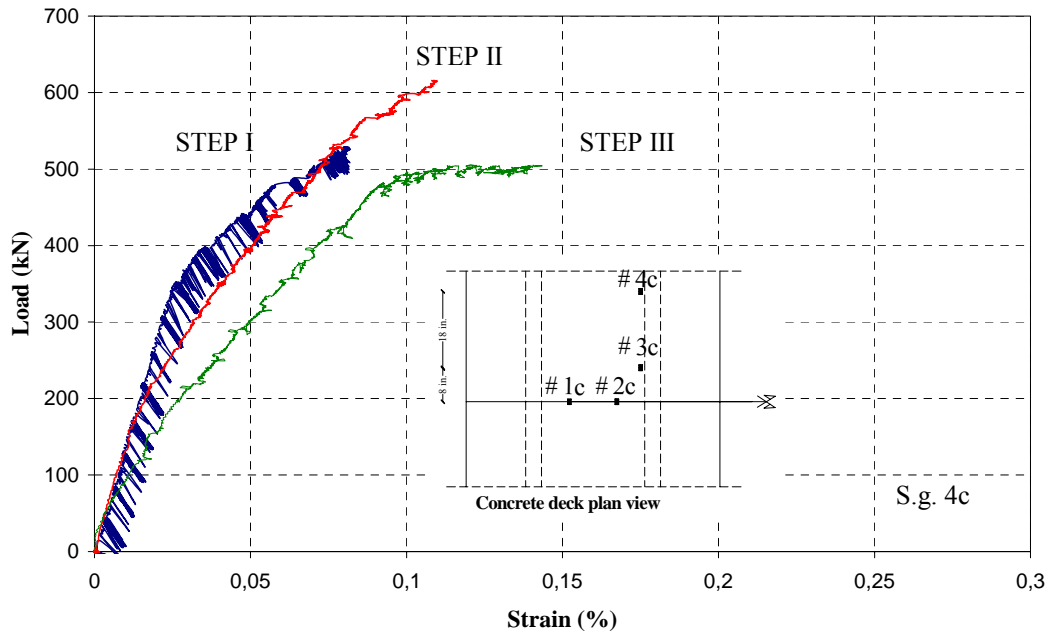


Figure III-7-20– Load-strain on concrete deck (66.0 cm (26 in.) from mid-span cross-section strain gage 4c)

Six strain gages were applied on CFRP reinforcement on bottom surface, two at mid-span cross-section, two 10.2 cm (4 in.) and two 55.9 cm (22 in.) symmetrically placed from mid-span. The curves obtained by data provided from these strain gages are below shown (see Figure III-7-21, Figure III-7-22, Figure III-7-21 and Figure III-7-22). Both curves concerning two strain gages placed at mid-span are reported considering that, due to the 2 tendons cut, the cross-section is asymmetrical; as concern the other four strain gages symmetrically placed from mid-span only two curves, one for each couple of symmetrical strain gages, are, instead, depicted. In each diagram two curves are depicted: one represent the load-strain with reference to first loading phase (step I) and one depict the load-strain until 616 kN (139 kips) load value when CFRP failure occurred (step II).

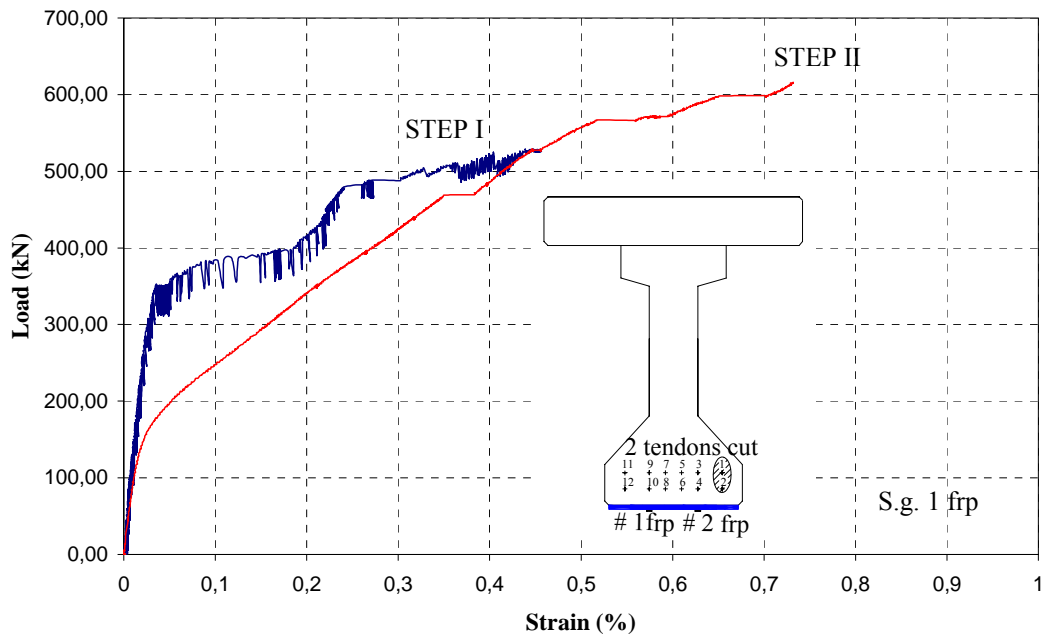


Figure III-7-21– *Load-strain on CFRP bottom surface (mid-span cross-section strain gage 1 frp)*

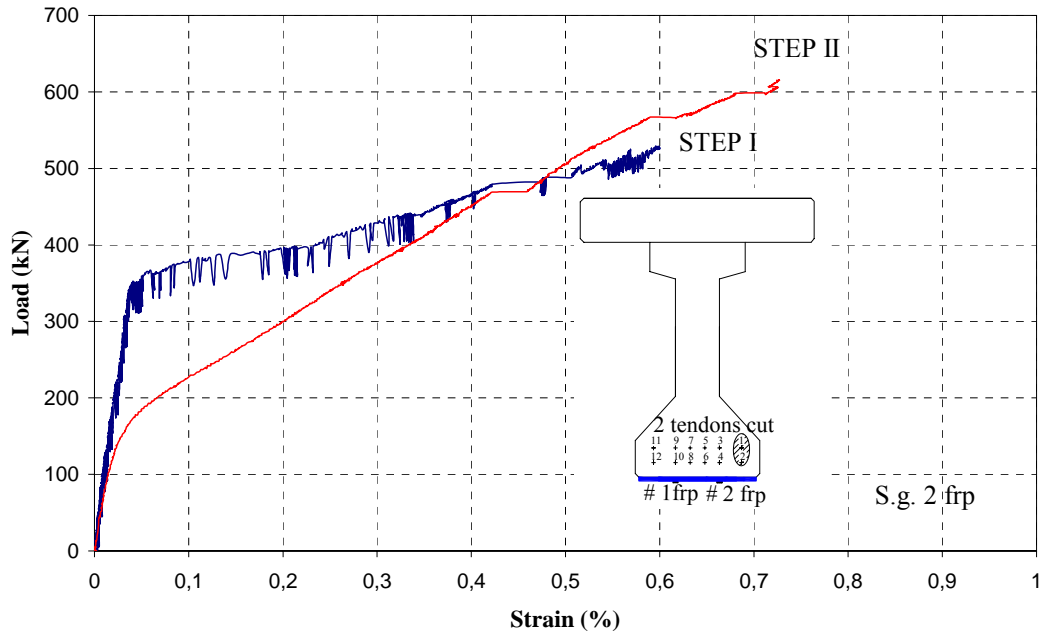


Figure III-7-22 - Load-strain on CFRP bottom surface (mid-span cross-section strain gage 2 frp)

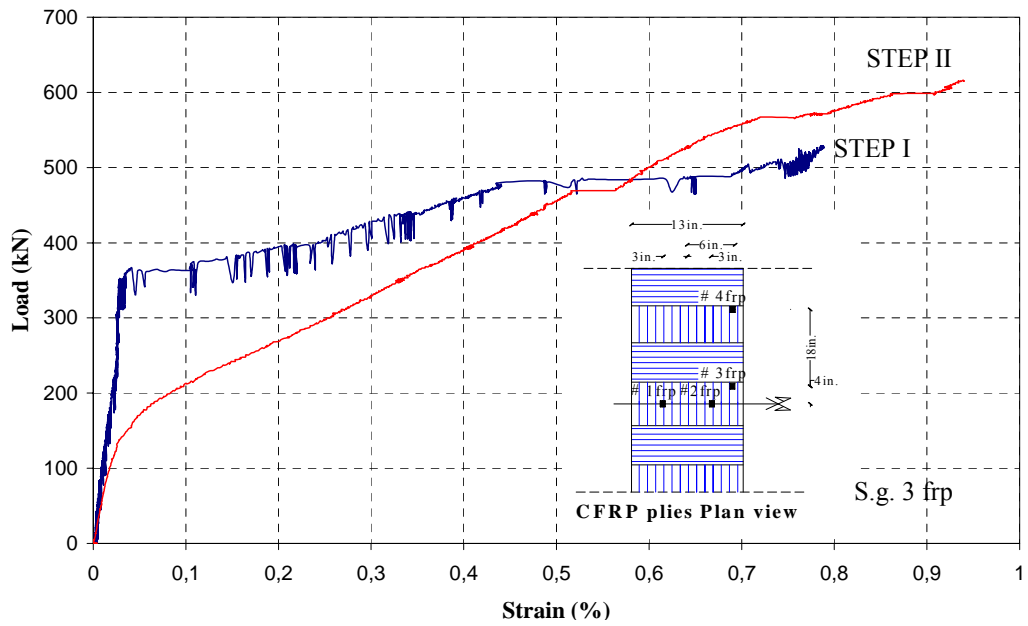


Figure III-7-23— Load-strain on CFRP bottom surface (10.2 cm (4 in.) from mid-span cross-section strain gage 3 frp)

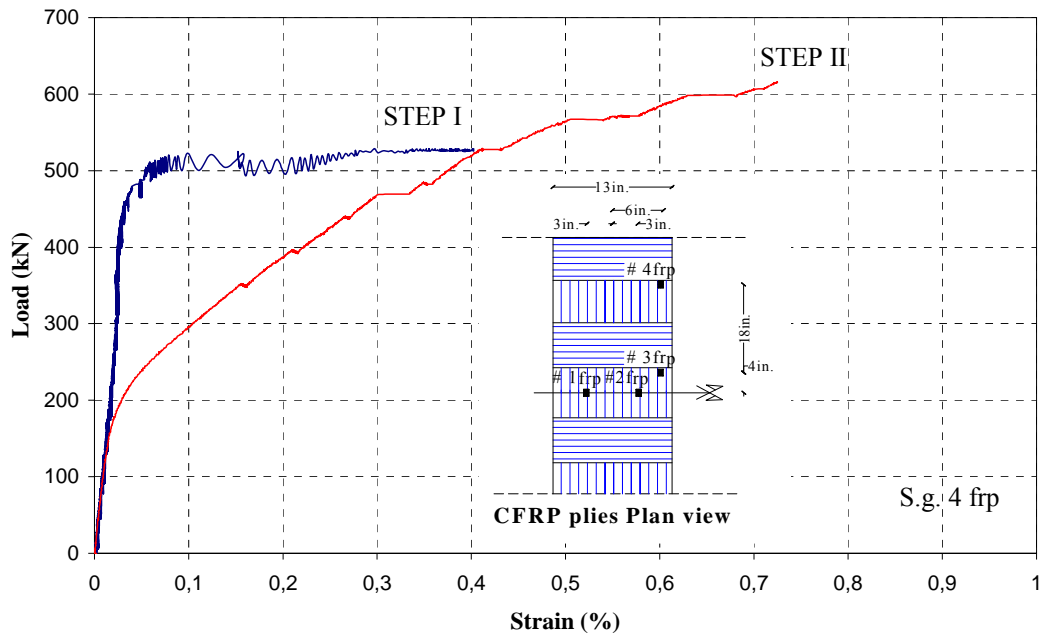


Figure III-7-24– Load-strain on CFRP bottom surface (55.9 cm(22 in.) from mid-span cross-section strain gage 4 frp)

In * Including *strain due to prestress*

Table III-7-5 strain values at cracking load , at ultimate load for each strain gage on concrete, CFRP reinforcement and tendons are summarized. Furthermore in the last column are shown the ultimate strain value recorded by strain gages on concrete surface with reference to the virgin damaged specimen.

Strain gage	Strain at Cracking load (%)	Strain at Ultimate load (%)	Strain at Ultimate load after FRP failure (%)
#2-3 tendon*	0.66	1.06	-
#2-9 tendon*	0.66	1.35	-
#2-1 tendon*	0.66	0.74	-
#2-1 tendon*	0.66	0.831	-
#1 - #2 concrete	0.04	0.16	0.28
#3 - #5 concrete	0.03	0.14	0.29
#4 - #6 concrete	0.03	0.10	0.14
#1 - #2 CFRP	0.05	0.72	-
#3 - #5 CFRP	0.04	0.94	-
#4 - #6 CFRP	0.03	0.72	-

* Including strain due to prestress

Table III-7-5- Strain on concrete and tendons

The maximum value recorded from the strain gauges applied on the tendons was 1.06 % on tendon #2-3. The maximum value recorded from the strain gauges applied on the concrete was achieved at midspan cross-section and was 0.16 % with reference to intentionally damaged and upgraded specimen, while on the virgin damaged the maximum strain at failure was 0.29 % at 20.3 cm (8 in) from mid-span.

Finally the maximum strain recorded by strain on CFRP was 0.94 % at 10.2 cm (4 in.) from mid-span.

Using strain data provided by strain gages applied on concrete and CFRP reinforcement placed in the same position at mid-span cross-section, it was possible to represent two moment-curvature diagram each for every couple of strain gages. Both moment-curvature diagram are reported below (see Figure III-7-25 and Figure III-7-26). In each case two curves are depicted, one in order to show the cracking phase (step I) and one to consider the moment-curvature until CFRP failure (step II).

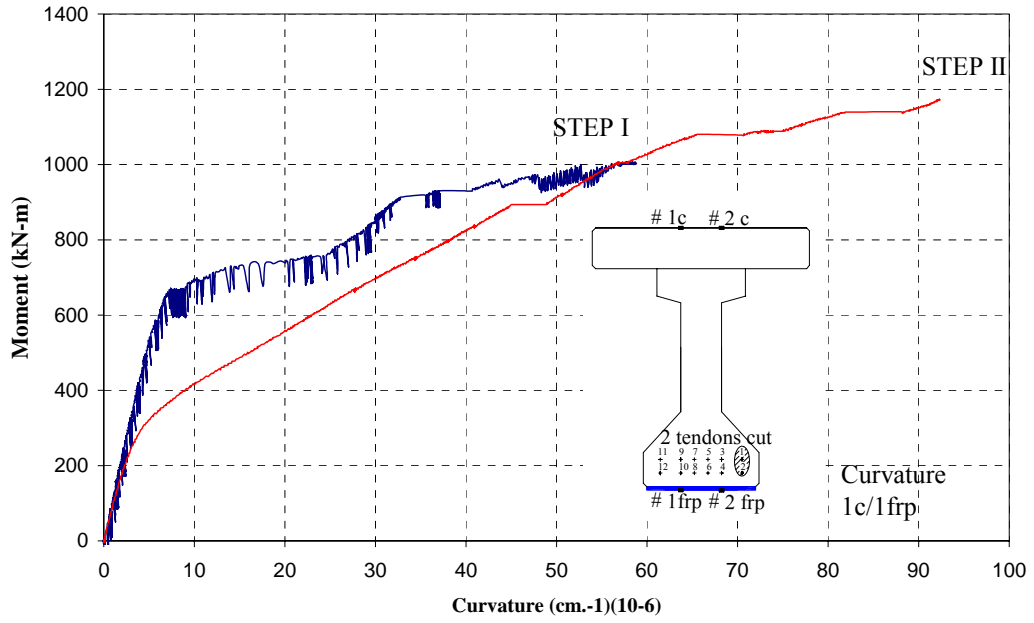


Figure III-7-25– *Moment- curvature 1c-1frp*

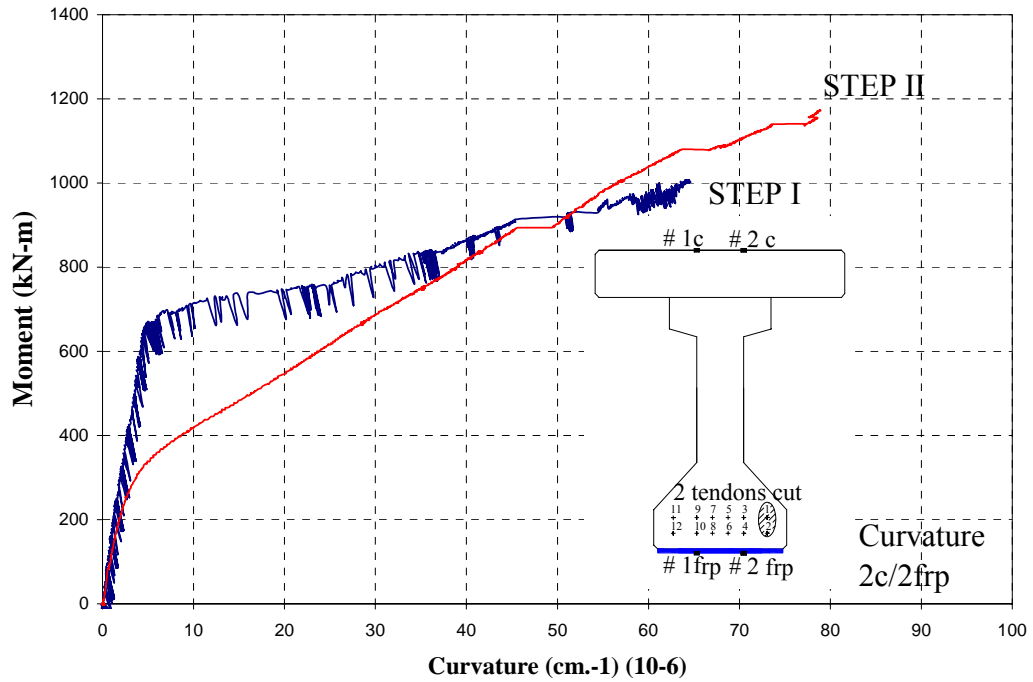


Figure III-7-26 - Moment- curvature 2c-2frp

In Table III-7-6 cracking and maximum moment with corresponding curvature values are summarized:

	Cracking Moment $M_{cr.} = 668 \text{ kN-m (492 kips-ft)}$	Ultimate Moment $M_{max.} = 1174 \text{ kN-m (866 kips-ft)}$
Curvature 1c/1frp $\text{cm}^{-1} (\text{in.}^{-1})$	7.70	92.27
Curvature 2c/2frp $\text{cm}^{-1} (\text{in.}^{-1})$	6.15	78.86

Table III-7-6– Curvature value at cracking and ultimate load respectively

8. DISCUSSION OF TEST RESULTS

Experimental comparison

First an experimental comparison between virgin and CFRP strengthened specimen is reported in this paragraph.

In Figure III-8-1 a comparison between data obtained from stringer LVDT's at mid-span in both cases is depicted.

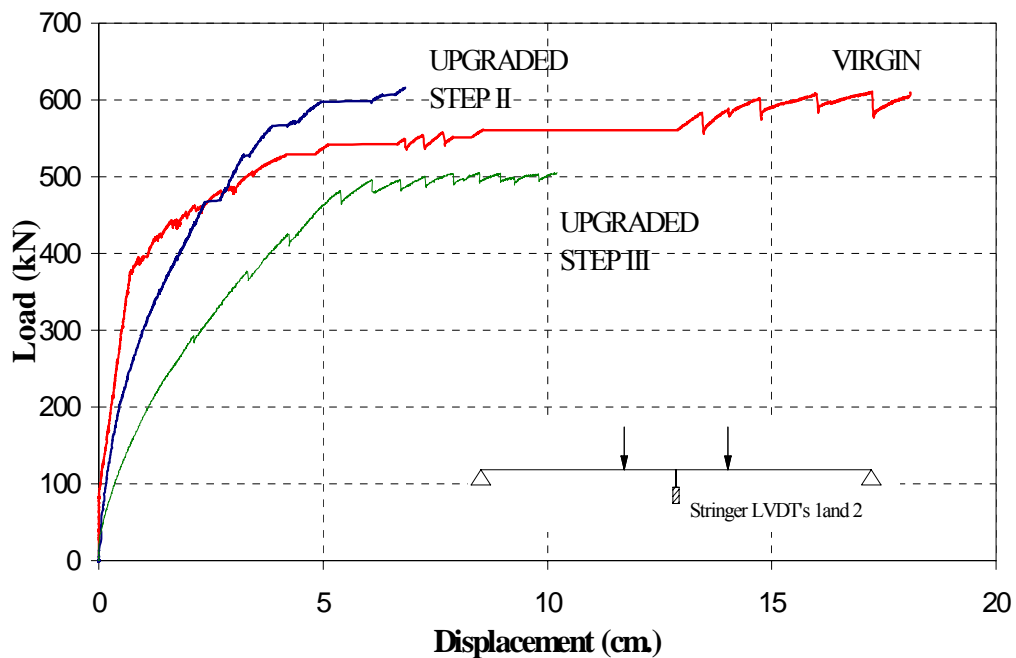


Figure III-8-1- *Load-displacement string LVDT's comparison between virgin and CFRP upgraded specimens*

This diagram shows that the maximum load achieved in both cases was equal and this confirms that the upgrade technique was effective in restoring the original flexural capacity. .

With reference to LVDT's 3 (1.37 m (4.5 ft) from mid-span) the same comparison is below depicted (see Figure III-8-2)

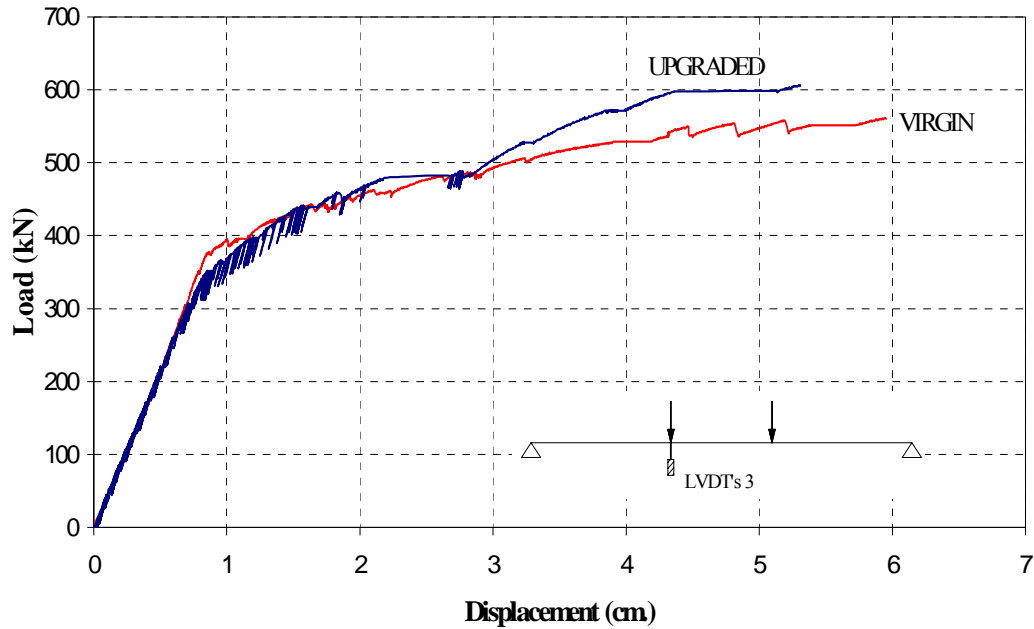


Figure III-8-2- *Load-displacement LVDT's 3 comparison between virgin and CFRP upgraded specimens*

This diagram shows that the stiffness of virgin and upgraded specimens was exactly the same; this underlines that **alarg** with the flexural capacity, the FRPstrengthening allowed to restore also the stiffness of the original beam. This information was not available in Figure III-8-1 as already mentioned in paragraph 7.

Comparison in terms of load-strain in the tendons and in the concrete are depicted in Figure III-8-3 and Figura 8-4).

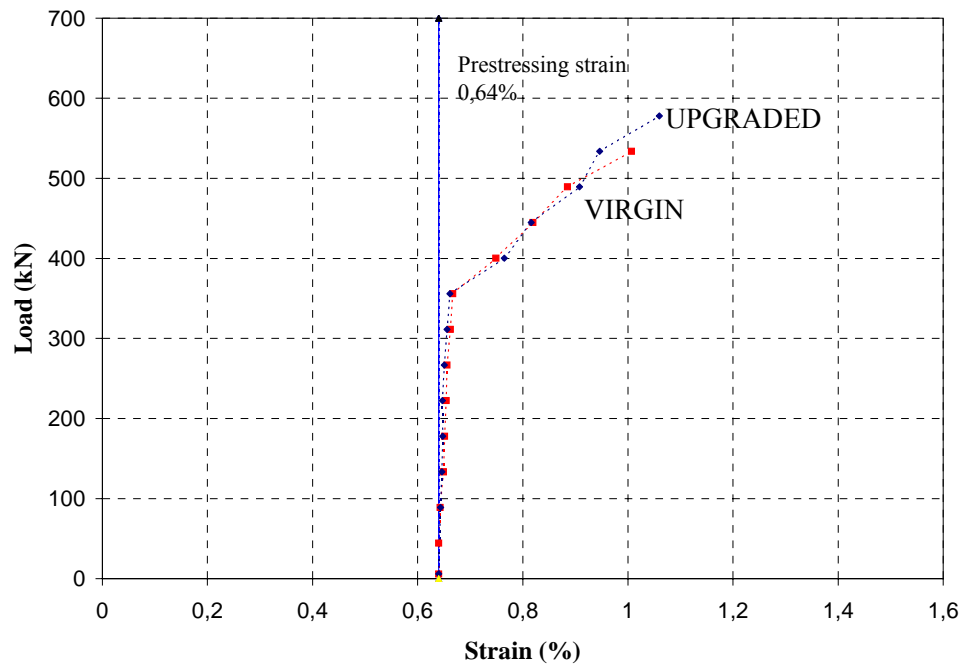


Figure III-8-3 – Comparison between strain in the tendons between virgin and CFRP upgraded specimens

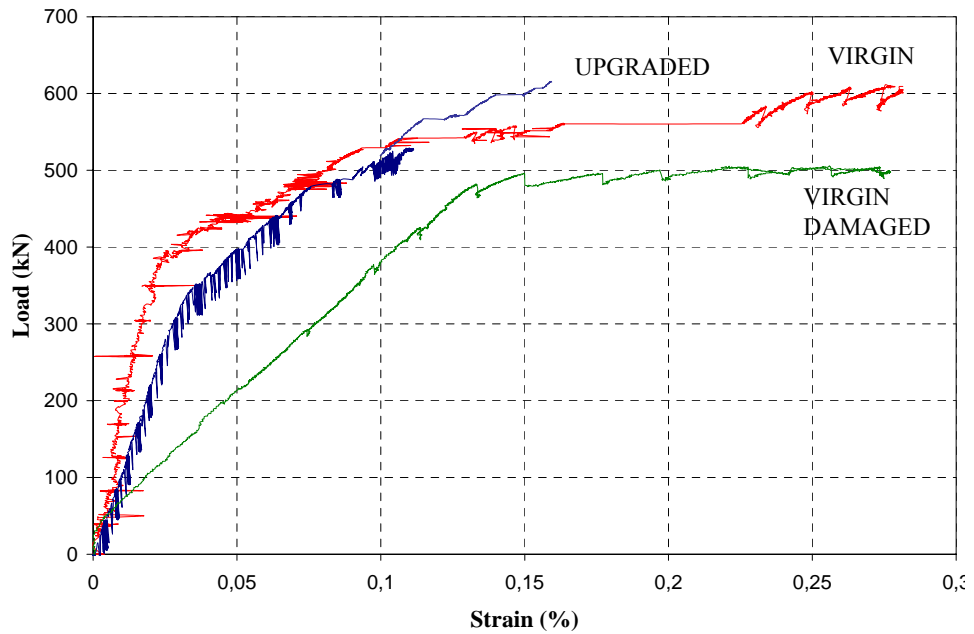


Figura 8-4- Comparison between strain in concrete between virgin and CFRP upgraded specimens

Finally experimental moment-curvature concerning virgin and upgraded specimen are compared in Figure III-8-5)

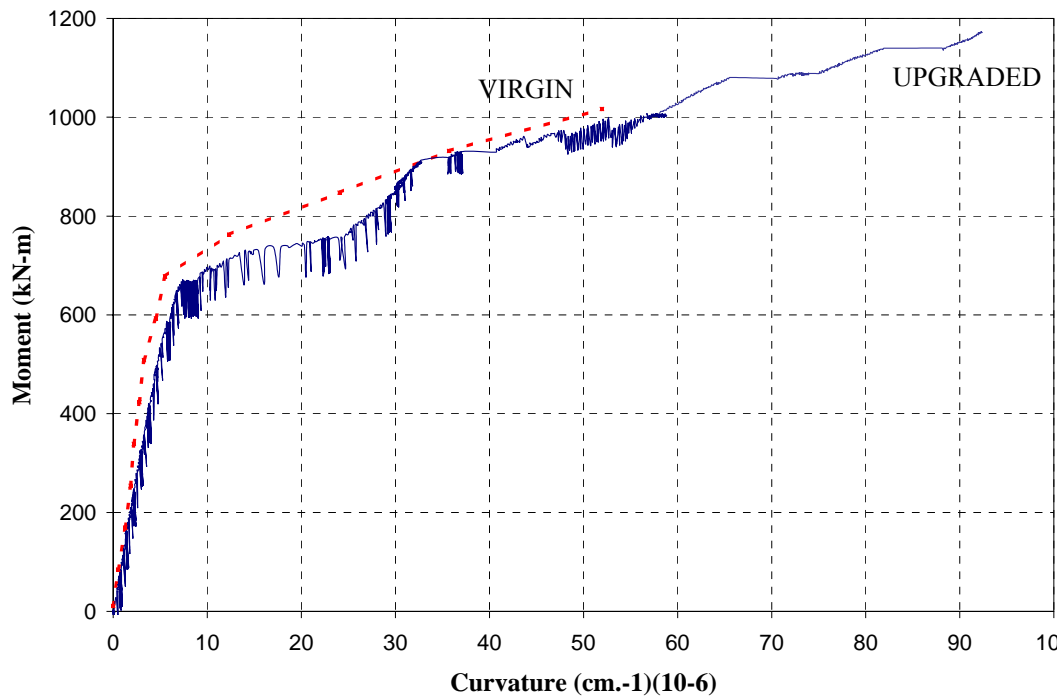


Figure III-8-5 – *Moment-curvature comparison between virgin and CFRP upgraded specimens*

This diagram shows that CFRP reinforcement allowed to restore completely the stiffness of the specimen cross-section.

Theoretical and experimental comparison

Same experimental theoretical comparisons have been performed.

In particular tri-linear moment-curvature for both tested beams have been evaluated. (see

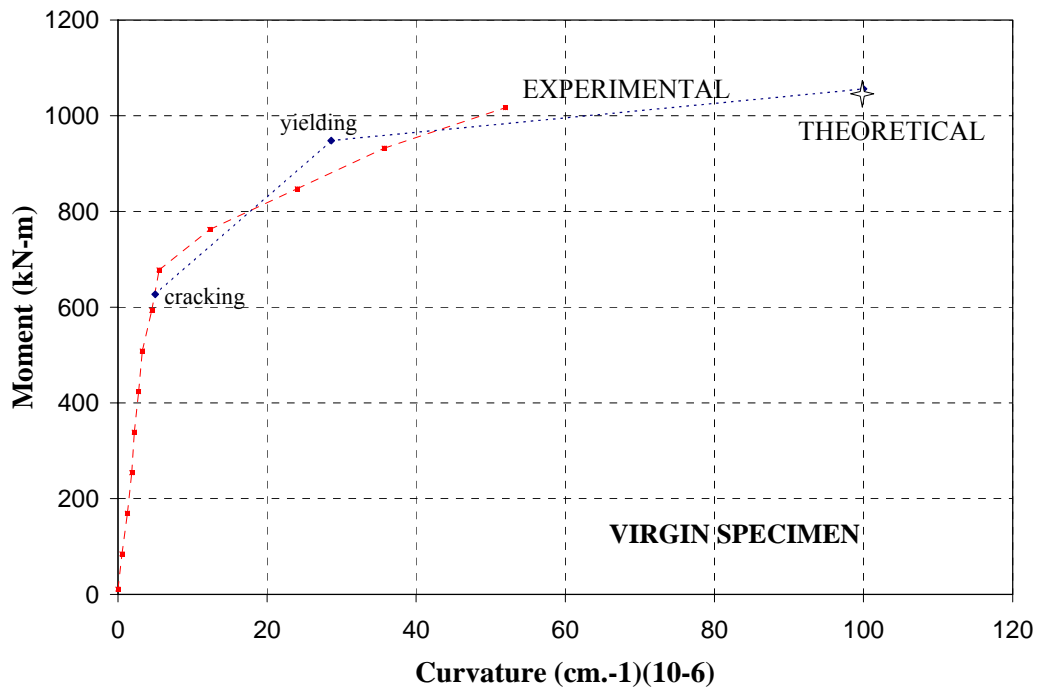


Figure III-8-6 and Figura III-8-7)

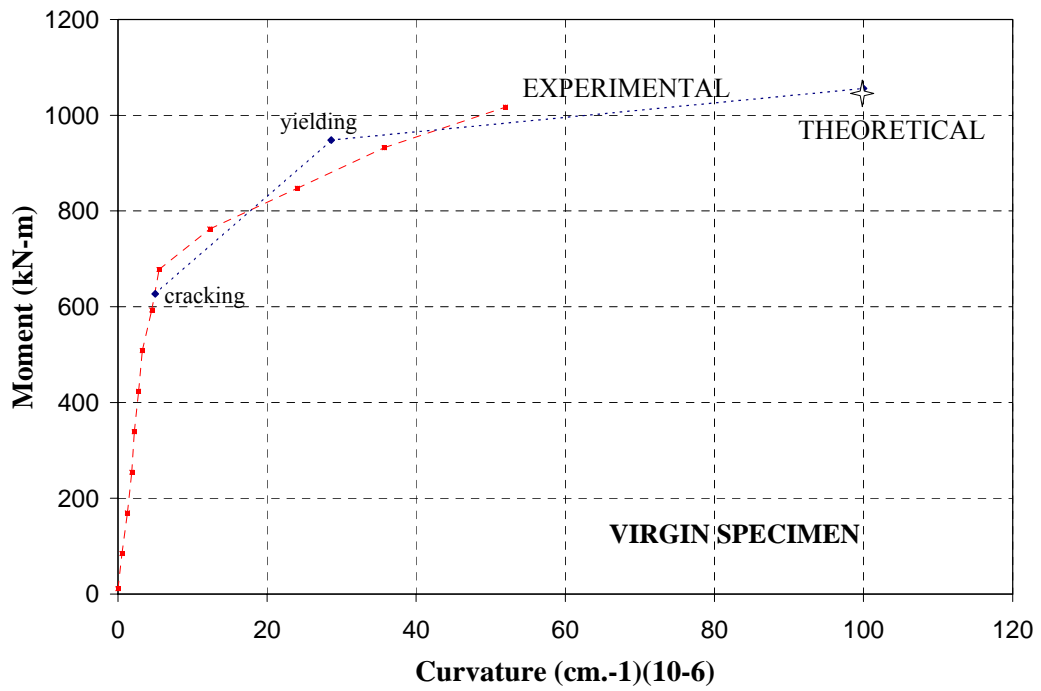


Figure III-8-6 - Moment-curvature theoretical and experimental comparison virgin specimen

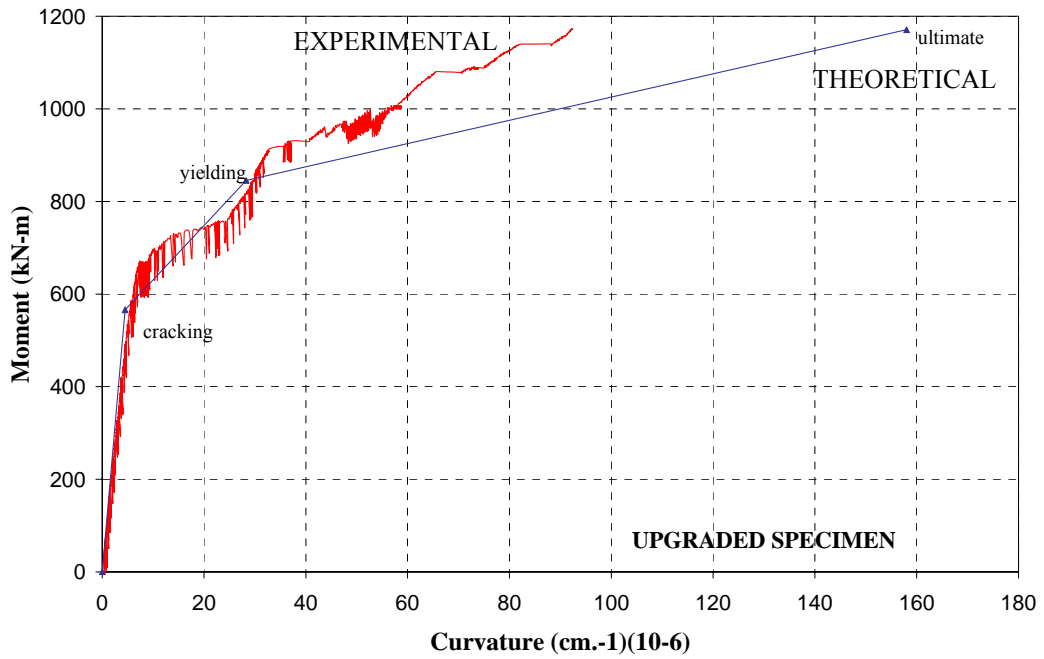


Figura III-8-7 – Moment-curvature theoretical and experimental comparison upgraded specimen

Load displacement for both tested beams with theoretical cracking and yielding loads are below reported. (see Figure III- 8-8 andFigure III-8-9)

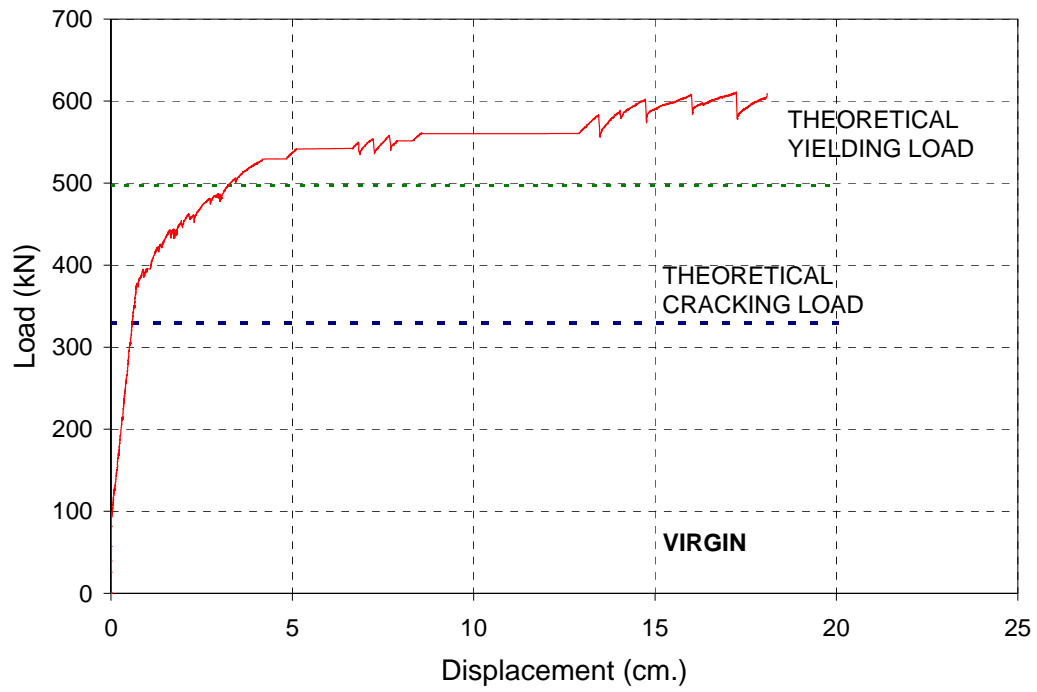


Figure III- 8-8- Load –displacement virgin specimen, cracking and yielding load

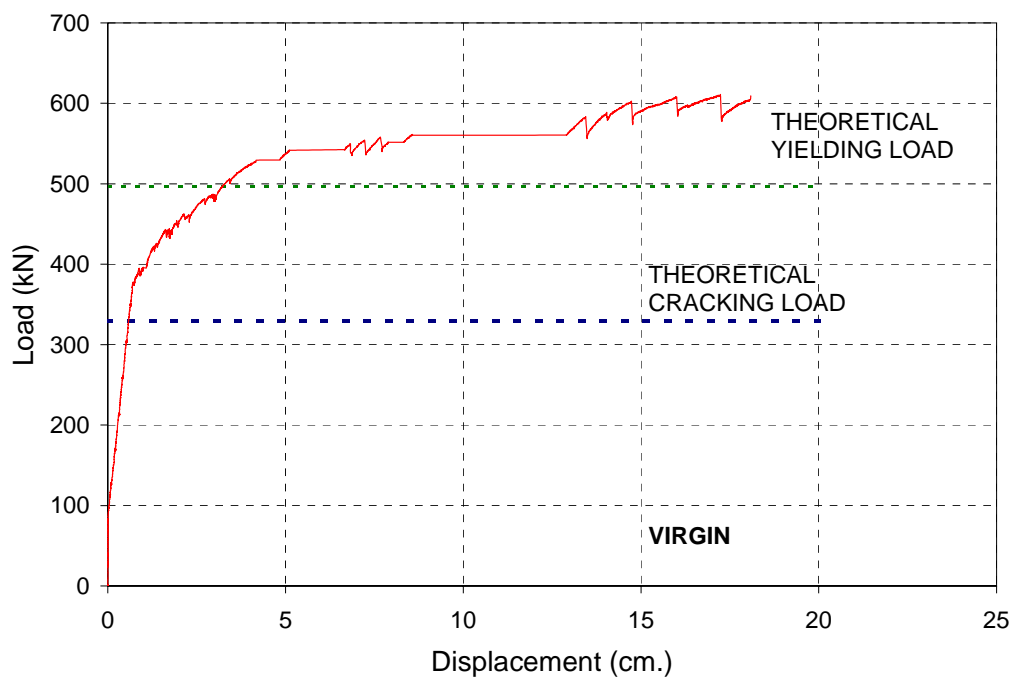


Figure III-8-9- *Load –displacement upgraded specimen, cracking and yielding load*

In Table III-8-1 and Table III- 8-2 the mains aspects of theoretical and experimental comparison are summarized

	CRACK. MOMENT kN-m (kips-ft)		YIELD. MOMENT kN-m (kips-ft)		ULTIMATE MOMENT kN-m (kips-ft)	
	EXP.	THEOR.	EXP.	THEOR.	EXP.	THEOR.
VIRGIN	520 (705)	627 (463)	-	948 (699)	834* (1131)	995 (734)
UPGRADED	474 (643)	566 (417)	-	845 (623)	1173 (865)	1082 (798)
UPGRADED AFTER FRP FAILURE	-	557 (410)	-	-	689 (508)	834 (615)

**Maximum moment*

Table III-8-1 – *Final results comparison, cracking, yielding, ultimate load*

	CURVATURE AT CRACK. cm ⁻¹ (10-6) in. ⁻¹ (10-6)		CURVATURE AT YIELD. cm ⁻¹ (10-6) in. ⁻¹ (10-6)		ULTIMATE CURVATURE cm ⁻¹ (10-6) in. ⁻¹ (10-6)	
	EXP.	THEOR.	EXP.	THEOR.	EXP.	THEOR.
VIRGIN	5.1	5.0	-	28.6	51*	365
UPGRADED	5.4	4.5	-	28.3	78.9	158

**Maximum moment*

Table III- 8-2- *Final results comparison cracking, yielding, ultimate curvature*

This tables show that theoretical prediction and experimental results are very similar and that the upgrade technique used was definitely effective.

TABLE OF CONTENTS

CHAPTER III 83

RESEARCH PROGRAM 83

1. INTRODUCTION 83

2. THEORETICAL BACKGROUND 84

-Nominal moment strength of undamaged beam	84
-Nominal moment strength of CFRP upgraded beam.....	94
- Length of FRP reinforcement	103
-Cracking –Load Moment	104

3. SPECIMEN DESCRIPTION 106

-Specimen 1 (undamaged).....	106
-Specimen 2 (intentionally damaged and upgraded).....	110

4. MATERIALS CHARACTERIZATION 115

-Girder concrete	115
- Deck concrete	116
-Prestressed concrete strand	118

-Mild steel	118
-------------------	-----

5. THEORETICAL PREDICTIONS 120

-Undamaged beam	120
- Virgin damaged beam.....	123
- Intentionally damaged and CFRP upgraded beam	125

6. TEST SETUP AND INSTRUMENTATION 131

-Instrumentation Specimen 1 (undamaged)	133
-Instrumentation Specimen 2 (intentionally damaged and repaired)	136

7. TEST RESULTS 140

-Specimen 1 (undamaged).....	140
-Specimen 2 (damaged and CFRP upgraded)	147

LIST OF FIGURES

Figure III-2-1- <i>Stress distribution throughout loading history for a PC beam. (a) Beam section. (b) Initial prestressing stage. (c) Self-weight and effective prestress. (d) Full dead load plus effective prestress. (e) Full service load plus effective prestress. (f) Limit state of stress at ultimate load for underreinforced beam. (Edward G. Navy, Prestressed concrete)</i>	85
Figure III-2-2- <i>Load-deformation curve of typical prestressed beam. (Edward G. Navy, Prestressed concrete)</i>	86
Figure III-2-3-(a) <i>strain distribution due to self weight and effective prestress-(b)strain distribution due to full service load-(c)strain distribution due to (a) plus (b).</i>	88
Figure III-2-4- <i>Stress and strain distribution across beam depth at ultimate load . (a) strain distribution due to self weight and effective prestress; (b) strain distribution due to external load; (c) strain distribution at failure[(a) plus (b)];(d) actual stress block;(e) assumed equivalent stress block</i>	89
Figure III-2-5- <i>Typical stress-strain curve, 7 wire low-relaxation prestressing strand.</i>	93
Figure III-2-6- <i>Internal strain and stress distribution under flexure at ultimate stage</i>	99
Figure III-3-1- <i>Girder cross section (1 in.=2.54 cm)</i>	107
Figure III-3-2- <i>Specimen 1 cross section (1 in.=2.54 cm)</i>	108

Figure III-3-3 – <i>Tendons cut and intentionally damaged area on specimen 2</i>	110
Figure III-3-4 - <i>Two plies of CFRP laminate (1 in.=2.54 cm)</i>	111
Figure III-3-5 – <i>CFRP Strips U-Wrapped around the Girder Bulb on specimen 2 (1 in.=2.54 cm)</i>	112
Figure III-3-6- <i>Second Specimen mid-span cross section (1 in.=2.54 cm)</i>	114
Six cylinders were manufactured in order to verify mechanical properties of girder concrete. Their dimensions were 102 by 203 mm (4 by 8 in.) (see Figure III-4-1). Compression tests were performed under a Tinius Olsen Test machine (Figure III-4-2). Test results are presented in Table III-4-1	115
Figure III-4-2- <i>Girder Concrete cylinders</i>	115
Figure III-4-3- <i>Compression test under a Tinius Olsen Test machine</i>	116
Figure III-4-4 - <i>Deck concrete cylinders</i>	117
Figure III-6-1- <i>Test Set up</i>	132
Figure III-6-2- <i>Strain gages on the specimen 1(1 in.=2.54 cm)</i>	134
Figure III-6-3- <i>Detail strain gauges on the tendon and on the concrete</i>	135
Figure III-6-4- <i>Stringer LVDTs and LVDTs positions</i>	136
Figure III-6-5 – <i>Strain gage on CFRP detail</i>	138
Figure III-6-6 – <i>Strain gages on specimen 2(1 in.=)2.54 cm)</i>	139
Figure III-7-1- <i>Flexural cracks</i>	141
Figure III-7-2- <i>Load-displacement stringer LVDTs #1 and #2</i>	141
Figure III-7-3- <i>Load-displacement LVDTs #3(1.37 m (4.5 ft) from mid-span)</i>	142
Figure III-7-4- <i>Strain on tendons placed at mid-span</i>	143
Figure III-7-5- <i>Strain on concrete placed at mid-span</i>	144
Figure III-7-6– <i>Moment-curvature curvature 1c/ 1-3t</i>	145
Figure III-7-7 – <i>Moment-curvature 2c/1-9t</i>	146
Figure III-7-8 – <i>Cracks pattern</i>	148
Figure III-7-9 – <i>CFRP failure</i>	148
Figure III-7-10- <i>Load-displacement stringer LVDTs #1 (mid-span)</i> ...	150
Figure III-7-11– <i>Load-displacement stringer LVDTs #2 (mid-span)</i>	150
Figure III-7-12– <i>Load-displacement LVDT #3 (1.4 m. (4.5 ft) from mid-span cross - section)</i>	151
Figure III-7-13 – <i>Load-strain on tendon 9 (mid-span cross-section)</i> .	153
Figure III-7-14– <i>Load-strain on tendon 3 (mid-span cross-section)</i>	153

Figure III-7-15- – <i>Load-strain on tendon 1 (20.3cm (8 in.) from mid-span cross-section)</i>	154
Figure III-7-16– <i>Load-strain on tendon 1 (66.0 cm (26 in.) from mid-span cross-section)</i>	154
Figure III-7-17 – <i>Load-strain on concrete deck (mid-span cross-section strain gage 1c)</i>	156
Figure III-7-18 - <i>Load-strain on concrete deck (mid-span cross-section strain gage 2c)</i>	156
Figure III-7-19– <i>Load-strain on concrete deck (8 in. (20.3) from mid-span cross-section strain gage 3c)</i>	157
Figure III-7-20– <i>Load-strain on concrete deck (26 in. (66.0) from mid-span cross-section strain gage 4c)</i>	157
Figure III-7-21– <i>Load-strain on CFRP bottom surface (mid-span cross-section strain gage 1 frp)</i>	158
Figure III-7-22 - <i>Load-strain on CFRP bottom surface (mid-span cross-section strain gage 2 frp)</i>	159
Figure III-7-23– <i>Load-strain on CFRP bottom surface (10.2 cm (4 in.) from mid-span cross-section strain gage 3 frp)</i>	159
Figure III-7-24– <i>Load-strain on CFRP bottom surface (55.9 cm(22 in.) from mid-span cross-section strain gage 4 frp)</i>	160
Figure III-7-25– <i>Moment- curvature 1c-1frp</i>	163
Figure III-7-26 - <i>Moment- curvature 2c-2frp</i>	164

LIST OF TABLES

Table III-3-1- <i>Material quantity and properties</i>	109
Table III-3-2- <i>CFRP 130 properties</i>	113
Table III-4-1- <i>Test results for girder concrete cylinders</i>	116
Table III-4-2- <i>Test results for deck concrete cylinders</i>	117
Table III-4-3- <i>Prestressed concrete strands properties</i>	118
Table III-4-4- <i>Mild steel properties</i>	119
Table III-5-1- <i>Theoretical results</i>	129
Table III-6-1- <i>Load cycles</i>	133
Table III-6-2 – <i>Strain on tendons due to prestress</i>	133
Table III- 6-3 - <i>Strain on tendons due to prestress</i>	137
Table III-7-1- <i>Displacement in.(cm) at cracking and maximum load</i> ..	142
Table III-7-2 – <i>Strain on concrete and tendons</i>	144
Table III-7-3– <i>Curvature value at cracking and maximum load</i>	146
Table III-7-4– <i>Displacement cm (in.) at cracking and maximum load</i>	152

Table III-7-5- *Strain on concrete and tendons* 161
Table III-7-6- *Curvature value at cracking and ultimate load
respectively* 164

CHAPTER IV

REPAIR AND STRENGTHENING OF A PC BRIDGE GIRDER WITH NSM CFRP RECTANGULAR BARS

This chapter focuses on the use of carbon fiber reinforced polymer (CFRP) rectangular bars installed as near surface mounted (NSM) reinforcement for shear strengthening in conjunction with an externally bonded pre-cured CFRP laminate to increase the flexural capacity of a prestressed concrete (PC) bridge girder. The specimen was removed from an overloaded bridge in Graham County, Kansas, strengthened and tested in the laboratory. Test results showed that the proposed technique represents an effective solution to increase both shear and flexural capacity with emphasis on the former.

1. BACKGROUND

Numerous bridges throughout the state of Kansas utilize prestressed concrete (PC) members. In many cases, frequent overloading has occurred due to the heavier vehicles now traveling on these structures. This has led to significant cracking of the prestressed members and in some cases spalling of concrete. Because cracked PC members are susceptible to strand fatigue as well as corrosion, the damaged girders on these bridges need to be repaired or replaced.

One such bridge in which multiple overloads have occurred is Bridge #56 in Graham County, Kansas. The four-span bridge was composed of 1.8 m (6 ft) wide PC double-T members. The inspection of the bridge showed that most of the stems of the 12.2 m (40 ft) interior double-T's were severely cracked and in some cases spalling had occurred. Because of the numerous existing bridges in need of upgrade and considering cost and inconvenience of replacing damaged bridge members, the state Departments of Transportation of Kansas and Missouri decided to support research in order to investigate the feasibility of repairing PC members with carbon fiber reinforced polymer (CFRP) systems.

Three of the damaged PC double-T's from Bridge #56 were set aside for upgrade and testing. Each of the three members was saw cut in half longitudinally to provide a total of six 915 mm (36 in) wide by 12.2 m (40 ft) long single-T specimens. The specimens were 585 mm (23 in) deep, with a 130 mm (5 in) thick flange. They had four (4) rows of prestressing reinforcement, each row consisting of a single 13 mm (0.5 in) diameter strand. The strands were single point depressed at mid-span to a height of 51 mm (2 in) from the bottom face. In addition, there were two rows of mild-steel reinforcement running longitudinally and two rows running laterally. Shear reinforcement consisted of single-legged 12-mm (# 4) rebar, positioned at the center of the web. The bars terminated 102 mm (4 in) from the bottom face and were spaced at approximately 255 mm (10 in) on center.(see Figure IV-1-1)

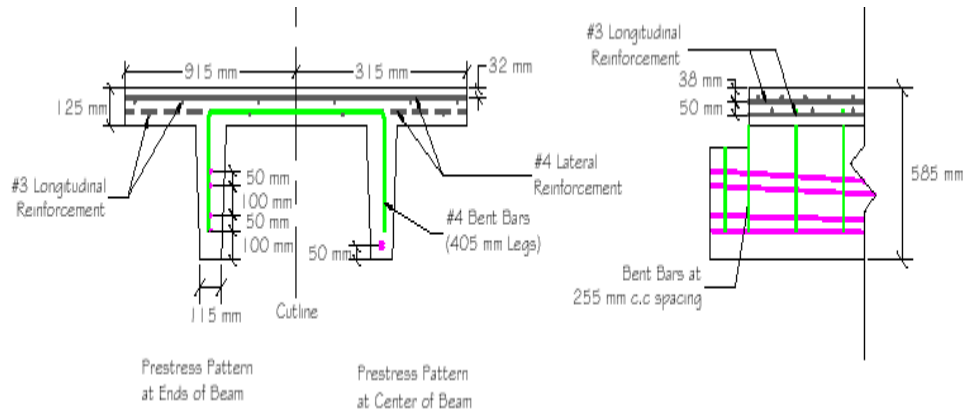


Figure IV-1-1- Dimensions of test specimen before cutting (25.4 mm=1 in.)

Three of these specimens were tested at Civil Infrastructure Systems Testing Lab (CISL) at Kansas State University with a 3 point bending configuration as is depicted in Figure IV-1-2 (Phase 1) and one was set aside for the University of Missouri-Rolla where this study was completed (Phase 2).

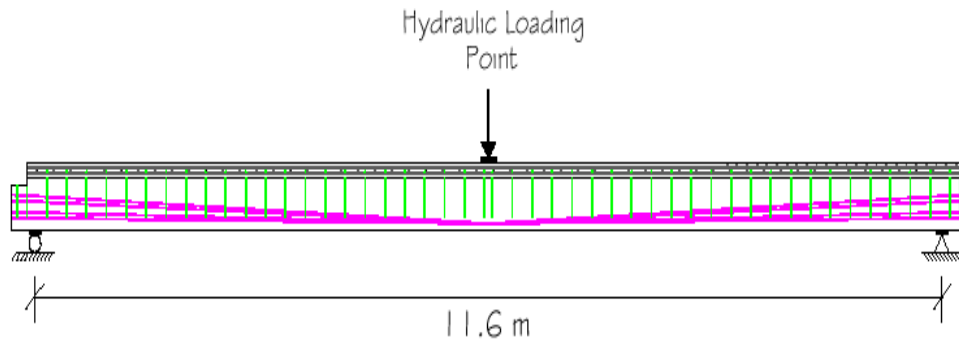


Figure IV-1-2 - Geometry of test setup for Phase 1

The first of the three specimens that were tested in Phase 1, used as a control, showed that the damaged girders were still able to withstand the original design live load corresponding to an H-15 truck (AASHTO 1996). The second specimen tested was strengthened with two plies of FRP laminate applied to the bottom of the web and

extending for 95 mm (3.7 in.) on each side of the web as depicted in Figure 3. The laminate was installed by manual lay-up and each ply had a fiber thickness of 0.16 mm (0.0065 in) and a total width of 305 mm (12 in.). Finally, in order to prevent its peeling at the laminate ends, a one ply U-wrap was installed as shown in Figure IV-1-3.

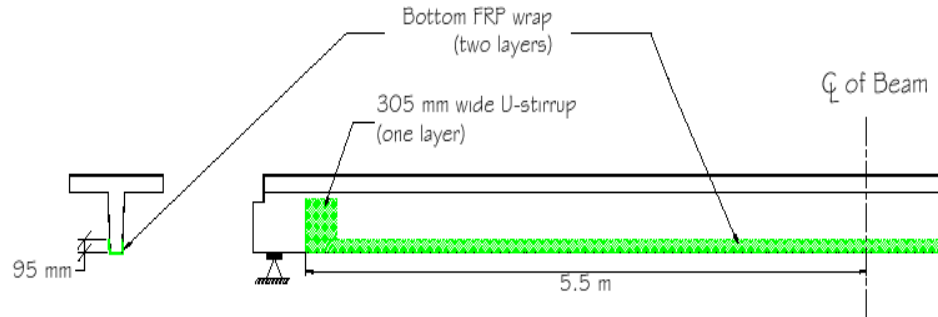


Figure IV-1-3 - FRP layout of specimen S2 (25.4 mm = 1 in, 1 m = 3.28 ft)

Test results on this specimen showed that the upgrade scheme could increase the flexural capacity of the original girder. However, due to shear deficiency, the full flexural capacity was not realized and a premature horizontal shear failure at the level of prestressing steel occurred in the girder prior to FRP rupture. A shear friction approach was used to design the FRP U-wrap for the third specimen (see Figure IV-1-4) that reached its full flexural capacity and failed due to flexural FRP rupture.

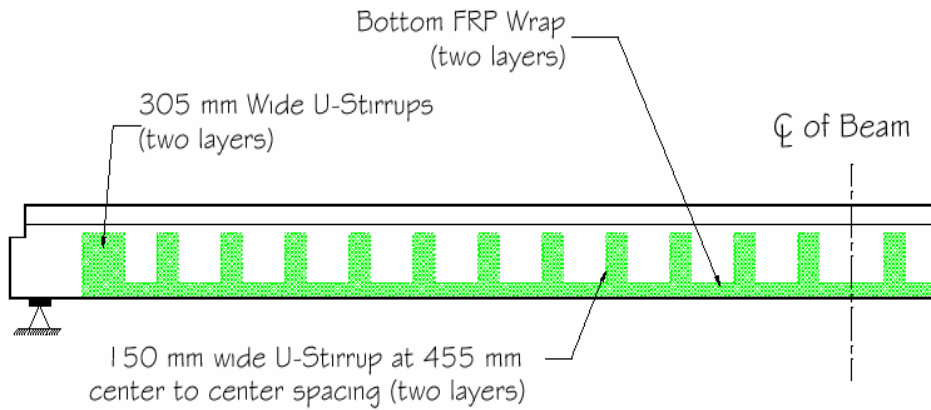


Figure IV-1-4 - FRP layout of specimen S3 (25.4 mm = 1 in)

Test results of Phase 1 are summarized in **Table IV-1-1**.

Specimen	Ultimate load kN (Kips)	Ultimate Moment Capacity (M_n) kN-m (Kips-ft)	Ultimate Shear Capacity (V_n) kN (Kips)	Failure Mode
S1	130 (29.2)	324 (440)	65 (14.6)	Flexure
S2	160 (36.0)	395 (535)	80 (18.0)	Shear
S3	162 (36.5)	400 (540)	81 (18.2)	Flexure (FRP rupture)

Table IV-1-1 - Test results of Phase 1

2. TEST PHASE II

One of the six single-T PC specimens was tested at High-Bay Structures Laboratory of the University of Missouri-Rolla. The objective of this test was to investigate the effectiveness of the strengthening techniques based on CFRP rectangular bars installed as

near surface mounted (NSM) reinforcement for shear upgrade, and externally bonded pre-cured FRP laminate for flexural upgrade.

-Flexural Strengthening

Flexural strengthening consisted of a pre-cured CFRP laminate 100 mm (4 in.) wide and 1.4 mm (0.055 in.) thick (ref- S&P) applied on the bottom surface of the web, as depicted in Figure IV-2-1 (Figure IV-2-2).

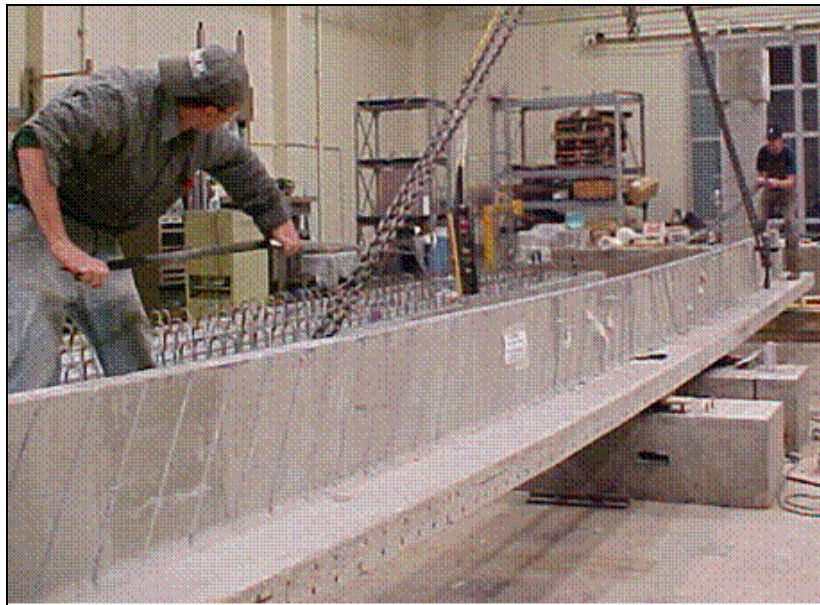


Figure IV-2-1 - Flexural strengthening installation



Figure IV-2-2 - Removal of excess resin

The mechanical properties of laminate used for flexural strengthening are summarized in Table IV-2-1.

The pre-cured CFRP laminate was produced by pultrusion, a continuous manufacturing process where fibers are impregnated with a thermoset resin and form a composite molded and cured through a dye. A laminate produced by pultrusion may have a fiber volume fraction of approximately 70%.

The installation procedure was simple and involved: 1) cutting the laminate to length; 2) applying the epoxy adhesive on the laminate; 3) pressing the laminate onto the concrete surface; and 4) removing excess resin (see Figure 6). Finally, to prevent the laminate ends peeling, a two-ply CFRP wrap, each 508 mm. (20 in) wide and 0.16 mm/ply (0.0065 in/ply) thick was placed at each end of the longitudinal FRP laminate. The properties of the wrap are reported in Table IV-2-1.

-Shear strengthening

The shear strengthening was attained with CFRP rectangular bars spaced at 203 mm (8 in) along the girder with an inclination of 60 degrees. The rectangular FRP bars had dimensions 2 by 16 mm (0.079 by 0.63 in) with mechanical properties as listed in Table IV-2-1. The groove cut into the concrete to receive the FRP bar had dimensions of 6 by 19 mm (0.25 by 0.75 in).

The advantages of using CFRP rectangular bars for structural strengthening installed with the NSM technique include:

- Surface preparation is minimized
- Grooving is obtained with a single saw cut without any concrete chipping
- After installation, the NSM bar is protected from mechanical damage, and
- Quality of concrete inside the groove typically better than surface concrete

The installation of the CFRP rectangular bars is performed according to the following sequence :

- Using a diamond blade concrete saw or grinder, a groove of 6 by 9 mm (0.25 by 0.75 in) is cut
- The groove is masked to prevent excess adhesive from marring the exposed concrete surface
- The groove is thoroughly cleaned using a vacuum and/or compressed air
- The groove is filled with the adhesive. Care should be made to avoid entrapped air

- The CFRP rectangular bar is placed on edge into the groove, and

Removal of excessive adhesive and general clean-up. (see Figure IV-2-3 and Figure IV-2-4)



Figure IV-2-3 - *Installation of rectangular CFRP bar for shear strengthening*



Figure IV-2-4 – Instrumented bars for shear strengthening

Property	Pre-cured Laminate	U-wrap Anchor	Rectangular Bar
Modulus of Elasticity N/mm ² (ksi)	205,000 (29,700)	227,535 (33,000)	131,000 (19,000)
Ultimate tensile strength N/mm ² (ksi)	2,400-2,600 (345-365)	3,800 (550)	2,070 (300)
Ultimate strain	0.0116	0.0167	0.0157

Table IV-2-1 - FRP system properties for specimen S4

-Test set-up

The specimen was tested upside down under a four-point load configuration with a clear test span of 9.14 m (30 ft). The constant moment region was 1.8 m (6 ft) (Figure IV-2-5).

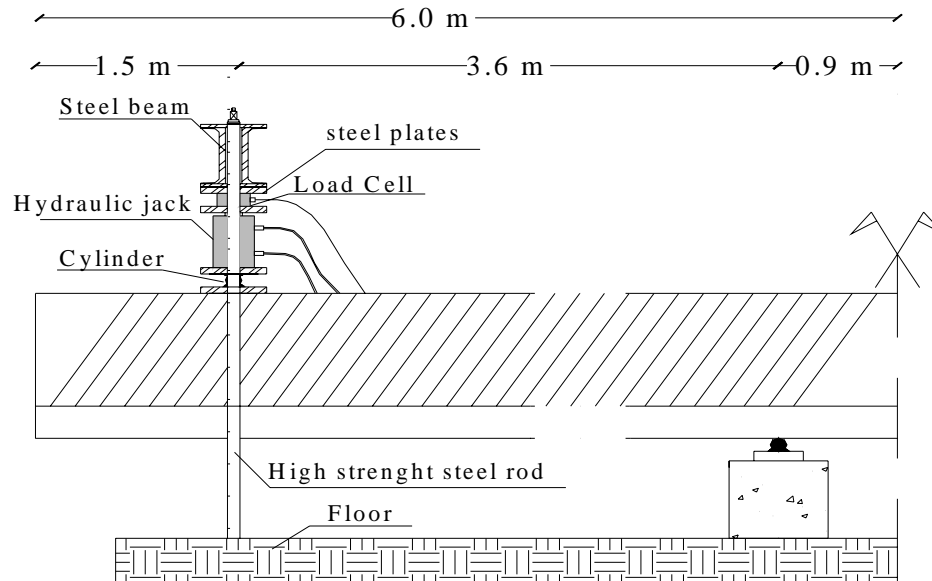


Figure IV-2-5 - Test setup for specimen S4 (25.4 mm = 1 in, 1 m = 3.28 ft)

Such test setup ensured more stability during the test and allowed a clear view of the FRP performance.

Two hydraulic jacks equipped with 890 kN (200 kips) load cells were used to apply and measure the load. Real time recording of structural response was achieved using an electronic data acquisition system. Two linear variable displacement transducers (LVDTs) were positioned (one on each side of the flange) at mid-span and two stringer-type LVDTs were placed close to the ends of the girder to measure deflection at the location of the jacks. Finally, 13 strain gages were applied on the FRP rectangular bars where maximum shear was expected (see Figure IV-2-4), two strain gages were applied on the FRP laminates at 100 mm (4 in) from each side of the span centerline, and two strain gages were applied on the concrete top flange at the same positions (see Figure IV-2-6).

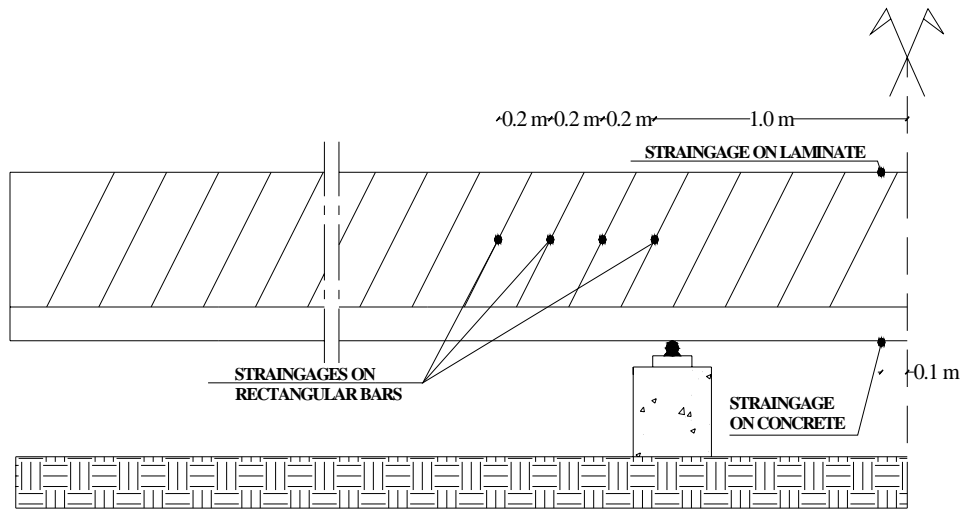


Figure IV-2-6 - Strain gage positions for specimen S4 (25.4 mm = 1 in, 1 m = 3.28 ft)

The load was applied in cycles of load and unload as shown in Table IV-2-2.

Cycle	Load Range KN (kips)
1	0-44.6-0 (0-10-0)
2	0-89.2-0 (0-20-0)
3	0-135.6-0 (0-30-0)
4	0-178.0-0 (0-40-0)
5	0-failure

Table IV-2-2 - Load-unload cycles for specimen S4

Experimental Results

A partial debonding of the laminate used for flexural reinforcement at load of 153.0 kN (34.6 kips) was observed and a total debonding followed at an ultimate load of 210 kN (47.2 kips). This corresponds to a maximum moment of 437 kN-m (322.5 kips-ft) and a maximum shear of 125.5 kN (28.2 kips) combining the effects of the point loads and girder self-weight.

The maximum deflections at the end of the girder was 203 mm (8 in.) (see Figure IV-2-7) while at mid-span it was 20 mm (0.8 in.), so that an effective total deflection of 223 mm (8.8 in.) was achieved at ultimate.

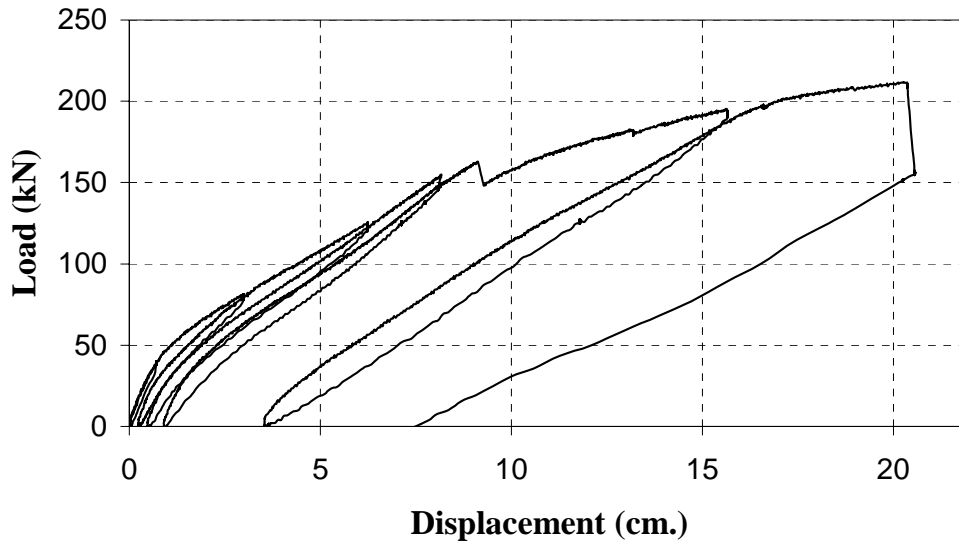


Figure IV-2-7- *Load-displacement as measured at the location of the jack (stringer LVDTs)*

The highest recorded level of strain on the flexural CFRP laminate before failure was 12,000 $\mu\epsilon$ as is shown in Figure IV-2-8. Finally, the highest recorded strain on the rectangular bars due to shear and corresponding to the ultimate load was approximately 6,500 $\mu\epsilon$. (see Figure IV-2-9).

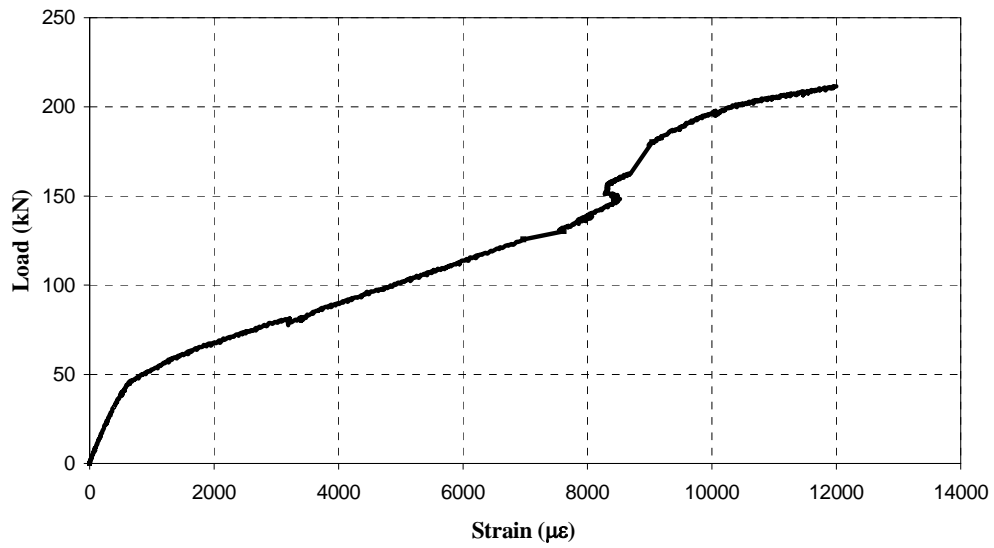


Figure IV-2-8 - *Strain measured in the flexural pre-cured FRP laminate*

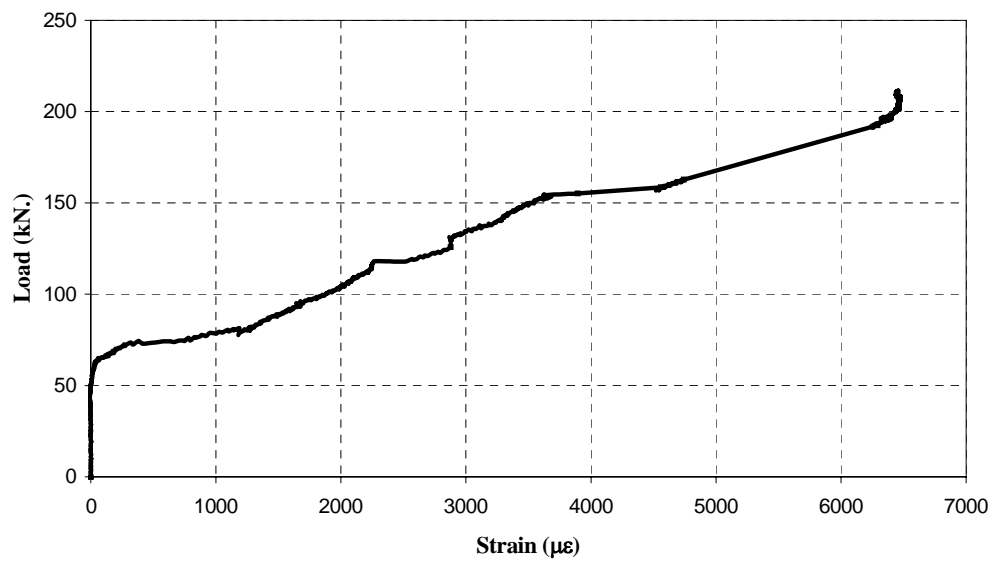


Figure IV-2-9 - *Strain measured in the FRP rectangular bar for shear*

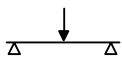
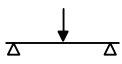
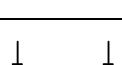
3. DISCUSSION

The objective of the proposed investigation was to evaluate the shear and flexural improvement provided by CFRP NSM rectangular bars and the pre-cured laminate, respectively. In order to perform a comparison between the test results of Phases 1 and 2, the maximum shear and bending moment obtained in the three specimens of Phase 1 (i.e., S1, S2, and S3) were recomputed at a cross-section at 0.9 m (3 ft) from mid-span. This is the location where maximum shear and bending moment were obtained in specimen S4 (Phase II).

- Flexural Evaluation

In order to evaluate the flexural capacity improvement given by the pre-cured FRP laminate, the nominal moment capacity of S4 was compared to the maximum moment of specimen S1 at the same cross-section. Specimen S1 was unstrengthened and showed a flexure-type failure mode. Considering the sum of both applied load and self weight, the ultimate moment of specimen S4 at 0.9 m (3 ft) from midspan was 437 kN-m (322.5 kips-ft), where as, the moment recorded at failure for specimen S1 was 384 kN-m (283.5 kips-ft) at the same cross-section. Thus the use of the FRP laminate increased the moment capacity by a factor of 13.8 % as compared to the control specimen. For specimens S2 and S3, the maximum moment (at 0.9 m (3 ft) from midspan) when failure occurred, were 458.2 kN-m (338.5 kips-ft) and 463.6 kN-m (342.5 kips-ft) giving a moment increments of 19.3 and 20.7 %, respectively. These results are summarized in Table IV- 3-1 where the normalized increment is calculated by dividing the moment increment by the axial stiffness ratio of flexural

CFRP laminate over flexural steel reinforcement. This parameter provides a measure of the efficiency of the different systems. Its validity is somehow relative, simply because the failure modes of the four girders were not all flexure-controlled.

Specimen	Test Setup	$E_f A_f / E_s A_s$ (%)	Failure load, P kN (kips)	Maximum Moment* kN-m (kips-ft)	Moment Increment (%)	Normalized Increment
S1		-	130.0 (29.2)	384.0 (283.5)	-	-
S2		10.8	160.0 (36.0)	458.2 (338.5)	19.3	1.8
S3		10.8	162.0 (36.5)	463.6 (342.5)	20.7	1.9
S4		40.9	251.0 (56.4)	437.0 (322.5)	13.8	0.3

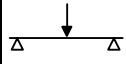
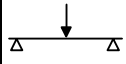
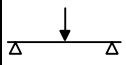
*Includes specimen self-weight

Table IV- 3-1- Comparison of test results for Phases 1 and 2 - flexure (cross-section at 914 mm (3 ft) from mid-span)

- Shear Evaluation

Considering both applied load and self weight, the shear in specimen S4, when the flexural failure occurred, was 125.5 kN (28.2 kips) compared to the maximum shear of specimen S1 equal to 81.8 kN (18.4 kips). This shows that the improvement was 88.1% over the control specimen S1.

The ultimate shear in S2, that had a shear-controlled failure, was 81.8 kN (18.4 kips); thus specimen S4 showed an improvement in shear capacity of at least of 36.9 % over this base strength. This value may be considered as a lower bound since S4 failed due to flexural FRP laminate debonding that did not allow achieving full shear capacity. Finally, specimen S3 that experienced a flexure-controlled failure, showed a maximum shear value of 83.2 kN (18.7 kips). A summary of the shear results is shown in Table IV-3-2. In this table, the normalized increment is calculated by dividing the shear increment by the axial stiffness ratio of the CFRP bars over steel stirrups reinforcement. The consideration made for the case of flexure in the previous section also pertains to shear. The maximum normalized increment was achieved in specimen S4 confirming the effectiveness of the NSM technique for shear strengthening.

	Test Setup	$\frac{E_f A_f}{E_s A_s}$ [§] (%)	Failure load, P kN (kips)	Maximum Shear* kN (kips)	Shear Increment (%)	Normalized Increment
S1		-	130.0 (29.2)	66.7 (15.0)	-	-
S2		18.0	160.0 (36.0)	81.8 (18.4)	22.6	1.2
S3		45.9	162.0 (36.5)	83.2 (18.7)	24.7	0.5
S4		6.2	251.0 (56.4)	125.5 (28.2)	88.1	14.2

[§]Per unit length *Include specimen self-weight

Table IV-3-2- Comparison of test results for Phases 1 and 2 - shear
(cross-section at 914 mm (3 ft) from mid-span)

4. MODELING CONSIDERATION

The approach used to calculate the nominal shear capacity of a member strengthened using NSM bars is similar to that used in ACI 440 (2002) for the case of externally bonded FRP laminates (Parretti and Nanni 2002). The equation below is applicable for NSM systems.

$$V_n = V_c + V_s + V_f$$

Several parameters influence the NSM FRP bars contribution to the shear capacity (V_f), such as quality of bond, FRP rebar type, groove dimensions, and quality of substrate material. When computing V_f , two strain limits need to be taken into account (De Lorenzis and Nanni 2001-a) namely: strain from bond-controlled failure, and maximum strain threshold of 0.004 . The latter is suggested to maintain the shear integrity of the concrete (Khalifa et al. 1998), and to avoid large shear cracks that could compromise the aggregate interlock mechanism.

The shear strength provided by the NSM reinforcement can be determined by calculating the force resulting from the tensile stress in the FRP bars across the assumed crack, and it is expressed by following equation for rectangular bars.

$$V_f = 4(a + b)\tau_b L_{tot}$$

where a and b represent the cross-sectional dimension for the rectangular FRP bar, and τ_b represents the average bond stress of the bars crossed by a shear crack.. Experimental data available on 10-mm (#3) carbon FRP deformed bars demonstrate that when using an epoxy based resin in a groove size at least 1.5 times the bar diameter, a

conservative value of $\tau_b=6.9 \text{ MPa}$ (1.0 ksi) can be used (De Lorenzis and Nanni, 2001b).

L_{tot} can be expressed as $L_{tot} = \sum_i L_i$ where L_i represents the length of each single NSM bar crossed by a shear crack and can be expressed as:

$$L_i = \begin{cases} \min\left(l_{0.004}, \frac{s \cdot i}{\sin \alpha}\right) & i = 1 \dots \frac{n}{2} \\ \min\left(l_{0.004}, d_{net} - \frac{s \cdot i}{\sin \alpha}\right) \geq 0 & i = \frac{n}{2} + 1 \dots n \end{cases}$$

where α represents the slope of the FRP bar with respect to the longitudinal axis of the beam, and s is the FRP bar spacing.

The first limit $l_{0.004}$, takes into account the shear integrity of the concrete by limiting at 0.004 the maximum strain in the FRP reinforcement. From the force equilibrium condition, $l_{0.004}$ can be determined as follows for rectangular bars:

$$l_{0.004} = 0.002 \frac{a \cdot b}{a + b} \frac{E_f}{\tau_b}$$

where A_b and E_f represent cross sectional area and elastic modulus of one FRP bar.

The second limit in equation up reported, takes into account bond as the controlling failure mechanism, and represents the minimum effective length of an FRP bar crossed by a shear crack. It is expressed by $s \cdot i / \sin \alpha$ or $d_{net} - s \cdot i / \sin \alpha$ depending on the value assumed by the term:

$$n = \frac{d_{net}}{s}$$

where n is taken as the smallest integer (e.g., $n = 32/3 = 10.7 \Rightarrow n = 10$).

A reduced value for the effective length of FRP bar, d_{net} , is suggested to take into account the formation of vertical flexural cracks in the shear regions that could compromise the bond between FRP bars and surrounding concrete :

$$d_{net} = d_r - \frac{2c_c}{\sin \alpha}$$

where d_r is the actual length of the bar, and c_c is the clear concrete cover of the internal longitudinal reinforcement.

Based on conventional PC theory and the proposed model, the nominal shear capacity of the girder prior and after strengthening were computed and compared to the experimental values as shown in Table IV-4-1. The reported data show a good match.

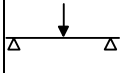
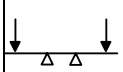
Specimen	Test Setup	V_c kN (kips)	V_s kN (kips)	V_f kN (kips)	V_n kN (kips)	Max Shear, V_u kN (kips)	V_n/V_u (%)
S2		14.7	0	0	14.7	81.8 (18.4) [shear failure]	80
S4		14.7	0	19.6	34.4	125.5 (28.2) [flex. failure]	123

Table IV-4-1- Shear theoretical predictions

5. CONCLUSIVE REMARKS

This research allowed to compare and check the effectiveness of numerous FRP upgrade systems with reference to both shear and flexural strengthening. The results of Phase I show that CFRP laminates applied on the bottom surface of the specimens are definitely valid for flexural upgrade, while Phase II shows that CFRP rectangular bars based on the NSM technique represents an innovative and effective system for shear strengthening. This result is confirmed by high strain values recorded by strain gages applied on CFRP bars during the test. For what concerns the flexural strengthening, the precured laminates tested in Phase II appeared to provide lower performance if compared to laminates. Furthermore, a comparison between the results provided by Phase I and II underlines that the specimen failure mode could be changed depending on the selected upgrade system.

Further investigations will be necessary in order to optimize the combination of flexural and shear upgrade and in particular to prevent debonding of the flexural strengthening.

CONCLUSIONS

The present thesis deal with the strengthening of PC members using composites. In particular, the motivation was given by the accident occurred on the A5657 Bridge, on Route 28 over the Gasconade River, South of Dixon, Missouri, U.S.A. One of its PC girders was accidentally damaged during the construction by the contractor; removal of lost concrete showed that two prestressing tendons were fractured due to the impact. The Missouri Department of Transportation, owner of the bridge, accepted the proposed upgrade solution submitted by the contractor; however, that caused that MODOT subtracted from the payments owed to the contractor five times the cost of the strengthening to cover possible future replacements.

This case highlighted the importance of implementing effective and fast strengthening techniques to use in similar situations as well as of demonstrating their reliability and structural validity. Uncertainties about these two aspects could result in social consequences (replacement of the bridge would have a strong impact on communications and economic activities) and economic disadvantages (contractor strongly penalized to cover uncertainties).

In order to provide a contribution toward the solution of these issues, an experimental campaign was designed and developed at the Highbay Laboratory of the University of Missouri-Rolla. The work

dealt with composite beams having a PC girder and a top deck. The behaviour of the reference beam was compared to that of an equivalent member damaged (two tendons cut) and strengthened using the FRP technology.

In this context, first the thesis discusses the field application on the A5657 Bridge. The strengthening solution is presented and the steps involving the installation are outlined along with some aspects that characterize the specific case. Then, the experimental analysis on beams that simulated the members of the real bridge is described. The disposed instrumentation allowed to record interesting information about the global (in terms of load-deflection) and local (in terms moment-curvature) behaviour of tested members. The laboratory work confirmed the validity of the proposed technique and demonstrated that CFRP could be a promising tool to restore both capacity and stiffness of damaged PC girders. The experimental validation was finally extended to another upgrade scheme that was tested on a real girder taken from a replaced bridge. Such experimental study provided insights about the opportunities of combining laminates and bars for flexural and shear strengthening of PC girders.

APPENDIX A

**STRENGTHENING OF IMPACT-DAMAGED BRIDGE
GIRDER USING FRP LAMINATES**

CFRP PLYS INSTALLATION ON BRIDGE A5657



Figure A-1- *Bridge A5657 on Route 28 over Gasconade River, South of Dixon, Missouri (Mo), U.S.A*



Figure A-2- *Damaged span of the bridge*



Figure A-3- *Detail of the damaged area*



Figure A-4- *Spalled concrete and two tendons fractured*



Figure A-5- *Formwork application to restore damaged area*



Figure A-6- *Patch material for concrete repair*



Figure A-7- *Bottom edges of the girder rounded for proper installation*



Figure A-8- *Sandblasting of the repaired area*



Figure A-9- *Primer preparation*



Figure A-10- *Primer application*



Figure A-11- *Application of primer completed*



Figure A-12- *Application of first layer of saturant*

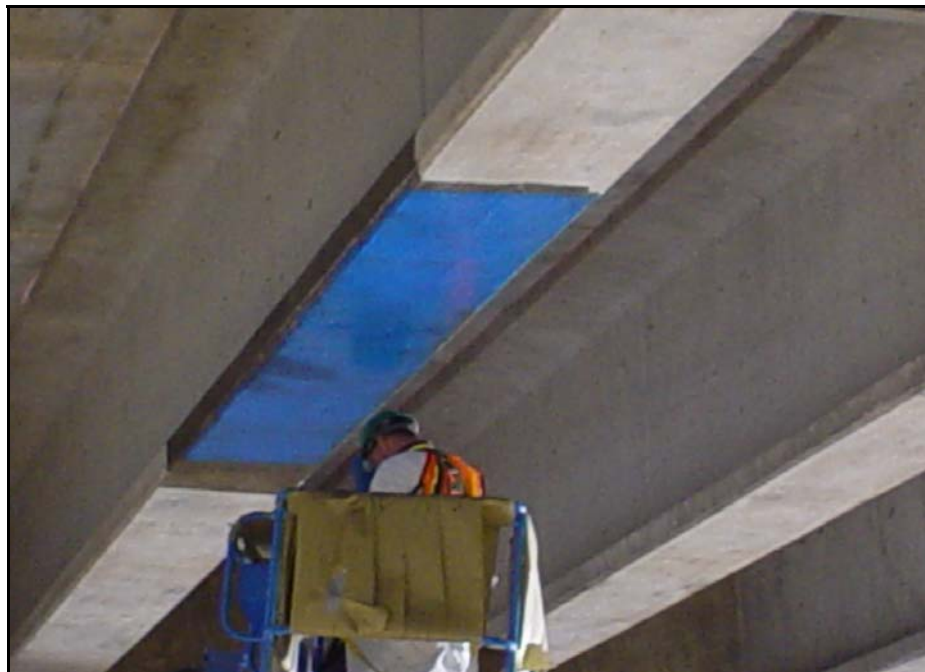


Figure A-13- *Application of first layer of saturant completed*



Figure A-14- *Application of FRP laminate*



Figure A-15- *Application of second layer of saturant*

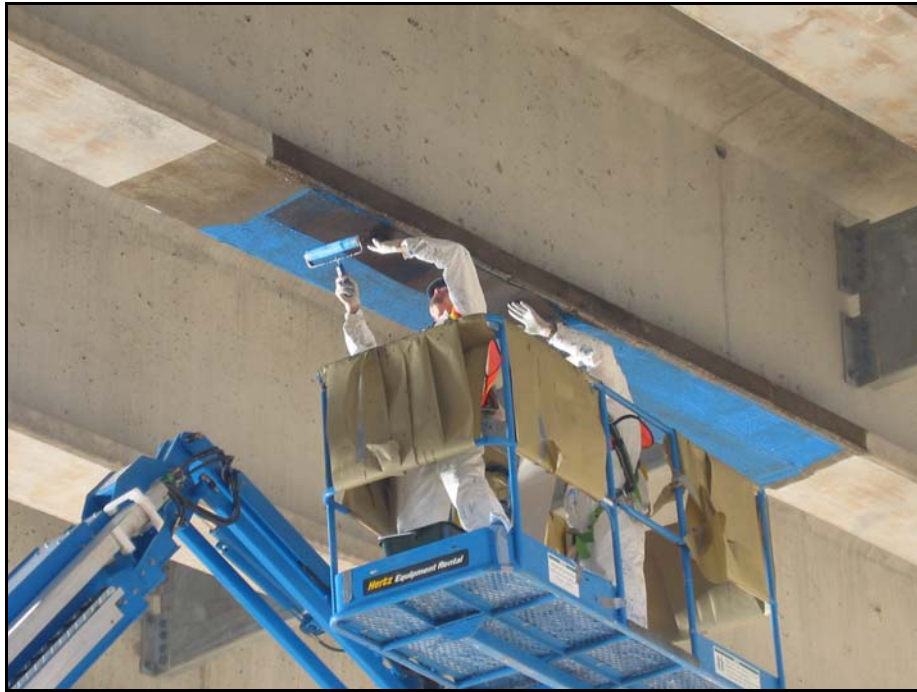


Figure A-16- *Completing of first ply of CFRP application*



Figure A-17- *First ply of CFRP application completed*



Figure A-18- *U-wrap installation*

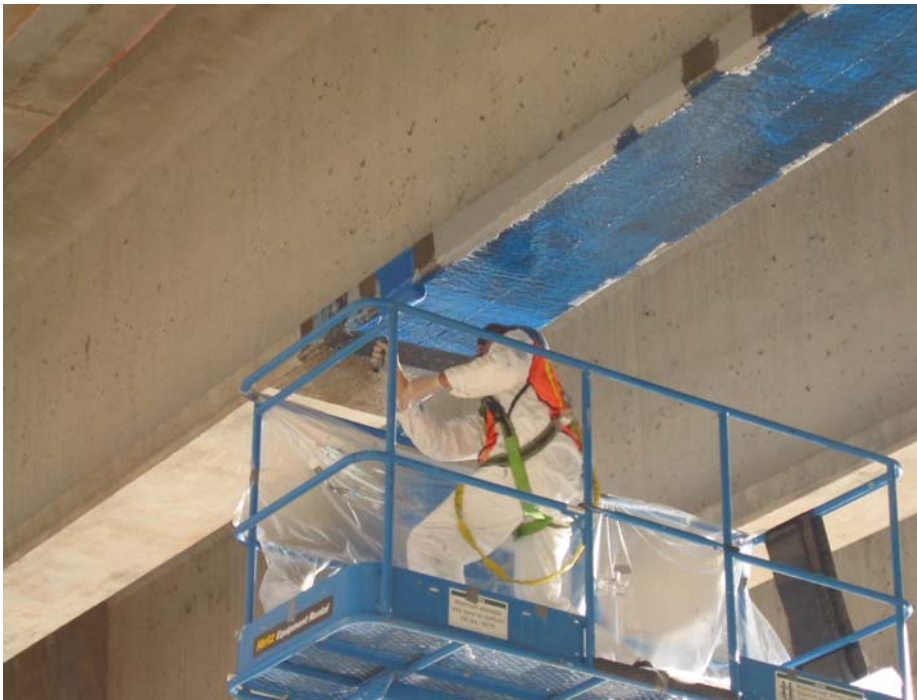


Figure A-19- *U-wrap installation: application of first layer of saturant*



Figure A-20- *U wrap installation: strips application*

APPENDIX B

LABORATORY TESTS ON PC BEAMS BRIDGE MODEL

SPECIMEN CONSTRUCTION

1. STRAIN GAGES APPLICATION ON THE TENDONS



Figure B-1- *Strain gages characteristics: resistance $350 \pm 0.5\%$; gage factor $2.105 \pm 0.5\%$ transverse sensitivity at $24^\circ \text{C} + 0.9 \pm 0.2\%$*



Figure B-2- *Application strain gages on the strands*



Figure B-3- *Strain gage installation*



FigureB-4- *Strain gage installation*



Figure B 5- *Strain gage installation*

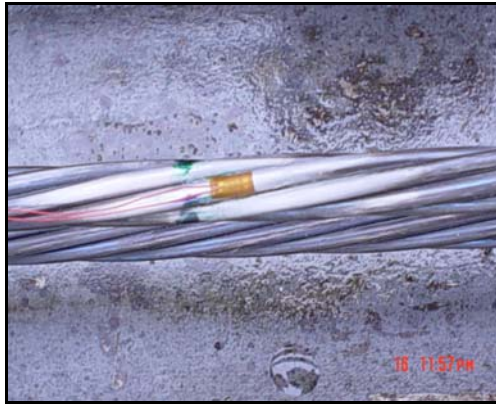


Figure B-6- *Strain gage installed*



Figure B-7- *Strain gage protection*



Figure B-8- *Location of strain gage applied on the undamaged girder*



Figure B-9- *Location of strain gages applied on the intentionally damaged and repair girder*

2. GIRDER CASTING



Figure B-10- *Stirrups installation*



FigureB- 11- *Stirrups installation*



Figure B-12- *Formworks installation*



Figure B-13- Girder casting



Figure B-14- Girder Concrete vibration



Figure B-15- Carrying girder in laboratory

3. DECK CASTING



Figure B-16- *Formworks preparation*



Figure B-17- *Formwork preparation*



Figure B-18- *Steel reinforcement installation*



Figure B-19- *Deck casting*



Figure B-20- *Complete specimen view*

REFERENCES

AASHTO, Standard Specifications for Highway Bridges (Sixteenth Edition), American Association of State Highway Traffic Officials, Washington D.C., 1996.

Aboutaha, R, R.T. Leon, and A.H. Zureick, (1997), “Rehabilitation of Damaged AASHTO Type II Prestressed Girder Using CFRP,” Proc., II Symposium on Practical Solutions for Bridge Strengthening and Rehabilitation, Kansas City, MO, April, pp. 293-301.

ACI Committee 440, ACI440.2R-02 (2002), “Guide for the Design and Construction of Externally Bonded FRP Systems for Strengthening Concrete Structures”

ACI Committee 318, “Building Code Requirements for Structural Concrete (ACI 318-99) and Commentary (ACI 318R-99),” American Concrete Institute, Farmington Mills, MI, 1999.

Alkhrdaji, T., Nanni, A., Mayo, R. “Upgrading Missouri Transportation Infrastructure: Solid Reinforced-Concrete Decks Strengthened

with Fiber-Reinforced Polymer Systems.” Transportation Research Record no. 1740. National Academy Press, Washington, D.C., 2000, pp 157-163.

Arduini, M., and Nanni, A., “Behavior of Pre-cracked RC Beams Strengthened with carbon FRP Sheets.” Journal of Composites for Construction. May 1997.

ASTM D3039/D 3039M –00. “Standard Test Method for Tensile Properties of Polymer Matrix Composite Materials.” American Standards of Testing and Materials

Benmokrane B., S. Faza, H.V.S. GangaRao, V.M. Karbhari, and M. Porter, “Gap Analysis for Durability of Fiber Reinforced Polymer Composites in Civil Infrastructure – Effects of Alkaline Environment”, CERF, 2001

Chin J.W., J. Martin, and T. Nguyen, “Gap Analysis for Durability of Fiber Reinforced Polymer Composites in Civil Infrastructure – Effects of Ultraviolet (UV) Radiation”, CERF, 2001

De Lorenzis, L., and Nanni, A., 2001-a, “Strengthening of Reinforced Concrete Beams with Near-Surface Mounted Fiber-Reinforced Polymer Bars”, *Structural Journal*, ACI, V. 98, No. 1, pp. 60-68.

De Lorenzis, L., and Nanni, A., 2001b; “Characterization of FRP Bars as Near Surface Mounted Reinforcement”, *Journal of Composites for Construction*, ASCE, V. 5, No. 2, pp. 114-121.

Dolan, C.W., S. Rizkalla and A. Nanni, Editors, (1999), *Fiber Reinforced-Polymer Reinforcement for Concrete Structures – Fourth International Symposium (FRPRCS4)*, ACI Special Publication No. 188, American Concrete Institute, Farmington Hills, MI, 1182 pp.

Fukuyama, H. (1999): “Fibre-Reinforced Polymers in Japan”, *Structural Engineering International*, 4/99, S. 263-266.

Furuta T., Kanakubo T., Nemoto T., Takahashi K. and Fukuyama H. (2000?), “Sprayed-up FRP Strengthening for Concrete Structures”

Hunston D., T. Juska, V.M. Karbhari, R. Morgan, and C. Williams, “Gap Analysis for Durability of Fiber Reinforced Polymer Composites in Civil Infrastructure – Effects of Moisture/Aqueous Solutions”, CERF, 2001

Japan Concrete Institute (1997), “Non-Metallic (FRP) Reinforcement for Concrete Structures”, 3rd Int. Symposium on Non-Metallic (FRP) Reinforcement for Concrete Structures

Juska T., P. Dutta, L. Carlsson, and J. Weitsman, “Gap Analysis for Durability of Fiber Reinforced Polymer Composites in Civil Infrastructure – Thermal Effects“, CERF, 2001

Karbhari V.M., “Gap Analysis for Durability of Fiber Reinforced Polymer Composites in Civil Infrastructure – Introduction”, CERF, 2001

Khalifa A., Alkhrdaji T., Nanni A., Lansburg S. (1999), “Anchorage of Surface Mounted FRP Reinforcement”

Khalifa, A., Gold, W.J., Nanni, A., and Abdel Aziz, M.I., 1998; “Contribution of Externally Bonded FRP to Shear Capacity of RC Flexural Member”, *Journal of Composites for Construction*, ASCE, V. 2, No. 4, pp. 195-202.

Khataukar, A. (2001), “Effect of Environmental Conditions on the Installation Process of Bonded FRP Materials,” MSc. Thesis, UMR, in print

Klaiber, F.W., T.J. Wipf, F.M. Russo, R.R. Paradis, and R.E. Mateega, (1999), “Field/ Laboratory Testing of Damaged Prestressed Concrete Girder Bridges,” Iowa DOT Report HR-397, Iowa State Univ., Ames, Iowa, Dec., 261 pp.

Lesko J., K. Reifsnider, S. Phifer, C. Bakis, A. Nanni, and C. Heil, "Gap Analysis for Durability of Fiber Reinforced Polymer Composites in Civil Infrastructure – Effects of Fatigue“, CERF, 2001

Master Builders Technologies, "MBrace Composite Strengthening System-Engineering Design Guidelines," (Second Edition), Cleveland, OH, 1998.

Morgan R., C. Dunn, and C. Edwards, "Gap Analysis for Durability of Fiber Reinforced Polymer Composites in Civil Infrastructure – Effects of Creep and Relaxation", CERF, 2001

Nakaba K., Kanakubo T., Furuta T. and Yoshizawa H. (2001), "Bond Behavior between Fiber-Reinforced Polymer Laminates and Concrete", ACI Structural Journal/May-June 2001, Title no. 98-S34

Nanni, A. "FRP Reinforcement for Bridge Structures," Proceedings, Structural Engineering Conference, The University of Kansas, Lawrence, KS, March 16, 2000, 5 pp.

Nanni, A., Huang, P.C., Tumialan, J.G., "Strengthening of Impact – Damaged Bridge Girder Using FRP Laminates," 9th Int. Conf., Structural Faults and Repair, London UK, July 4-6, 2001, 7 pp.

- Nanni, A. "Concrete Repair with Externally Bonded FRP Reinforcement: Examples from Japan." ACI Concrete International, June 1995, 22-26.
- Nanni, A., (1997) "Carbon FRP Strengthening: New Technology Becomes Mainstream," Concrete International: Design and Construction, Vol. 19, No. 6, June, pp. 19-23.
- Nawy, E.G., Prestressed Concrete A Fundamental Approach (Second Edition), William J. Hall Editor, New Jersey, 1996.
- Nilson, A. H., Design of Prestressed Concrete (Second edition) John Wiley and Sons, Inc., New York, NY, 1987.
- Olson, S.A., C. W. French, and R.T. Leon, (1992), "Reusability and Impact Damage Repair of Twenty-Year-Old AASHTO Type III Girders," Research Report No. 93-04, Univ. of Minnesota, Minneapolis, MN, May.
- Park, R., and Paulay, T., Reinforced Concrete Structure, John Wiley and Sons, Inc., New York, N.Y., 1975.
- Parretti, R. and A. Nanni, "Strengthening of RC Members Using NSM Composites: Design Overview," ASCE Journal of Structural Engineering, April 2002 (submitted)

Peterman, R., and Reed C.E., “Repair and Strengthening of Severely Damaged 32-Year Old Prestressed Concrete Bridge Girders with Externally Bonded FRP Reinforcement,” November 2001

Precast/Prestressed Concrete Institute. “PCI Design Handbook 5th Edition.” Chicago,

Russo, F.M., Terry, J.W., Klaiber, F. W. and Paradis,R. , “ Diagnostic Load Tests of a Prestressed Concrete Bridge Damaged by Overheight Vehicle Impact .” Transportation Research Record, Conference Paper, 2000, pp. 8

Scherer J., S&P Reinforcement, “Fiber reinforced polymer FRP systems for external strengthening of concrete structures.” ACI Spring Convention March 14 – 19, 1999, Chicago, IL.

Shahawy, M.A., Beitelman, T., (1996), “ Structural Repair and Strengthening of Damaged Prestressed Concrete Bridges Utilizing Externally Bonded Carbon Materials,” Florida Departement of Trasportation, March 24-28, 1996

Shanafelt, G.O., and W.B. Horn, (1980), “Damage Evaluation and Repair Methods for Prestressed Bridge Members,” Transportation Research Board, Washington, DC, NCHRP Report 226.

Shanafelt, G.O., and W.B. Horn, (1985), "Guidelines for Evaluation and Repair of Prestressed Concrete Bridge Members," NCHRP Report 280, Transportation Research Board, Washington, DC.

Sorathia U., T. Ohlemiller, R. Lyon, J. Riffle, and N. Schultz, "Gap Analysis for Durability of Fiber Reinforced Polymer Composites in Civil Infrastructure – Effects of Fire", CERF, 2001

Stone, D., A. Prota, and A. Nanni, "Performance Evaluation of an FRP-Reinforced Concrete Bridge", Transportation Research Board 81st Annual Meeting, Washington, D. C., January 13-17, 2002

Stone, D., S. Watkins, H. Nystrom and A. Nanni, "Investigation of FRP Materials for Bridge Construction," Proc., 5th Nat. Workshop on Bridge Research in Progress, C.K. Shield and A.E. Schultz, Eds., U. Minnesota, Twin Cities, Oct. 8-10, 2001, pp. 145-150.

Tanao H., Masuda Y., Sakashita M., Oono Y., Nonomura K. and Satake K. (1997) "Tensile Properties at High Temperatures of Continuous Fiber Bars and Deflections of Continuous Fiber Reinforced Concrete Beams Under High-Temperature Loading" Proceedings 3rd International Symposium FRPRCS-3, JCI 1997.

Tavakkolizadeh M., Saadatmanesh H. (2001), “Galvanic Corrosion of Carbon and Steel in Aggressive Environments”. Teng J.G. CICE 2001, “FRP Composites in Civil Engineering”.

Uomoto T. and Nishimura T., (1999) “The Deterioration of Aramid ,Glass and Carbon Fibers due to Alkali, Acid and Water in Different Temperatures” Proceeding 4th International Symposium FRPRCS-4, ACI SP-188 , American Concrete Institute, 1999, 515-522

Yang X., Miller B., Nanni A., Bakis C., “Characterization of CFRP Bars used as Near-Surface-Mounted Reinforcement” Proceedings of the 8th International Structural Faults and Repair Conference, Engineering Techniques Press, Edinburgh, Scotland, 1999, pp 340-350

Yang X., Nanni A, Haug S., Sun C.L. (2001), “Strength and Modulus Degradation of CFRP Laminates from Fiber Misalignment”.

Yang X., Nanni A. (2002), “Lap Splice Length and Fatigue Performance of FRP Laminates”.

Zobel, R.S, J.O. Jirsa, D.W. Fowler, and R.L. Carrasquillo, (1997), “Evaluation and Repair of Impact-Damaged Prestressed Concrete Bridge Girders,” Report CTR 1370-3F, Univ. of Texas, Austin, TX.

